The Evolution of the Galápagos Mantle Plume:

From Large Igneous Province to Ocean Island Basalt

Jarek Trela

Dissertation submitted to the faculty of the Virginia Polytechnic Institute and State University in partial fulfillment of the requirements for the degree of

Doctor of Philosophy

In

Geosciences

Esteban Gazel, Chair

Claude Herzberg

Mark J. Caddick

Ying Zhou

March 22nd, 2017

Blacksburg, Virginia

The Evolution of the Galápagos Mantle Plume:

From Large Igneous Province to Ocean Island Basalt

Jarek Trela

Abstract

Mantle plumes are anomalously hot, narrow upwellings of mantle material that originate at the core-mantle boundary. As plumes rise they may form volumetrically large "heads" (~1000 km in diameter) with narrower (~100 km) "tails". Plume head melting is thought to form Large Igneous Provinces (LIPs), vast outpourings of basaltic lava (~10^6 km^3), while plume tail melting forms linear chains of ocean island basalts (OIBs) similar the Emperor-Hawaii Seamount chain. Mantle plume derived melts indicate that these structures sample deep Earth geochemical and lithological heterogeneities. Studying plume-derived lavas can clarify important planetary-scale questions relating to the accretion of the Earth, primordial geochemical reservoirs, the fate of subducted materials, planetary differentiation, and convective mixing.

Although much research exists on plumes, the complete geochemical evolution from the LIP to OIB stage has not been constrained. The Galápagos hotspot provides an exceptional opportunity to reconstruct plume evolution due to the on-land accessibility of LIP terranes in the Caribbean and Costa and accreted OIB terranes along the west coast of Panama and Costa. This dissertation aims at clarifying the life-death cycle of the Galapagos mantle plume, addresses why plumes cool and stop producing melts, and effect of recycled crustal lithologies on the temperature of the plume and geochemistry of melts and olivine phenocrysts.

In Chapter 1 we closely examined the transitional phase of the Galápagos Plume

LIP to OIB forming stages. Our petrological evidence suggests that the maximum mantle potential temperature (T_p) of the plume changed from ~1650° to ~1550°C between 90-70 Ma. This change correlates with a dominant pyroxenite component (recycled oceanic crust) in the Galapagos source as indicated by high Ni and Fe/Mn and low Ca olivines relative to those that crystallized in normal peridotite derived melts. The Galápagos plume at 70 Ma represents elevated pyroxenite melt productivity relative to peridotite in a cooling lithologically heterogeneous mantle.

In Chapter 2 we showed that 89 Ma lavas from the Galapagos Plume-related Tortugal Suite record mantle temperatures as high as Archean komatiites and ~400°C hotter than the modern ambient mantle. These results are also supported by highly magnesian olivine phenocrysts and Al-in-olivine crystallization temperatures. Since mantle plumes are chemically and thermally heterogeneous, we interpret these rocks as the result of melting the hot core of the plume head that produced the Caribbean LIP. The Tortugal Suite represents the hottest Phanerozoic lavas.

In Chapter 3 we investigated the spatial and temporal evolution of the four isotopic end members of the mantle plume using Sr-Nd-Pb isotopic modeling. We find that the spatial relationship between each of the classically defined Domains has remained relatively constant over the last 90 Ma as evidenced by the isotopic compositions of accreted terranes in Costa Rica and Panama. Our new results extend the time scale of distinct isotopic heterogeneity in the source of the plume to at least 70 Ma for the Southern Domain and 90 Ma for the Central, and Northern Domains, suggesting that geochemically zoned plumes rising through the mantle preserve distinct isotopic heterogeneity on the time scale of tens to hundreds of millions of years.

The Evolution of the Galápagos Mantle Plume:

From Large Igneous Province to Ocean Island Basalt

Jarek Trela

General Audience Abstract

Mantle plumes are hot, narrow upwellings of plastically flowing mantle material. These structures are thought to originate at the core-mantle boundary. Because mantle plumes originate in the deep interior of the planet, they are though to sample both primitive materials that are remnants of Earth's formation as well as recycled crustal materials that have been subducted from the surface into the deep interior of the planet. When mantle plumes near the surface of the planet they begin to partially melt during a process known as adiabatic decompression melting. When these melts cool, they crystallize to form basalts. These rocks and their associated minerals can be studied to determine lava temperatures and pressures of formation.

The geologic record suggests that relatively recently mantle plumes cool and eventually become magmatically inactive. In this project, we used the Galapagos plume as a case study to investigate why it has systematically cooled over the last 90 Ma. The Galapagos mantle plume is possibly the oldest active plume and records a 90 Ma volcanic evolution. We studied Galapagos-related lavas and olivine crystals across the entire 90 Ma evolution of the plume to better understand the life-death cycle of mantle plumes. Our data suggest that the plume may be cooling due to an increase in the amount of recycled oceanic crust. Alternatively, a recycled oceanic crust component could have always been present in the source of the plume, though was diluted during high degrees of partial melting when it was hottest at 90 Ma.

Acknowledgements

There are so many extraordinary individuals that contributed to making this project successful and I would not have completed it without their help. Particularly, my advisor and mentor Dr. Esteban Gazel. I feel honored that he let me work on many exciting projects with during this project and took me on once-in-a-life-time adventures to Central America. His energy and endless enthusiasm always motivated come up with creative solutions to problems. I will always remember the excitement of studying the hottest lavas of the Phanerozoic with him.

I am very thankful for the support of my committee members: Mark Caddick, Ying Zhou, and Claude Herzberg. We had some excellent meetings together and they always asked challenging big-picture questions that lead to many great discoveries in Galapagos-related lavas. I will always be grateful to Claude for our lengthy correspondences and discussion about olivine, petrologic modeling, and the mysteries of the mantle. I thank Percy Denyer, Denis Soto, and Cornelia Class for helping us collect samples. I appreciate all of the technical and analytical support form our collaborators including Alex Sobolev, Valentina Batanova, Michael Bizmis, Luca Fedele, Brian Jicha, Ian Godwin, and Bob Tracy. I am grateful for all the members of the VT Volcanoes group for supporting me during the ups and downs of a dissertation. They include: Denis Zamboni, Pilar Madrigal, Sarah Mazza, Lowell Moore, Ty and Lisa Whalen, Besim Dragovic, and Claudia Adam. I am very grateful to my fiancé, Madison Pitcher, for all of her support, love, strength, and amazing cuisine that kept me fueled over the last few years. Finally, I thank my family for always believing in and encouraging me to do my best in all things.

Attributions

Many talented geoscientists contributed during the research, writing, and intellectual developments of this project and its associated manuscripts and their efforts must be attributed in this dissertation.

Chapter 1 was published as Trela, J., Vidito, C., Gazel, E., Herzberg, C. Class, C., Whalen, W., Jicha, B., Bizimis, M., Alvarado, G. 2015. Recycled crust in the Galapagos Plume source at 70 Ma: Implications for plume evolution: EPSL. v. 425, 268-277.

Chapter 2 was accepted to Nature Geoscience as Trela, J., Gazel, E., Moore, L., Sobolev, A., Bizimis, M., Jicha, B., Batanova, V., 2016. The hottest lavas of the Phanerozoic and the survival of ancient Archean reservoirs: Nature Geoscience (4/20/17).

Chapter 3 is currently under preparation for submission as Trela, J., Gazel, E., Sobolev, A.V., Bizimis, M., Jicha, B.R. Long-lived Sr-Nd-Pb heterogeneities in the Galapagos mantle plume. In preparation for G-cubed.

All of the coauthors helped tremendously in improving and driving the science behind these manuscripts.

Table of contents

Introduction

Although mantle plumes have been studied in great detail over the past several decades, the complete thermal and geochemical evolution of any mantle plume has yet to be constrained. The Galápagos hotspot provides an exceptional opportunity to reconstruct plume evolution due to the on-land accessibility of LIP terranes in the Caribbean and Costa Rica and accreted OIB terranes along the west coast of Panama and Costa Rica. Our recent petrological studies showed that lavas part of the Caribbean LIP melted more extensively and at higher temperatures than lavas from the modern Galapagos Islands suggesting that the plume is systematically cooling over time. My dissertation aims at understanding if the entrainment of dense recycled crustal components affect the thermal evolution of mantle plumes and influence the geochemical, isotopic, and olivine compositions that have erupted at the Galapagos hotspot over the past 90 Ma. Ultimately, this project explores the question of whether or not the progressive entrainment of recycled crustal components is responsible for secular Galapagos plume cooling and to constrain the life-death cycle of mantle plumes globally. By sampling the erupted Galapagos material we aim to clarify how the plume evolved both isotopically and lithologically in space and time over the last 90 Ma. The overarching theme of my research is to elucidate the complex geochemical recycling system of our planet to better understand the fate of subducted Earth materials.

Chapter 1 of this dissertation examined the LIP-OIB transitional phase of the Galápagos Plume and was published in EPSL (Trela et al., 2015). This study showed that the maximum mantle potential temperature of the Galapagos plume decreased by ~100°C during the LIP-OIB transition at 70 Ma. This marked decrease in temperature correlates

with the appearance of a dominant pyroxenite component source as indicated by high Ni and Fe/Mn and low Ca olivines. The Sr–Nd–Pb radiogenic isotopic compositions suggest that the OIB lavas are more radiogenic than the LIP lavas, suggesting an enrichment in the source of the plume, probably the result of a recycled oceanic crust component.

Chapter 1 was published as Trela, J., Vidito, C., Gazel, E., Herzberg, C. Class, C., Whalen, W., Jicha, B., Bizimis, M., Alvarado, G. 2015. Recycled crust in the Galapagos Plume source at 70 Ma: Implications for plume evolution: EPSL. v. 425, 268-277.

Chapter 2 of this dissertation shows that ~89 Ma lavas from the Galapagos Plume related Tortugal Suite in Costa Rica record mantle temperatures as high as ancient Archean komatiites and ~400°C hotter than the modern ambient mantle. Our results are supported by highly magnesian (Mg# = 94.2) olivines from primitive melts and Al-in-olivine crystallization temperatures up to 1602 °C (higher than most Archean komatiites), ~ 300 °C higher than those recorded by mid-ocean ridge basalts. Since mantle plumes are chemically and thermally heterogeneous, we interpret these rocks as the result of melting the hot core of the plume head that produced the Caribbean Large Igneous Province. The Tortugal Suite represents the hottest Phanerozoic lavas (relative to other hot LIPs and OIBs, e.g., Hawaii, Iceland, Emeishan) as well as the hottest terrane related to the secularly cooling Galapagos Plume. We suggest in this study that a reservoir as hot as the one that produced Archean komatiites survived Eons of convection in the deep Earth and it is still tapped by recent mantle plumes, though less frequently due to the secular cooling of the planet, entrainment of recycled lithologies during ascent and interaction with and mid-ocean ridges.

Chapter 2 was accepted to Nature Geoscience as Trela, J., Gazel, E., Moore, L., Sobolev, A., Bizimis, M., Jicha, B., Batanova, V., 2016. The hottest lavas of the Phanerozoic and the survival of ancient Archean reservoirs: Nature Geoscience (3/29/2017).

Chapter 3 of this dissertation focuses on understanding the isotopic evolution of the Galapagos plume over the last 90 Ma. In this study, we investigate the spatial and temporal evolution of the four isotopically distinct end members that define the plume using Sr-Nd-Pb isotopic modeling and source inversion techniques. Interestingly, the spatial relationship between each of the classically defined Galapagos Domains has remained relatively constant over the last 90 Ma as evidenced by the isotopic compositions of accreted terranes in Costa Rica and Panama. Our new results extend the time scale of distinct isotopic heterogeneity in the source of the plume to at least 70 Ma for the Southern Domain and 90 Ma for the Central, Northern, and Eastern Domains, suggesting that geochemically zoned plumes rising through the mantle preserve distinct isotopic heterogeneity on the time scale of tens to hundreds of Ma.

Chapter 3 is in preparation for submission as Trela, J., Gazel, E., Sobolev, A.V., Bizimis, M., Jicha, B.R. Long-lived Sr-Nd-Pb heterogeneities in the Galapagos mantle plume. In preparation for G-cubed. To be submitted before end of spring semester 2017.

Chapter 1: Recycled crust in the Galápagos Plume source at 70 Ma: Implications for plume evolution

Abstract

Galápagos plume-related lavas in the accreted terranes of the Caribbean and along the west coast of Costa Rica and Panama provide evidence on the evolution of the Galápagos mantle plume, specifically its mantle temperature, size and composition of heterogeneities, and dynamics. Here we provide new $^{40}Ar/^{39}Ar$ ages, major and trace element data, Sr-Nd-Pb isotopic compositions, and high-precision olivine analyses for samples from the Quepos terrane (Costa Rica) to closely examine the transitional phase of the Galápagos Plume from Large Igneous Province (LIP) to ocean island basalt (OIB) forming stages. The new ages indicate that the record of Quepos volcanism began at 70 Ma and persisted for 10 Ma. Petrological evidence suggests that the maximum mantle potential temperature (T_p) of the plume changed from ~1650° to ~1550°C between 90-70 Ma. This change correlates with a dominant pyroxenite component in the Galapagos source as indicated by high Ni and Fe/Mn and low Ca olivines relative to those that crystallized in normal peridotite derived melts. The decrease in T_p also correlates with an increase in high-field strength element enrichments, e.g., Nb/Nb*, of the erupted lavas. Radiogenic isotope ratios (Nd-Pb) suggest that the Quepos terrane samples have intermediate (Central Domain) radiogenic signatures. The Galápagos plume at 70 Ma represents elevated pyroxenite melt productivity relative to peridotite in a cooling lithologically heterogeneous mantle.

Introduction

The initial melting of mantle plumes produces unparalleled volumes (5-40 x 10^6

km^3) of lava that form continental flood basalts and oceanic plateaus, which represent the most significant igneous structures on Earth (e.g., Coffin and Eldholm, 1994; Mahoney and Coffin, 1997; Saunders, 2005; Coffin et al., 2006). This type of intra-plate magmatism originates at a deep thermal boundary layer below the upper mantle, (possibly the core-mantle boundary, e.g., Morgan, 1972; Tolstikhin and Hofmann, 2005; Torvisk et al., 2010; Burke et al., 2011). During ascent, a plume may develop a volumetrically large "head", followed by a narrower conduit or "tail". Geodynamic models suggest that melting of a 500-2000 km wide plume head (Arndt, 2000) forms large igneous provinces (LIPs), characterized by high degrees of partial melting, high mantle potential temperatures (T_p), and widespread lava flows ($> 10^5$ km^2) (Richards et al., 1989; Coffin and Eldholm, 1994, Herzberg and Gazel, 2009). These events were sometimes so large that they affected environmental change leading to catastrophic mass extinctions or oceanic anoxic events (e.g., Courtillot and Renne, 2004; Kerr, 2005; Blackburn et al., 2013). Subsequent melting of a plume conduit will form ocean island basalts (OIBs), which may manifest themselves as tracks of linear ocean islands and seamount chains. Most older LIPS were hotter and melted more extensively than their younger OIB counterparts (Herzberg and Gazel, 2009).

The Galápagos hotspot provides an exceptional opportunity to reconstruct plume evolution due to the on-land accessibility of LIP terranes in the Caribbean and Costa Rica (Alvarado et al., 1997; Denyer and Gazel, 2009; Loewen et al., 2013) and accreted OIB terranes along the west coast of Panama and Costa Rica (Hoernle et al., 2002). Recent petrological studies suggested that the Caribbean LIP (CLIP) melted more extensively and at higher temperatures than lavas from the modern Galápagos Islands (Herzberg and

Gazel, 2009). The maximum T_p of the plume was ~1620 °C during the Cretaceous and cooled to ~1500 °C at present time at a rate of ~1 °C/Ma assuming a linear decrease (Herzberg and Gazel, 2009). Therefore, understanding the evolution of the Galápagos mantle plume has significant global implications for understanding mantle dynamics.

The amount, age, and contribution of subducted slab sources (eclogite, pyroxenite, or refertilized peridotite) fingerprinted in mantle plume geochemistry are also important. Although a recycled crust signature has been identified in plumes through the use of radiogenic isotopes and trace-element signatures (e.g., Zindler and Hart, 1986; Hofmann, 1997; Chauvel et al., 2008) and more recently through the use of major element signatures (e.g., Jackson and Dasgupta, 2008; Shorttle and Maclennan, 2011; Jackson et al., 2012) and numerical models (Ballmer et al., 2013) the exact nature of geochemical exchanges and mixing of pyroxenite with mantle end members requires further investigation. Global scale recycling of crustal material undoubtedly plays a key role in the development and evolution of deep geochemical reservoirs as well as affecting the thermodynamic cooling of Earth. Furthermore, when compared with a primitive mantle reference, typical OIB trace element signatures show positive high field strength element (e.g., Nb and Ta) anomalies, suggesting a subducted slab reservoir in the mantle (McDonough, 1991; Rudnick et al., 2000; Kamber and Collerson, 2000; Jackson et al., 2008). This reservoir could represent the mantle domain component common in all plumes (e.g., C, FOZO) (Zindler and Hart, 1986; Hart et al., 1992; Stracke et al., 2005).

Our objective is to characterize the sources of the lavas present in the Quepos terrane and their effect on plume evolution during the important LIP-OIB transition. This "transition" marks a major decrease in the magmatic productivity when head stage

melting ceases and tail stage melting begins during a plume's evolution. In this study we use integrated petrological, geochemical, isotopic, and high-precision olivine geochemical analyses to compare our new results to preexisting data sets to show a decrease in T_p evident in the Quepos lavas that corresponds to a dominant pyroxenite component in the Galápagos Plume.

Background

The formation of the Caribbean Large Igneous Province (CLIP) began ~90 Ma with the incipient melting of the Galápagos plume head (Duncan and Hargraves, 1984; Richards et al., 1989; Pindel and Barrett, 1990; Kerr, et al., 1996a; Kerr et al., 1996b; Hauff et al., 1997; Sinton et al., 1997; Hauff et al., 2000a;). The Caribbean plate represents an over-thickened section of oceanic crust (up to 20 km) and is interpreted as the product Galápagos plume head melting (Duncan and Hargraves, 1984; Hauff et al., 1997, 2000a,b; Sinton et al., 1998; Kerr et al., 1996a; Hoernle et al., 2002, 2004). The CLIP then migrated northeast with the Farallon Plate where it collided with the Greater Antilles Arc (e.g., Duncan and Hargraves, 1984; Hauff et al., 2000; Geldmacher et al., 2003, Gazel et al., 2011). This collision triggered a reversal in subduction polarity, which initiated subduction along the western edge of the CLIP margin (Duncan and Hargraves, 1984; Geldmacher et al., 2003). The reversal in polarity facilitated the migration of the CLIP farther northeast between the converging North and South Americas between Late Cretaceous to Tertiary time (e.g., Duncan and Hargraves, 1984; Hauff et al., 2000a; Hoernle et al., 2002; Geldmacher et al., 2003).

Petrological and geochemical research of the Burica, Osa, and Quepos terranes in western Costa Rica (Fig. 1) together with Azuero and Sona terranes in Panama, provide

strong evidence that these areas represent accreted Galápagos OIB terranes, which resulted from melting of the plume tail post CLIP formation (Hauff et al., 2000a; Hoernle et al., 2002; Denyer and Gazel, 2009). These terranes are markedly younger than CLIP related lavas (85-95 Ma) with $^{40}Ar/^{39}Ar$ ages between 65-40 Ma and represent ancestral Galápagos plume tail segments accreted to Central America (Sinton et al., 1997; Hauff et al., 2000a; Hoernle et al., 2002). Around 23 Ma the Farallon Plate began spreading to form the Nazca and Cocos plates (e.g., Lonsdale, 2005). During the next 20 Ma the Galápagos hotspot and the Cocos-Nazca ridge experienced a series of complex interactions (Werner et al., 2003). The ridge-hotspot interactions subsequently formed the Cocos and Carnegie aseismic ridges located on the northeastward and eastward migrating Cocos and Nazca Plates respectively.

The present day Galápagos archipelago is currently divided into four domains, characterized by unique isotopic variations in Nd-Sr-Pb and $^{3}He/^{4}He$ (Hoernle et al., 2000; Harpp and White, 2001). The Eastern Domain represents the most depleted isotopic end-member (Hoernle et al., 2000; Harpp and White, 2001) with compositions similar mid ocean ridge basalt (MORB). Lavas from Floreana define the most isotopically enriched end member (Southern Domain) with high radiogenic $^{87}Sr/^{86}Sr$ and $^{206}Pb/^{204}Pb$ ratios (Harpp and White, 2001). Lavas in the Wolf-Darwin Lineament (Northern Domain) typically display minor ^{207}Pb and ^{208}Pb enrichments and $^{3}He/^{4}He$ ratios between 8.8-6.9 R/R_A (Harpp and White, 2001; Vidito et al., 2013) though they are depleted in $^{87}Sr/^{86}Sr$ and $^{206}Pb/^{204}Pb$ relative to Floreana lavas (Harpp and White, 2001). Islands in the Central Domain (e.g., Fernandina) most likely resemble the true "plume" composition and show intermediate enrichments in Sr, Nd, Pb (Harpp and White, 2001)

with high $^{3}He/^{4}He$ (up to 30.3 R/R_A; Kurz et al., 2014).

The Quepos terrane (focus of this study) is one of six fault-bounded oceanic igneous terranes located on the Pacific Costa Rican coast (Fig. 1). An intra-plate Galápagos origin is now generally accepted to explain the formation of Quepos based on petrological evidence, field-based observations, and trace element data and represents the oldest accreted segments of the Galápagos OIB stage (Frisch et al., 1992; Hauff et al., 1997; Denyer and Gazel, 2009). The lava stratigraphy of Quepos is dominated by a transitional tholeiitic to alkaline series with incompatible trace element patterns indicative of an OIB source with a clear Galápagos isotopic signature (Hauff et al., 2000; Geldmacher et al., 2003).

Materials and Methods

Picrite, diabase, and basalt samples were collected in the Quepos terrane, from in-situ outcrops or fresh, meter-size boulders along the shoreline to take advantage of active surf erosion exposures.

At the University of Wisconsin-Madison Rare Gas Geochronology Laboratory, $^{40}Ar/^{39}Ar$ incremental heating experiments were conducted on groundmass and mineral separates using a 25 Watt CO_2 laser and analyzed using a MAP 215–50 following the procedures in Jicha and Brown (2014). Isotope data was reduced using ArArCalc software version 2.5 (http://earthref.org/ArArCALC/). Ages are reported with 2σ uncertainties (includes the J uncertainty) and are calculated relative to a Fish Canyon standard age of 28.201 ± 0.046 Ma (Kuiper et al., 2008) and a value for $\lambda^{40}K$ of 5.463 ± 0.107 x 10^{-10} yr^{-1} (Min et al., 2000).

Alteration-free rock chips were selected under stereoscopic microscope and powdered in an alumina mill at the Department of Geosciences at Virginia Tech. From these powders, whole rock major and trace element compositions were collected at Washington State University by XRF and ICP-MS (protocols in Johnson et al., 1999). Curacao picrite samples were processed and analyzed in the geochemistry laboratory at the Department of Geosciences at Virginia Tech following the procedures described in Mazza et al. (2014). Major elements were collected by X-ray fluorescence (XRF), the Relative Standard Deviation (RSD) for 10 replicates of BHVO-2g was <2.70% for all major elements and accuracy better than 1.74%, with the excpetion of P_2O_5. Trace elements as well as P_2O_5 were collected from the same fluxed glasses with an Agilent 7500ce ICPMS coupled with a Geolas laser ablation system, following the procedures detailed in Mazza et al. (2014). Data were calibrated against USGS standards BCR-2, BHVO-2, G-2, and BIR-1a, using Ti from XRF as an internal standard and the standard element values reported in Kelley et al. (2003). The accuracy for 4 replicates of BHVO-2g was better than 5 % for all elements except for Ba, Hf, and Ge (7-9 %). The accuracy for 4 replicates of BIR-1a was better than 5 % for most elements except for Ga, Ge, Ce, Pr, Eu, Tb, Dy, Ho, Tm, Er, Yb, and Lu (5-9 %).

Acid-digested aliquots of the same powdered material was used to collect radiogenic isotope ratios of Pb, Nd, and Sr on a Neptune multi collector ICPMS at the Center for Elemental Mass Spectrometry (CEMS), University of South Carolina (USC). Pb isotope ratios were determined by the Tl-addition technique (White et al., 2000) using $^{203}Tl/^{205}Tl = 0.418922$ and assuming identical fractionation factors between Tl and Pb. The Pb/Tl ratio ($^{208}Pb/^{205}Tl \sim 7$) of the samples was kept near identical to the NBS

981 standard by first performing dip checks in the samples and spiking Tl to the appropriate level. The NBS-981 standard was determined at $^{206}Pb/^{204}Pb = 16.936 \pm 0.001$, $^{207}Pb/^{204}Pb = 15.490 \pm 0.001$, $^{208}Pb/^{204}Pb = 36.694 \pm 0.003$ (2 standard deviations, = 13). Isotopic ratios for Nd were normalized to $^{146}Nd/^{144}Nd = 0.7219$ and the Nd standard JNd_i was measured at $^{143}Nd/^{144}Nd = 0.5121$ and 0.512112 ± 0.000007 (n=6) at USC. Isotopic ratios for Sr were normalized to $^{86}Sr/^{88}Sr = 0.1194$ and replicate analyses of $^{87}Sr/^{86}Sr$ at 0.710320 ± 0.000012. All Sr measurements are reported relative to NBS-987 where $^{87}Sr/^{86}Sr = 0.710250$.

Radiogenic isotope ratios of seven new Quepos samples (this study) were age corrected to initial eruptive values at 65 Ma. Additionally, we calculated the radiogenic composition of the Quepos and CLIP sources at 65 Ma and 90 Ma respectively by inverting primary magma compositions of Quepos and CLIP lavas assuming a modal composition of a refertilized peridotite and a melt fraction of 10%. We then projected these values to 0 Ma (assuming a radiogenic ingrowth corresponding to the source parent/daughter ratios). This method allows for proper comparison of Quepos and CLIP lavas to the present day isotopic domains in the Galápagos archipelago. We tested the sensitivity of radiogenic source compositions to the degree of partial melting and found negligible changes 10, 20, and 30%.

We performed high-precision trace element analyses on Quepos olivines using Rutgers University's JEOL JXA-8200 Superprobe. A modified version of the Sobolev et al. (2007) protocol was used to obtain high precision trace-element data. Samples were analyzed with a focused beam (~1 mm) at 20 kV and 300 nA. Peak count times were as follows: Si : 50s; Mg : 80s; Fe : 100s; Ni : 150s; Ca : 150s and Mn : 150s. The San

Carlos olivine standard was analyzed at regular intervals during each run in order to correct for instrumental drift. All oxide totals from the olivine analyses were normalized to 100%. Olivine data are also reported from Curacao lavas (Kerr et al., 1996b for sample 92-8 and Revillon et al., 1999 for sample 94-54).

Petrological Modeling

Our goal is to use high precision olivine data to infer the lithology of the source that melted to produce the Quepos picrites; additionally, we examine olivines from the older CLIP lavas from Curacao in order to provide constraints on how the source lithology changed from ~90 to 70 Ma. A detailed description of the method that was adopted for petrological modeling was provided previously (Herzberg, 2011; Herzberg et al., 2013; 2014). The model has the following components: 1) identification of a primary magma composition, 2) calculation of a liquid line of descent after variable proportions of olivine, clinopyroxene, and plagioclase have been subtracted, 3) calculation of the compositions of olivine that crystallize from these derivative magmas, 4) comparison of model and observed olivine compositions. The modeling requires use of the olivine/melt distribution coefficients D; for Ni we have chosen the Beattie-Jones model (Jones, 1984; Beattie et al., 1991); for Ca and Mn we use the models in Herzberg and O'Hara (2004) and for Fe-Mg exchange between olivine and melt we use the model of Toplis (2005). There are other olivine/liquid distribution models for Ni, and all are parameterizations of experimental data. Of these, the Beattie-Jones model has the minimum root mean square error (RMSE) (reproducing experimentally collected data (Herzberg et al., 2013; 2014).

Matzen et al. (2013) proposed that the partitioning of Ni between olivine and melt decreases as temperature increases, and the inference is that deep melting of peridotite

will produce Ni rich melts that crystallize Ni-rich olivine near the surface. They proposed that the NiO contents of olivines greater than 0.37% in mantle peridotites are proportional to the difference in temperature between melting in the mantle and crystallization near the surface, i.e., the ΔT effect. The difficulties with this model were previously examined (Herzberg et al., 2013; 2014) and we will draw attention to several points that compromise its use for interpreting the Curacao and Quepos olivine phenocrysts. The Beattie-Jones Ni partitioning model is more accurate than the Matzen et al. (2013) in describing the experimental data (Herzberg et al., 2013; 2014). The 1 RMSE for the Beattie-Jones model is 1.1; the 1 RMSE for the Matzen model is 2.5 (Herzberg et al., 2014). Therefore, the difference in olivine NiO between average Hawaii and spinel peridotite (i.e., 0.46% and 0.37%) discussed by Matzen et al. (2013) is fully accounted for by the 1 RMSE of 2.5. Thus, the ΔT interpretation for the high NiO in Hawaiian olivines is undermined by the uncertainty. In the Beattie-Jones model the effect of T on D_{Ni} is accounted for in the MgO content of the melt, but in the Matzen et al. (2013) model, the separation of T and melt MgO as independent variables likely accounts for the larger RMSE. As discussed below, olivine compositions from Curacao crystallized from hot peridotite-source primary magmas, yet they display no elevations in Ni. Additionally, the highest olivine Ni contents worldwide are found in subduction zone lavas from the Mexican Volcanic Belt (Straub et al., 2008), yet there is no thermal anomaly below this region. Finally, we reiterate that the inference of a pyroxenite or refertilized peridotite source from elevated Ni using the Beattie-Jones model is internally consistent with Ca and Fe/Mn, but no such consistency was provided in the Matzen et al. (2013) model.

Results

The matrix of three samples from Quepos (two basalts and one picrite) were dated by $^{40}Ar/^{39}Ar$, and yielded weighted mean plateau ages of 61.4 ± 0.6, 68.6 ± 0.3, 70.6 ± 1.2 Ma. Previously published $^{40}Ar/^{39}Ar$ ages of Quepos basalts yielded ages at 60-65 Ma (Sinton et al., 1997; Hoernle et al., 2002). Our new measurements agree with the ~60 Ma pulse and extend the maximum age of Quepos volcanism to 70 Ma, indicating that the formation of this complex may have occurred over a 10 Ma interval.

New major and trace element results are plotted in Figures 2 and 3. Quepos lavas belong to both alkaline and sub-alkaline series (Fig. 2A). These lavas are mostly classified as basalts, with some examples of basaltic andesites, trachybasalts, and one basanite (Fig. 2A). Quepos picrites fall within the picro-basalt/basalt compositional fields (Fig. 2A) but textural and petrological evidence suggest that they are not liquids but cumulates produced by olivine accumulation. Nevertheless, their olivine-controlled high MgO (>10 wt%) compositions and abundance of fresh olivines make them ideal for source composition determinations and petrological studies. Quepos picrites plot below the peridotite-pyroxenite discrimination line (Fig. 2B) defined by Herzberg and Asimow (2008). In contrast, the older Curacao picrites (Kerr et al., 1996b, this study) plot on or above the line, in range with other CLIP samples consistent with a peridotite source. Primitive mantle normalized spider-diagrams from Quepos samples display broad enrichment in incompatible elements (Fig. 3). These lavas show marked positive high-field strength element enrichments (positive Ta, Nb, and Ti anomalies) as well as depletions in fluid mobile elements (K, Rb, Th, U) relative to elements with similar compatibilities. Additionally, the trace element abundances of our samples closely

resemble the incompatible element patterns of current Galápagos hotspot tracks; the Cocos, Coiba, and Carnegie ridges (Fig. 3).

High precision data on olivine interpreted as derived from a mantle peridotite source from a wide range of tectonic environments contain a range of ~ 2800-3100 ppm Ni (Herzberg et al., 2013). These contents are consistent with values from olivine in primitive MORB from the East Pacific Rise and olivines inferred to have crystallized from primary magmas of Archean komatiites (Herzberg, 2011a; Herzberg et al., 2013). CLIP olivines from the ~ 90 Ma lavas of Curacao are another example of peridotite-source olivines (Fig. 4). Olivine compositions trend towards 3000 ppm Ni and 2000 ppm Ca, consistent with magmas derived from a peridotite source. Importantly, these olivines crystallized from hot primary magmas (T_p = 1540°C; MgO = 18%; Herzberg and Gazel, 2009; Hastie and Kerr, 2010), yet there is no evidence for elevated Ni in Curacao olivines that would support the ΔT model (Matzen et al., 2013). Curacao olivines have low Ni contents (Fig. 4), unlike high Ni Hawaiian olivines (Fig. 5).

When olivine Mg numbers are greater than 90, pyroxenite or refertilzed peridotite formed by reaction of partial melts of recycled crust with peridotite are often revealed in olivine phenocrysts with high Ni, low Ca, low Mn and high Fe/Mn compared to olivines that crystallize from melts of normal MORB-like peridotite (Sobolev et al., 2005; 2007; Gurenko et al., 2009; 2010; Herzberg, 2011; Herzberg et al., 2014). Olivines from Quepos (Fig. 5) are too high in Ni and Fe/Mn and too low in Ca to have crystallized from normal mantle peridotite such as the source of MORB, Archean komatiites, and Curacao lavas (Fig. 4). They are also similar to olivines from Mauna Kea for which a pyroxenite source has been inferred (Sobolev et al., 2007; Herzberg, 2011a).

Seven new sets of Sr-Nd-Pb isotope ratios are provided in this study (Fig. 6). These ratios were first age corrected using an average age of 65 Ma and then used to project the radiogenic ingrowth of the source, as described in the methods above. These values are plotted in Figure 6 along with modern Galápagos Plume isotopic domains (Hoernle et al. 2000; Harpp and White, 2001) and previously published CLIP and Nicoya data, also projected to present day (Hauff et al., 2000a, 2000b; Hoernle et al., 2004).

Discussion

The new $^{40}Ar/^{39}Ar$ ages presented in this study, suggest that Quepos volcanism lasted for approximately 10 Ma beginning at ~70 Ma and terminating at ~60 Ma. Our new data suggest that the initial melting event, which formed this terrane occurred ~5 Ma earlier than previously described (Hoernle et al., 2002). The trace-element patterns reveal similarities with the current Galápagos hotspot tracks; the Cocos, Coiba, and Carnegie Ridges (Fig. 3). Therefore, the Quepos terrane is possibly the oldest accreted Galápagos OIB terrane found in Central America and records the transitional phase between LIP and OIB-type volcanism.

CaO-MgO bulk rock compositions can be used as a first order discrimination between peridotite and pyroxenite source-derived melts (Herzberg and Asimow, 2008). Samples from the CLIP plot in the area consistent with a dominantly peridotitic source composition (Fig. 2B), although it is also possible that some pyroxenite lithologies can also produce high CaO magmas (Herzberg, 2011). Our new samples from Quepos plot below that line and are similar to the range exhibited by Mauna Kea (Hawaii) lavas, which have been interpreted to be derived from a pyroxenite source (Sobolev et al., 2007; Herzberg, 2011a). We note that no experimental melt compositions of peridotites have

been reported that plot below the discrimination line, supporting evidence that low CaO primary magmas originated by pyroxenite melting. Modern Galápagos archipelago lavas plot above and below the discrimination line, consistent with the presence of both peridotite and pyroxenite sources in the plume (Vidito et al. 2013). Also, one lava composition from Quepos reported by Tournon (1984) plots above the line, and this was used to model the olivines for peridotite source melts (Fig. 5).

New high-precision data from Quepos olivine phenocrysts show that they have higher Ni and Fe/Mn and lower Ca contents than those expected of a normal peridotite source (Fig. 5). While Quepos and Mauna Kea olivines share many similarities (Fig. 5), there are also differences that may be interpreted as variable amounts of olivine in the source, which may be present in Quepos and variably present or even absent in Mauna Kea (Sobolev et al., 2005; Herzberg, 2011a).

The observed trends in Ni and Ca in Quepos olivines suggest that sole crystallization of olivine is not sufficient to explain the data. Quepos olivines are too low in Ca and too high in Ni to be derived from a pure pyroxenite end member (Fig. 5). The best fit occurs when olivine and clinopyroxene crystallize along a cotectic. However, this is problematic for several reasons. First, Quepos picrites lack clinopyroxene. Although magmas can crystallize olivine + clinopyroxene at high-pressures and then only olivine within shallower crustal magma chambers (e.g. Thompson et al., 1980; O'Donnell and Presnall, 1980; Elthon et al., 1995), this process would be preserved in the geochemical signature of these picrites. The lack of decreasing Sc/Al and Ca/Al with decreasing MgO does not support polybaric crystallization for Quepos samples. However, fractional crystallization coupled with magma recharge and mixing from a pyroxenite source

provides a viable explanation to the Ni and Ca trends observed in Quepos olivines (Fig. 5). The recharge model shows that Quepos olivines crystallized from mixtures between the pyroxenite-derived primary magma and a derivative liquids with Mg# of 75 to 84 (Fig. 5). It is important to note that Ni and Ca are elements sensitive to magma recharge and mixing while Fe/Mn remains insensitive to this process.

Source-projected isotope variations in $^{143}Nd/^{144}Nd$ and $^{208}Pb/^{204}Pb$ and $^{206}Pb/^{204}Pb$ reveal that the Quepos terrane is most similar to the Central Domain of the Galápagos archipelago (Fig. 6). Nicoya and Curacao basalts also show similarity to the Central Domain, although are typically less radiogenic in Pb isotopic composition and more radiogenic in Nd isotopic composition than Quepos lavas. In the modern archipelago the Central Domain is by far the most widespread and defines lavas from Fernandina and Isabella (Harpp and White, 2001). This component dominates the center of the archipelago, whereas the other components prevail in the peripheral areas (Harpp and White, 2001). The trace element chemistry, radiogenic isotope ratios, and $^{3}He/^{4}He$ ratios (Graham et al., 1993; Kurz and Geist, 1999) of Fernandina all suggest that lavas erupted in the western reaches of the archipelago represent the most undegassed, primitive part of the Galápagos plume (Harpp and White, 2001).

Previous studies suggested some possible mechanisms leading to the formation of isotopically distinct domains in the Galápagos plume source include: 1) recycling and entrainment of ancient oceanic crust into the plume (Hart, 1984), 2) recycling of subducted sediment (Dupré and Allégre, 1983), 3) delamination of subcontinental lithosphere (Hart, 1984). Based on the new data presented here, we favor the interpretation that recycled oceanic crust is responsible for the more radiogenic Pb

isotopic nature of the Quepos terrane, relative to CLIP lavas.

Our new $^{40}Ar/^{39}Ar$ ages and geochemical data provide valuable insight into a crucial phase during the life cycle of the Galápagos plume during the LIP-OIB stage transition, thereby elucidating the "head-tail plume evolution". A fundamental question that remains is: what effect does recycled oceanic crust in the form of pyroxenite contribution have on the evolutionary history of the Galápagos plume? Herzberg and Gazel (2009) proposed that CLIP lavas melted hotter and more extensively than lavas from the 0-15 Ma archipelago and Carnegie and Cocos tracks (Fig. 7A). A significant decrease in T_p (~75 °C) is also observed between ~90 Ma CLIP lavas and ~65 Ma Quepos lavas (Herzberg and Gazel, 2009). Interestingly, there is also an increasing trend in high-field strength elements (HFSE), particularly Nb/Nb* (defined as $Nb_N/\sqrt{(Th_N \times La_N)}$) from ~90 to 0 Ma (Fig. 7B). HFSE's such as Nb are sequestered in refractory mineral phases, e.g., rutile, in a subducting slab, thus the increase in Nb/Nb* between 90 and 65 Ma may reflect a significant increase in recycled oceanic crust as the pyroxenite source for Quepos lavas. Jackson et al., (2008) presented evidence for a global enriched HFSE reservoir commonly sampled by OIBs with correspondingly high $^{3}He/^{4}He$, and radiogenic $^{187}Os/^{188}Os$ that collectively suggest the existence of a mantle source with a refractory eclogite (pyroxenite) component (Jackson et al., 2008). This result advocates important implications for the development of global mantle geochemical heterogeneity. The high $^{3}He/^{4}He$ ratios of erupted lavas at some hotspots (Galápagos, Hawaii, Samoa, Iceland) are interpreted to originate from a relatively primitive, undegassed mantle reservoir (Kurz et al., 1982; Farley et al., 1992), named PHEM (Farley et al., 1992), FOZO (Hart et al., 1992), or C (Hanan and Graham, 1996).

Understanding the nature of such a primitive, undegassed mantle reservoir and the development of a nonprimitive (nonchondritic?) mantle component is therefore crucial for understanding the formation of the high HFSE – high $^{3}He/^{4}He$ domain frequently sampled by some plumes (Galápagos, Iceland, Hawaii, Samoa), balancing Earth's HFSE budget from subduction to deep recycling, and evaluating large-scale planetary differentiation processes (Jackson et al., 2008).

Evidence is accumulating that the amount of recycled crust in the Galápagos mantle plume has been increasing with time. Peridotite-source melting is consistent with the ~90 Ma CLIP lavas that have high CaO contents (Fig. 2B) and olivine data that indicate a peridotite source provenance (Fig. 4). The first evidence for participation of a dominant recycled crust component is at ~ 70 Ma as documented in this paper by lavas from the Quepos terrane. And in modern lavas, olivine chemistry reveals the widespread occurrence of pyroxenite throughout the present-day Galápagos archipelago (Vidito et al., 2013). However, determining secular changes in the absolute amount of recycled crust contained in the Galápagos plume is difficult because of its lower solidus and higher melt productivity relative to peridotite (e.g., Morgan, 2001; Pertermann and Hirschmann, 2003; Ito and Mahoney, 2005; Sobolev et al., 2007; Shorttle and Maclennan, 2011). That is, given the same lithological mixture of peridotite and pyroxenite, if the plume is cooler for any reason, pyroxenite will preferentially melt owing to its lower melting temperature, and its elevated productivity will mean that pyroxenite-source melts will be overly abundant. However, these petrological constraints provide a qualitative framework for explaining the larger geodynamical framework for cooling the plume with time (Fig. 7A).

Petrological modeling suggests that most LIPS (Paleocene and older) were hotter and melted more extensively than younger ocean islands, maybe only with the exception of Hawaii (Herzberg and Gazel, 2009). It would be difficult to imagine a scenario of LIPs-producing plumes rooted in a hotter boundary layer at the base of the mantle than younger ocean island-producing plumes. If we assume that the Galápagos is representative of global plume evolution, and that recycled crust remains negatively buoyant relative to peridotite at all depths in the mantle (Hirose, 2006; Ricolleau et al., 2010), then it is possible that mantle plumes were triggered near the core-mantle boundary by instabilities of the buoyantly-favored perovskite-bearing peridotite equivalent, and that they progressively entrained more recycled crust with time. According to Davaille et al. (2002) entrainment of dense crust would require a hotter mantle to rise, which is not consistent with the Galápagos plume. An alternative explanation is that relative to the recycled crust-free peridotite equivalent, mantle plumes that entrain a limited amount of recycled crust of limited volume are expected to have a longer transit ascent time, creating opportunities for greater conductive heat loss to their surroundings (Farnetani and Samuel, 2005; Nolet et al., 2006; Kumagai et al., 2008). The problem with this model is that increased recycled crust entry into the root of the plume can be confused with increased melt productivity of recycled crust that is expected from cooling. Detailed work on the oldest 90 Ma CLIP lavas and additional Galápagos-related terranes might break this interpretative circularity if it can constrain whether the LIP source was free of recycled crust or if it was present, but completely exhausted and diluted during partial melting.

Conclusions

The new age constraints presented here indicate that the LIP-OIB transition in the history of the Galápagos Plume occurred at about 70-60 Ma, i.e. 20-30 Ma after the onset of CLIP volcanism. Our results show that a dominant pyroxenite source lithology is observed for the first time at ~70 Ma in the record of the Quepos terrane.

The maximum T_p of the plume changed from ~1650 to ~1550 °C between 90-70 Ma. This change corresponds to a dominant pyroxenite component in the Galápagos plume evident in the Quepos data. Furthermore, there is also an increase in HFSE contents relative to equally incompatible elements throughout the evolution of the plume. The petrological requirement of elevated melt productivity of pyroxenite relative to peridotite in a cooling lithologically heterogeneous mantle is well-illustrated by the Galápagos plume. However, with no obvious reason for plume material being cooler at the time of tail versus plume head formation, we consider an increased incorporation of pyroxenite into the plume tail as the cause for the secular cooling of the plume tail relative to the head most likely. This secular cooling would be caused due to the decreased buoyancy of the plume material with a higher pyroxenite proportion resulting in a slower ascent rate through the mantle and thus, a higher cooling rate. The increased pyroxenite contribution through time would in this case reflect the effect of an increased proportion in the plume tail combined with an increased melt production rate.

Sr-Nd-Pb radiogenic isotopic compositions suggest that the source of the ~65 Ma Quepos terrane contains intermediate signatures similar to the classically defined Central Domain and are more radiogenic than CLIP lavas, suggesting an enrichment in the source of the plume, probably the result of a recycled oceanic crust component.

References

Allan, J.F., Simkin, T., 2000. Fernandina Volcano's evolved, well-mixed basalts: Mineralogical and petrological constraints on the nature of the Galápagos plume. J. Geophys. Res. 105, 6041-6071.

Alvarado, G. E., Denyer, P., Sinton, C. W., 1997. The 89 Ma Tortugal komatiitic suite, Costa Rica: Implications for a common geological origin of the Caribbean and Eastern Pacific region from a mantle plume. Geology, 25 (5), 439-442.

Arndt, N., 2000. Hot heads and cold tails. Nature, 407, 458-461.

Ballmer, M.D., Ito, G., Wolfe, C.J., Solomon, S.C., 2013. Double layering of a thermochemical plume in the upper mantle beneath Hawaii. Earth Planet. Sci. Lett. 376, 155-164.

Blackburn, T.J., Olsen, P.E., Bowring, S.A., McLean, N.M., Kent, D.V., Puffer, J., McHone, G., Rasbury, E.T., Et-Touhami, M., 2013. Zircon U-Pb geochronology links the end-Triassic extinction with the Central Atlantic Magmatic Province. Science, 340, 941-945.

Blichert-Toft, J., White., W. M., 2001. Hf isotope geochemistry of the Galápagos Islands. Geochem. Geophys. Geosyst. 2, http://dx.doi.org2000GC000138.

Burke, K., 2011. Plate Tectonics, the Wilson Cycle, and Mantle Plumes: Geodynamics from the Top. Ann. Rev. Earth Planet. Sci. 39 (1), 1-29.

Beattie, P., Ford, C., Russell, D., 1991. Partition coefficients for olivine-melt and orthopyroxene-melt systems. Cont. Mineral. Petrol. 109, 212-224.

Danyushevsky, L. V., and Plechov, P., 2011. Petrolog3: Integrated software for modeling crystallization processes. Geochem. Geophys. Geosyst. 12 (7). http//dx.doi.org/10.1029/2011GC003516.

Chauvel, C., Lewin, E., Carpentier, M., Arndt, N. T., Marini, J.-C., 2008. Role of recycled oceanic basalt and sediment in generating the Hf–Nd mantle array. Nat. Geo. 1 (1), 64-67.

Coffin, M. F., Duncan, R. A., Eldholm, O., Fitton, J. G., Frey, F. A., Larsen, H. C., Mahoney,

J. J., Saunders, A. D., Schlich, R., Wallace, P. J., 2006. Large Igneous Provinces and Scientific Ocean Drilling status quo and a look ahead. Oceanography. 19, 150-160.

Coffin, M. F., Eldholm, O., 1994, Large igneous provinces: crustal structure, dimensions, and external consequences. Rev. Geophys, 32, 1-36.

Courtillot, V.E., Renne, P.R., 2003. On the ages of flood basalt events. Comptes Rendus Geoscience. 335, 113-140.

Denyer, P., Gazel, E., 2009. The Costa Rican Jurassic to Miocene oceanic complexes: Origin, tectonics and relations. J. South Am. Earth Sci. 28 (4), 429-442.

Duncan, R., Hargraves, R., 1984. Plate tectonic evolution of the Caribbean region in the mantle reference frame. Geol. Soc. Am. Mem. 162, 81-94.

Dupré, B., and Allegre, C. J., 1983. Pb-Sr isotope variation in Indian Ocean basalts and mixing phenomena. Nature. 303, 142-146.

Duran, P., 2013. Estudio vulcano-estructural y sedimentario del mélange en el

Promontorio de Quepos, Pacífico Central, Costa Rica. University of Costa Rica. Central American School of Geology. Masters Thesis.

Elthon, D.,Ross, D.K.,Meen, J.K., 1995. Compositional Variations of Basaltic Glasses from the Mid-Cayman Rise Spreading Center. J. Geophys. Res. 100 (B7), 12497-12512.

Farley, K. A., Craig, H., 1992. Mantle Plumes and Mantle Sources. Science, 258 (5083), 821-822.

Farnetani, C. G., Samuel, H., 2005. Beyond the thermal plume paradigm: Geophys. Res. Lett. 32, 1-4.

Frisch, W., Meschede, M., Sick, M., 1992. Origin of the Central American ophiolites: Evidence from paleomagnetic results. Geol. Soc. Am. Bull. 104 (10), 1301-1314.

Gale, A., Dalton, C.A., Langmuir, C.H., Su, Y., Schilling, J.-G., 2013. The mean composition of ocean ridge basalts. Geochem. Geophys. Geosyst. 14, 489-518. http://dx. doi:10.1029/2012GC004334

Gazel, E., Abbott R. N, Draper, G. 2011., Garnet-bearing ultramafic rocks from the Dominican Republic: Fossil mantle plume fragments in an ultra high pressure ceanic complex? Lithos. 125 (1-2), 393-404.

Geist, D., White, W.M., Albarede, F., Harpp, K., Reynolds, R., Blichert-Toft, J., Kurz, M.D., 2002. Volcanic evolution in the Galápagos: The dissected shield of Volcan Ecuador. Geochem. Geophys. Geosyst. 3 (1). http://dx. doi:10.1029/2002GC000355 of 32-32 of 32.

Geldmacher, J., Hanan, B. B., Blichert-Toft, J., Harpp, K., Hoernle, K., Hauff, F.,

Werner, R., Kerr, A. C., 2003. Hafnium isotopic variations in volcanic rocks from the Caribbean Large Igneous Province and Galápagos hot spot tracks. Geochem.Geophys.Geosyst. 4 (7). http://dx.doi.org/10.1029/2002GC000477

Graham, D. W., Christie, D. M., Harpp, K. S., Lupton, J. E., 1993. Mantle Plume Helium in Submarine Basalts from the Galápagos Platform. Science. 262, 2023-2026.

Hanan, B. B., Graham, D. W., 1996. Lead and helium isotope evidence from oceanic basalts for a common deep source of mantle plumes. Science. 272 (5264), 991-995.

Harpp, K. S., White, W. M., 2001. Tracing a mantle plume: Isotopic and trace element variations of Galápagos seamounts. Geochem. Geophys. Geosyst. 2, http://dx.doi.org/2000GC000137.

Hart, S., Hauri, E., Oschmann, L., Whitehead, J., 1992. Mantle plumes and entrainment: isotopic evidence. Science. 256, (5056) 517-520.

Hart, S. R., 1984. A large-scale isotope anomaly in the Southern Hemisphere mantle. Nature. 309, 753-757.

Hastie, A.R., Kerr, A.C., 2010. Mantle plume or slab window?: physical and geochemical constraints on the origin of the Caribbean oceanic plateau. Earth Sci. Rev., 98, 283-293.

Hauff, F., Hoernle, K., Schmincke, H.U., Werner, R., 1997. A Mid Cretaceous origin for the Galápagos hotspot: volcanological, petrological, and geochemical evidence from Costa Rican oceanic crustal segments. Geol. Rund. 86, 141-155.

Hauff, F., Hoernle, K., Tilton, G., Graham, D. W., Kerr, A. C., 2000a. Large volume recycling of oceanic lithosphere over short time scales: geochemical constraints from the Caribbean Large Igneous Province. Earth Planet Sci. Lett. 174, 247-263.

Hauff, F., Hoernle, K., van den Bogaard, P., Alvarado, G., Garbe-Schönberg, D., 2000b. Age and geochemistry of basaltic complexes in western Costa Rica: Contributions to the geotectonic evolution of Central America. Geochem. Geophys. Geosyst. 1 (5). http://dx.doi.org/10.1029/1999GC000020.

Herzberg, C., 2011a. Identification of Source Lithology in the Hawaiian and Canary Islands: Implications for Origins. J. Petrol. 52, 113-146.

Herzberg, C., Asimow, P. D., 2008. Petrology of some oceanic island basalts: PRIMELT2.XLS software for primary magma calculation. Geochem. Geophys. Geosyst. 9 (9). http://dx.doi.org/10.1029/2008GC002057

Herzberg, C., Asimow, P.D., Ionov, D.A., Vidito, C., Jackson, M.G., Geist, D., 2013. Nickel and helium evidence for melt above the core-mantle boundary. Nature 493, 393-397.

Herzberg, C., Cabral, R.A., Jackson, M.D., Vidito, C., Day, J.M.D., Hauri, E., 2014. Phantom Archean crust in Mangaia hotspot lavas and the meaning of heterogeneous mantle. Earth Planet. Sci. Lett. 396, 97-106.

Herzberg, C., Gazel, E., 2009. Petrological evidence for secular cooling in mantle Plumes. Nature. 458, 619-623.

Herzberg, C., O'Hara, M.J., 2002. Plume-associated ultramafic magmas of Phanerozoic age. J. Petrol. 43, 1857-1883.

Hirose, K., 2006. Postperovskite phase transition and its geophysical implications. Rev. Geophys. 44, 2005RG000186, RG3001.

Hoernle, K., Hauff, F., van den Bogaard, P, 2004, 70 m.y. history (139–69 Ma) for the Caribbean large igneous province. Geology. 32 (8), 697-700.

Hoernle, K., Werner, R., Phipps Morgan, J., Garbe-Schönberg, C.D., Bryce, J.G., Mrazek,

J., 2000. Existence of complex spatial zonation in the Galápagos plume for at least 14 m.y. Geology. 28, 435-438.

Hoernle, K., van den Bogaard, P., Werner, R., Lissinna, B., Hauff, F., Alvarado, G., Garbe-Schönberg, D., 2002. Missing history (16–71 Ma) of the Galápagos hotspot: Implications for the tectonic and biological evolution of the Americas. Geology. 30 (9), 795-798.

Hofmann, A. W., 1997. Mantle geochemistry: the message from oceanic volcanism. Nature. 385, 219-229.

Ito, G., Mahoney, J.J., 2005. Flow and melting of a heterogeneous mantle: 1. Method and importance to the geochemistry of ocean island and mid-ocean ridge basalts. Earth. Planet. Sci. Lett., 230, 29-46.

Jackson, M.G., Dasgupta, R., 2008. Compositions of HIMU, EM1, and EM2 from global trends between radiogenic isotopes and major elements in ocean island basalts. Earth. Planet. Sci. Lett., 276, 175-186.

Jackson, M. G., Hart, S. R., Saal, A. E., Shimizu, N., Kurz, M. D., Blusztajn, J. S., Skovgaard, A. C., 2008. Globally elevated titanium, tantalum, and niobium (TITAN) in ocean island basalts with high $^{3}He/^{4}He$. Geochem. Geophys. Geosyst.

9. http://dx.doi.org/10.1029/2007GC001876.

Jackson, M.G., Weis, D., Huang, S., 2012. Major element variations in Hawaiian shield lavas: Source features and perspectives from global ocean island basalt (OIB) systematics. Geochem. Geophys. Geosyst. 13. http://dx.doi:10.1029/2012GC004268

Jicha, B. R., Brown, F. H., 2014. An age on the Korath Range and the viability of $^{40}Ar/^{39}Ar$ dating of kaersutite in Late Pleistocene volcanics, Ethiopia, Quat. Geochron. 21, 53-57.

Johnson, D. M., Hooper, P. R., Conrey, R. M., 1999. XRF Analysis of rocks and minerals for major and trace elements on a single low dilution Li-tetraborate fused bead. Advances in X-ray Anal. 41, 843-867.

Kamber, B., Collerson, K., 2000. Zr/Nb systematics of ocean island basalts reassessed—the case for binary mixing. J. Petrol. 41 (7), 1007-1021.

Kerr, A. C., 2005. Oceanic LIPs: The Kiss of Death: Elements. 1, 289-292.

Kerr, A. C., Marriner, G. F., Arndt, N., Tarney, J., Nivia, A., Saunders, A. D., Duncan, R. A., 1996a. The petrogenesis of Gorgona komatiites, picrites and basalts: new field, petrographic and geochemical constraints. Lithos. 37, 245-260.

Kerr, A. C., Tarney, J., Marriner, G. F., Klaver, G. T., Saunders, A. D., Thirlwall, M. F., 1996b. The geochemistry and petrogenesis of the late-Cretaceous picrites and basalts of Curaçao, Netherlands Antilles: a remnant of an oceanic plateau: Cont. Mineral. Petrol. 124 (1), 29-43.

Kuiper, K.F., Deino, A., Hilgen, F.J., Krijgsman, W., Renne, P.R., Wijbrans, J.R., 2008. Synochronizing Rock Clocks of Earth History. Science 320, 500-504.

Kumagai, I., Davaille, A., Kurita, K., Stutzmann, E., 2008. Mantle plumes: Thin, fat, successful, or failing? Constraints to explain hot spot volcanism through time and space. Geophys. Res. Lett. 35 (16). http://dx.doi.org/10.1029/2008GL035079

Kurz, M. D., Jenkins, W. J., Hart, S. R., 1982. Helium isotopic systematics of oceanic islands and mantle heterogeneity. Nature. 297, 43-47.

Kurz, M. D., Geist, D., 1999. Dynamics of the Galápagos hotspot from helium isotope geochemistry. Geochim. Cosmochim Acta. 63 (23/24), 4139-4156.

Kurz, M. D., Rowland, S. K., Curtice, J., Saal, A. E., Naumann, T., 2014. Eruption Rates for Fernandina Volcano, The Galápagos. In Harpp, K.S., Mittelstaedt, E., d'Ozouville, N., Graham, D.W. (Eds.), A New Chronology at the Galápagos Hotspot Center. John Wiley & Sons Inc., Chapter 4, pp. 41-54.

Li, C., Ripley, E.M, 2010. The relative effects of composition and temperature on olivine-liquid Ni partitioning: Statistical deconvolution and implications for petrologic modeling. Chem. Geol. 275, 99-104.

Loewen, M. W., Duncan, R. A., Kent, A. J. R., Krawl, K., 2013. Prolonged plume volcanism in the Caribbean Large Igneous Province: New insights from Curaçao and Haiti. Geochem. Geophys. Geosyst. 14 (10). http://dx.doi.org/10.1002/ggge.20273.

Lonsdale, P., 2005. Creation of the Cocos and Nazca plates by fission of the Farallon plate. Tectonophys. 404 (3-4), 237-264.

Mahoney, J. J., Coffin, F. F., 1997. Large Igneous Provinces: Continental, oceanic, and planetary flood volcanism, Washington. Am. Geophys. Union Mono. 100. http://dx.doi.org/10.1029/GM100.

Matzen, A.K., Baker, M.B., Beckett, J.R., Stolper, E.M., 2013. The temperature and pressure dependence of nickel partitioning between olivine and silicate melt. J. Petrol. 54, 2521-2545.

Meschede, M., Frisch, W., 1994, Geochemical characteristics of basaltic rocks from the Central American ophiolites. Profil. 7, 71-85.

Morgan W. J., 1971. Convection plumes in the lower mantle. Nature 230, 42–43.

Morgan, J. P., 2001. Thermodynamics of pressure release melting of a veined plum pudding mantle. Geochem. Geosphys. Geosys. 2, 2000GC000049.

McDonough, W., 1991. Partial melting of subducted oceanic crust and isolation of its residual eclogitic lithology. Phil. Trans. Royal Soc. London. Series A. Physical and Engineering Sciences. 335 (1638), 407-418.

Min K., Mundil R., Renne P. R., Ludwig K. R., 2000. A test for systematic errors in $^{40}Ar/^{39}Ar$ geochronology through comparison with U/Pb analysis of a 1.1Ga rhyolite. Geochem. Cosmochem. Acta. 64, 73-98.

Morgan, W. J., 1972. Deep Mantle Convection Plumes and Plate Motion. Am. Assoc. Petrol. Geol. Bull. 56 (2), 203-213.

Naumann, T.R., Geist, D.J., 2002. Petrology and Geochemistry of Cerro Azul Volcano and the Origin of the Petrologic Diversity of the Western Galápagos Shield Volcanoes: An inter-volcano comparison of Cerro Azul, Alcedo, and Sierra Negra. J. Petrol. 43, 859-883.

Nolet, G., Karato, S., Montelli, R., 2006. Plume fluxes from seismic tomography. Earth Planet. Sci. Lett. 248 (3-4), 685-699.

O'Connor, J. M., Stoffers, P., Wijbrans, J. R., Worthington, T. J., 2007. Migration of

widespread long-lived volcanism across the Galápagos Volcanic Province: Evidence for a broad hotspot melting anomaly? Earth Planet. Sci. Lett. 263 (3–4), 339-354.

O'Donnell, T. H., Presnall, D.C., 1980, Chemical Variations of the Glass and Mineral Phases in Basalts Dredged from 25-Degrees-30-Degrees-N Along the Mid-Atlantic Ridge. Am. J. Sci. 280, 845-868.

O'Hara, M.J. 1968, The bearing of phase equilibria studies in synthetic and natural systems on the origin of basic and ultrabasic rocks. Earth Sci. Rev. 4, 69-133.

Pertermann, M., Hirschmann, M.M., 2003. Anhydrous partial melting experiments on MORB-like eclogite: phase relations, phase compositions and mineral-melt partitioning of major elements at 2-3 GPa. J. Petrol. **44**, 2173-2201.

Pindell, J. L., Barrett, S. F., 1990. Geological evolution of the Caribbean region: a plate tectonic perspective: The Caribbean region. In: Dengo, G., Case, J.E., (Eds.), Boulder, Colorado, Geological Society of America, The Geology of North America, H, pp. 405-432.

Richards, M. A., Duncan, R. A., Courtillot, V. E., 1989. Flood basalts and hot-spot tracks: Plume heads and tails. Science. 246 (4926), 103-107.

Ricolleau, A., Perrillat, J.-P., Fiquet, G., Daniel, I., Matas, J., Addad, A., Menguy, N., Cardon, H., Mezouar, M., Guignot, N., 2010. Phase relations and equation of state of a natural MORB: implications for the density profile of subducted oceanic crust. J. Geophy. Res. 115, B08202, doi:10.1029/2009JB006709.

Rudnick, R. L., Barth, M., Horn, I., McDonough, W. F., 2000. Rutile-bearing refractory

eclogites: missing link between continents and depleted mantle. Science. 287 (5451), 278-281.

Rudnick, R.L., Gao, S., 2003. The Composition of the Continental Crust, In: Holland, H.D. and Turekian, K.K. (Eds.), Treatise on Geochemistry, Elsevier-Pergamon, Oxford. 3, pp. 1-64.

Saunders, A. D., 2005. Large Igneous Provinces: Origin and Environmental Consequences. Elements. 1, 259-263.

Sinton, C. W., Duncan, R. A., Denyer, P., 1997. Nicoya Peninsula, Costa Rica: A single suite of Caribbean oceanic plateau magmas. J. Geophys. Res. 102 (B7), 15507-15520.

Sinton, C. W., Duncan, R. A., Storey, M., Lewis, J., Estrada, J. J., 1998. An oceanic flood basalt province within the Caribbean plate: Earth Planet. Sci. Lett. 155, 221-235.

Shorttle, O., Maclennan,J., 2011. Compositional trends of Icelandic basalts: Implications for short-length scale lithological heterogeneity in mantle plumes. Geochem. Geophys. Geosys. 12, Q11008, doi:10.1029/2011GC003748.

Sobolev, A.V., Hofmann, A.W., Sobolev, S.V., Nikogosian I.K., 2005. An olivine-free mantle source of Hawaiian shield basalts. Nature. 434, 590-597.

Sobolev, A. V., Hofmann, A. W., Kuzmin, D. V., Yaxley, G. M., Arndt, N. T., Chung, S. L., Danyushevsky, L. V., Elliott, T., Frey, F. A., Garcia, M. O., Gurenko, A. A., Kamenetsky, V. S., Kerr, A. C., Krivolutskaya, N. A., Matvienkov, V. V., Nikogosian, I. K., Rocholl, A., Sigurdsson, I. A., Sushchevskaya, N. M., Teklay, M., 2007. The amount of recycled crust in sources of mantle-derived melts. Science. 316, 412-417.

Stolper, E., Sherman, S., Michael, G., Baker, M., Seaman, C., 2004. Glass in the submarine section of the HSDP2 drill core, Hilo, Hawaii. Geochem. Geophys. Geosyst. 5 (7). http://dx.doi.org/10.1029/2003GC000553.

Stracke, A., Hofmann, A. W., Hart, S. R., 2005. FOZO, HIMU, and the rest of the mantle zoo: Geochem. Geophys. Geosyst. 6 (5). http://dx.doi/10.1029/2004GC000824.

Straub, S.M., LaGatta, A.B., Pozzo, A.L.M.-D. Langmuir, C.H., 2008. Evidence from high Ni olivines for a hybridized peridotite/pyroxenite source for orogenic andesites from the central Mexican Volcanic Belt. Geochem. Geophys. Geosys. 9, Q03007, doi: 10.1029GC001583.

Thompson, G., Bryan, W.G., Melson, W.G., 1980. Geological and geophysical investigation of the Mid-Cayman-Rise-Spreading-Center - geochemical variation and petrogenesis of basalt glasses. J. Geol. 88 (1), 41-55.

Toplis, M. J., 2005. The thermodynamics of iron and magnesium partitioning between olivine and liquid: criteria for assessing and predicting equilibrium in natural and experimental systems. Contrib. Mineral. Petrol. 149 (1), 22-39.

Tolstikhin, I., Hofmann, A. W., 2005. Early crust on top of the Earth's core. Phys. Earth Planet. Interiors. 148 (2-4), 109-130.

Torsvik, T. H., Burke, K., Steinberger, B., Webb, S. J., Ashwal, L. D., 2010. Diamonds sampled by plumes from the core-mantle boundary. Nature. 466 (7304), 352-355.

Vidito, C., Herzberg, C., Gazel, E., Geist, D., Harpp, K., 2013. Lithological structure of the Galápagos Plume. Geochem. Geophys. Geosyst. 14 (10). http://dx. doi.org/10.1002/ggge.20270.

Walter, M. J.,1998. Melting of Garnet Peridotite and the Origin of Komatiite and

Depleted Lithosphere, J. Petrol., 39 (1), 29–60.

Wegner, W., Worner, G., Harmon, R.S., Jicha, B.R., 2010. Magmatic history and evolution of the Central American Land Bridge in Panama since Cretaceous times. Geol. Soc. Am. Bull. 123, 703-724.

Werner, R., and Hoernle, K., 2003. New volcanological and volatile data provide strong support for the continuous existence of Galápagos Islands over the past 17 million years. Int. J. Earth Sci. 92 (6), 904-911.

White, W. M., Albarede, F., Telouk, P., 2000. High-precision analysis of Pb isotope ratios by multi-collector ICP-MS. Chem. Geol. 167, 257-270.

White, W. M., McBirney, A. R., Duncan, R. A., 1993. Petrology and geochemistry of the Galápagos Islands: Portrait of a pathological mantle plume. J. Geophys. Res. 98 (B11), 19533-19563.

Zindler, A., Hart, S., 1986. Chemical Geodynamics. Ann. Rev. Earth Planet. Sci. 14, 493-571.

Figures

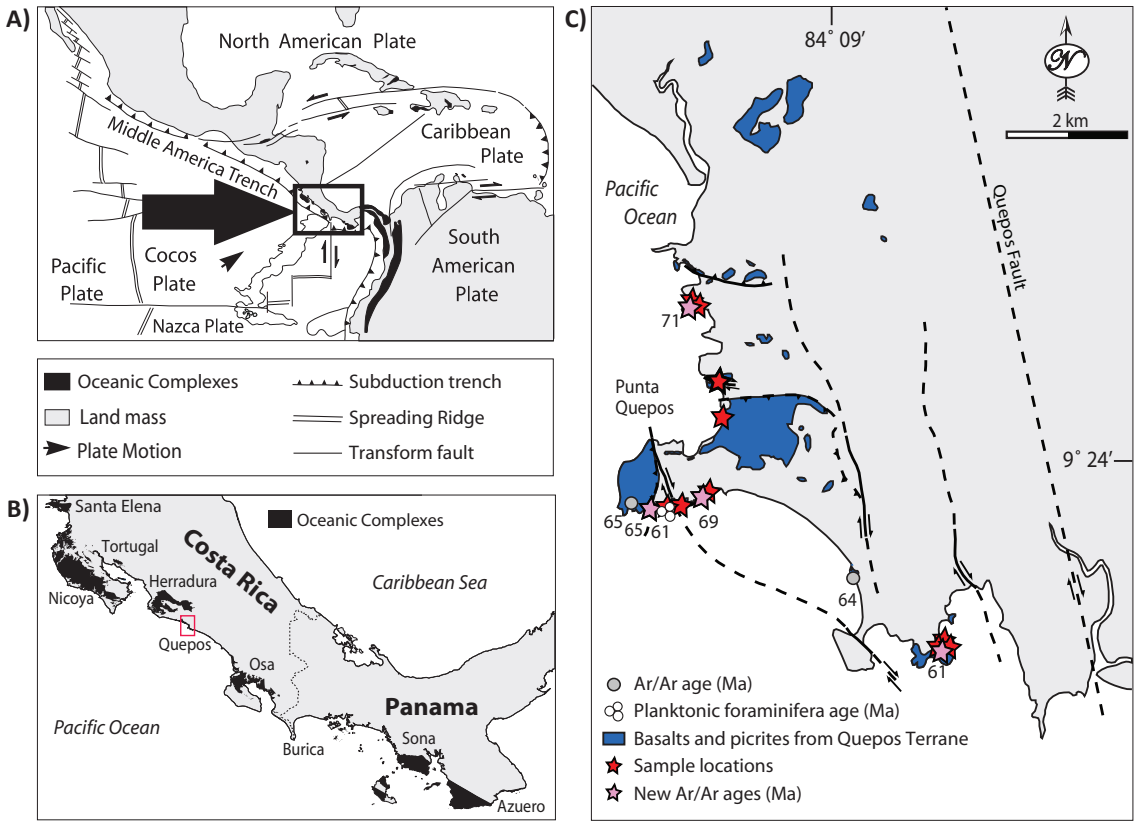

Fig. 1. A) Tectonic location of the study area (modified from Denyer and Gazel, 2009). B) Map of the accreted oceanic complexes along the coast of Costa Rica and Panama (modified from Denyer and Gazel, 2009). C) Geological map of the Quepos terrane showing sample locations, structures, and areas comprised by basalts and picrites modified from Duran (2013).

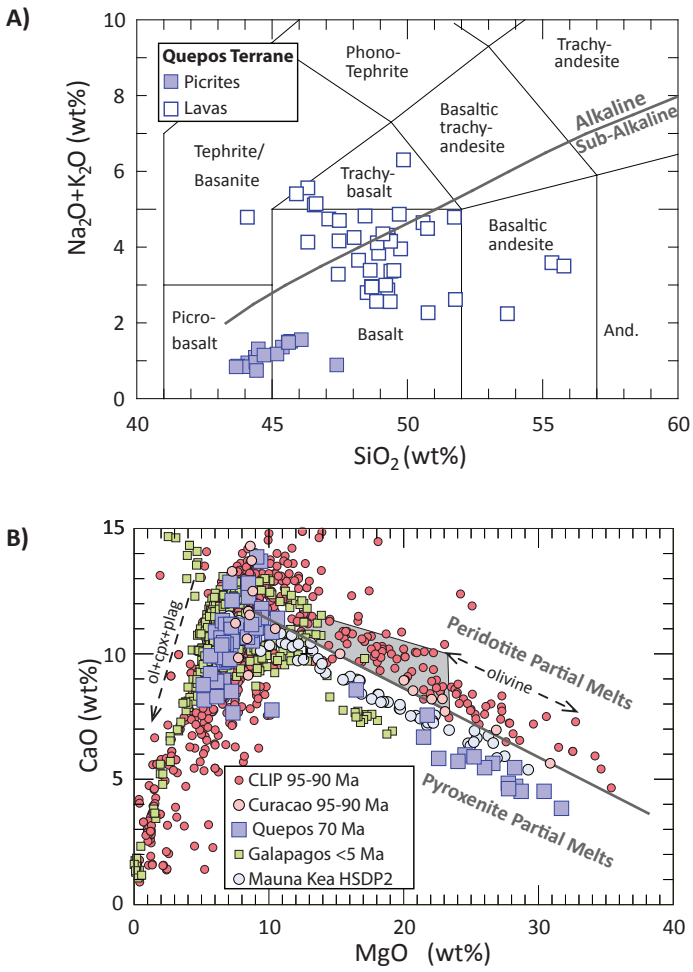

Fig. 2. A) Chemical classification of samples using the total alkali versus silica diagram (TAS). Literature data from Meschede and Frishe (1994), Sinton et al. (1997), and Hauff et al. (2000b). B) CaO-MgO discrimination diagram between peridotite and pyroxenite derived magmas from Herzberg and Asimow (2008). This model was developed for accumulated fractional melting of peridotite KR4003, and is validated by the fact that no experimental melt compositions from a pure peridotite source plot below the discrimination line. The grey shaded region represents primary magmas of fertile peridotite produced by accumulated fractional melting. Additional data from Stolper et al. (2004) for Mauna Kea and from White et al., 1993; Hauff et al., 1997; Allan and Simkin, 2000; Hauff et al., 2000a,b; Hoernle et al., 2000; Blichert-Toft and White, 2001; Geist et

al., 2002; Naumann et al., 2002; Werner et al., 2003; O'Connor et al., 2007; Wegner et al., 2010 for Galápagos related lavas including accreted terranes in Central America and parts of the CLIP including Nicoya and Curacao.

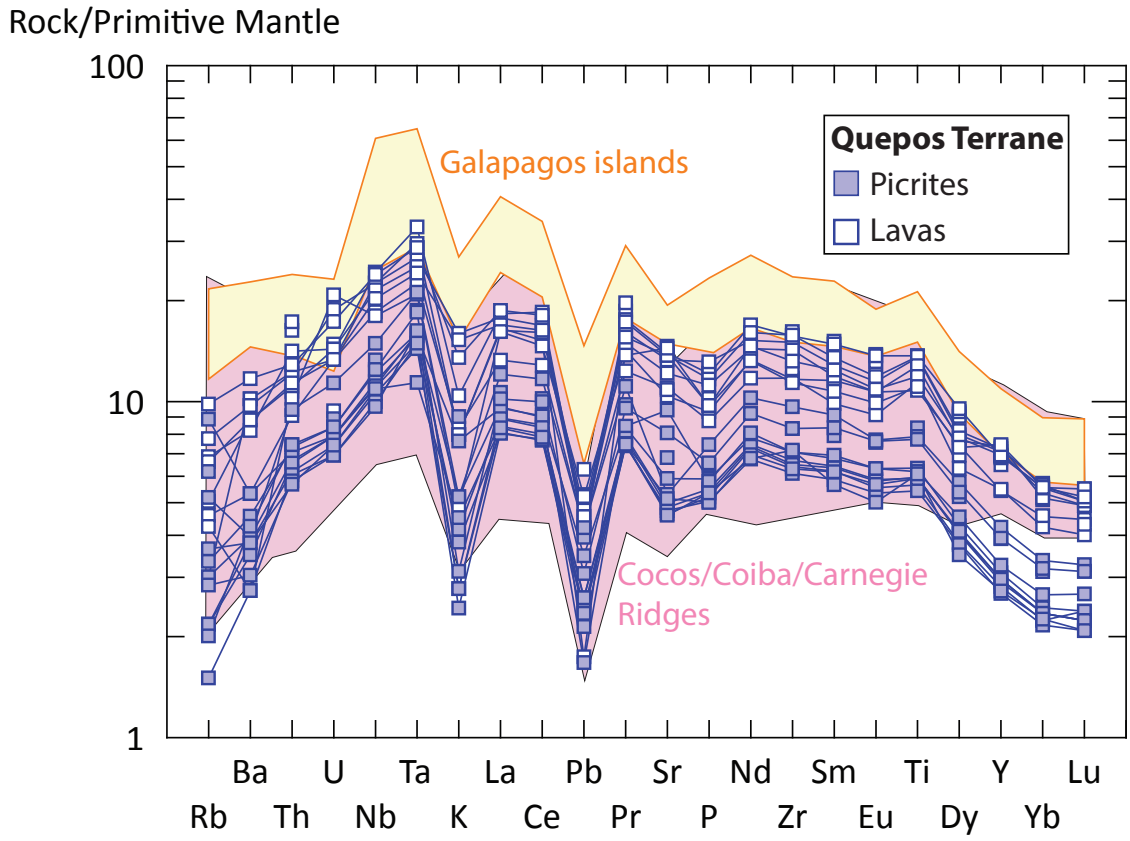

Fig. 3. Multi-element spider diagram normalized to primitive mantle (McDonough and Sun, 1995). Note how the new data from Quepos overlap with the current Galápagos tracks; the Cocos, Carnegie, and Coiba Ridges. Additional data from White et al., 1993; Hauff et al., 1997; Allan and Simkin, 2000; Hauff et al., 2000; Hoernle et al., 2000; Blichert-Toft and White, 2001; Geist et al., 2002; Naumann et al., 2002; Werner et al., 2003; O'Connor et al., 2007; Wegner et al., 2010 for Galápagos Domains.

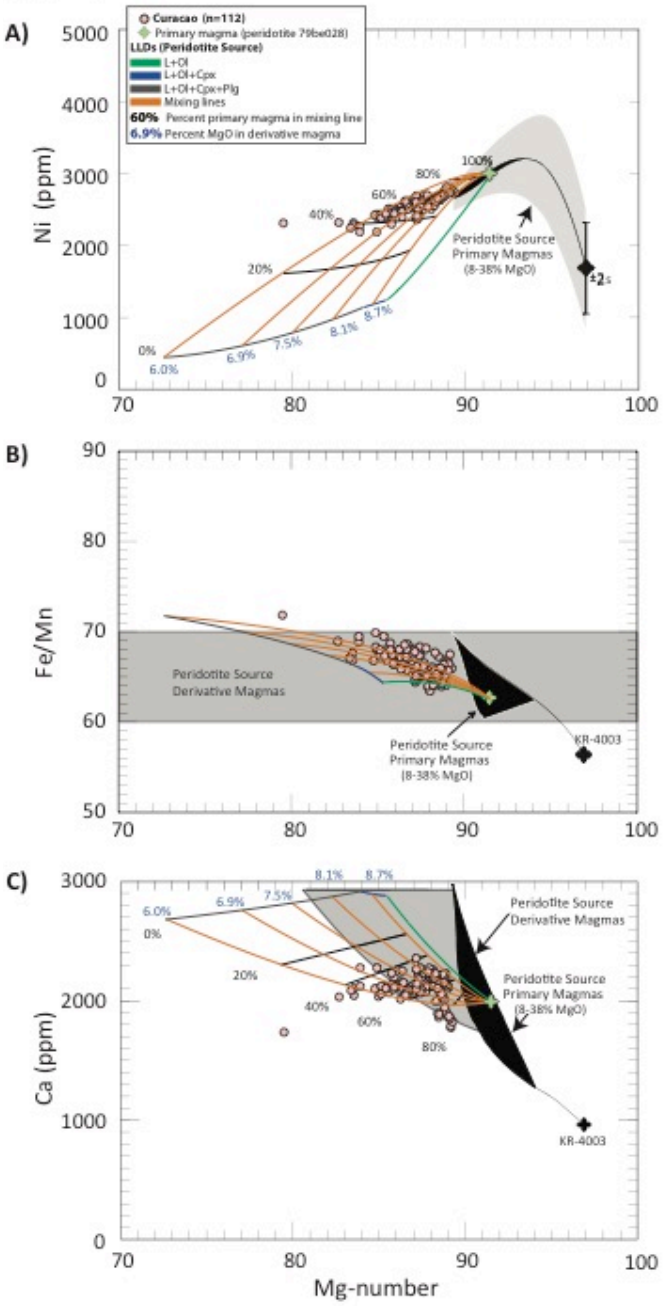

Fig. 4. Mg-numbers versus Ni and Ca contents and Fe/Mn for calculated olivines and high-precision olivines from ~ 90 Ma Curacao picrites. A Mg-number is defined as 100MgO/(MgO + FeO) in mole per cent. Black forms = calculated Ni and Ca in olivines that crystallize from all primary melts derived from a fertile peridotite source having 1960 ppm Ni, 3.45 wt% CaO and 0.13 wt% MnO (Herzberg, 2011a); the grey field in

panel A represents ±1σ uncertainty for Ni (Herzberg et al., 2013). The Curacao primary magma composition was computed from lava sample CR372T92 reported by Klaver (1987). The full range of model olivine Ca for peridotite-source melts far exceeds the 1700-2000 ppm range that is typically observed for MORB, komatiite, and other olivines of a peridotite source provenance; similarly the upper Fe/Mn model bound of 70 exceeds Fe/Mn of observed olivines of a peridotite source provenance. Curacao olivine compositions define trends towards peridotite-source olivines (see text).

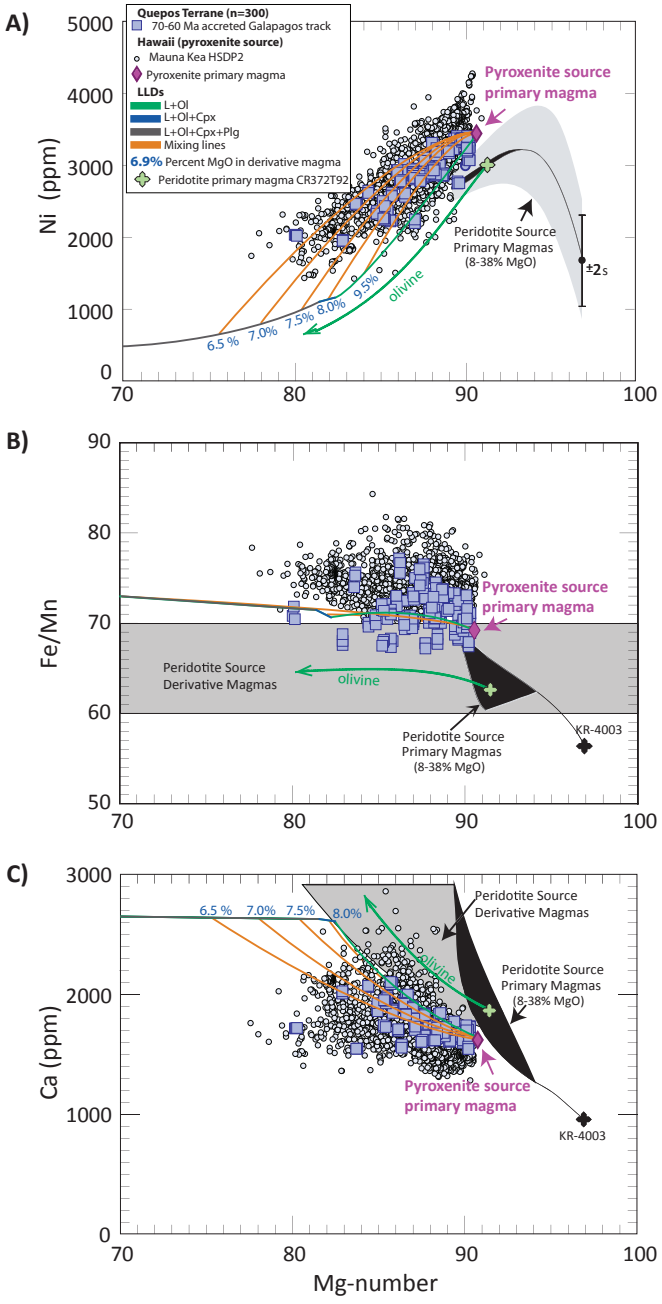

Fig. 5. Mg-numbers versus Ni and Ca contents and Fe/Mn for calculated olivines and high-precision olivines from picrites of the ~ 70 Ma Quepos terrane. Examples of olivines from a peridotite source primary magma and its derivatives are given by the green cross and arrow, computed from lava sample CR372T92 reported by Tournon (1984). Quepos olivine compositions are not consistent with derivation from a normal

peridotite source. Notice how the new Quepos data is within range of Mauna Kea data from Sobolev et al. (2007) interpreted as olivines that crystallized from a pyroxenite-derived primary magma. The trends can be explained by complex olivine+clinopyroxene fractional crystallization or magma recharge. Independent of the explanation, these crystallization trends do not extrapolate to peridotite source primary magmas.

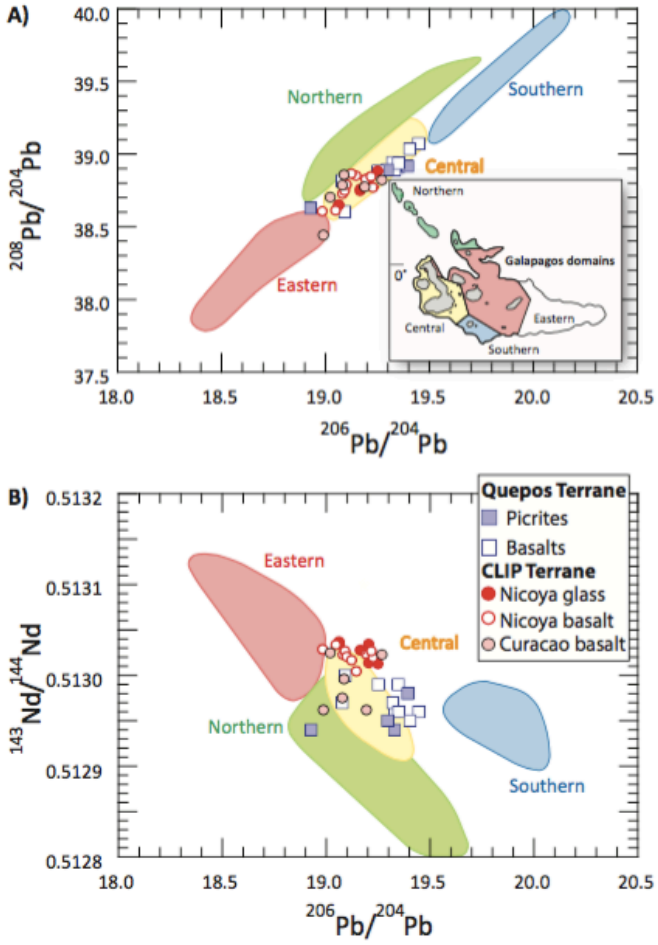

Fig. 6. Source projected Pb and Nd isotopes of picrite and basalt samples from the CLIP and Quepos terrane. Most Quepos samples fall within the Central Galápagos Domain. Shaded Galápagos Domains for the present day archipelago from Hoernle et al. (2000).

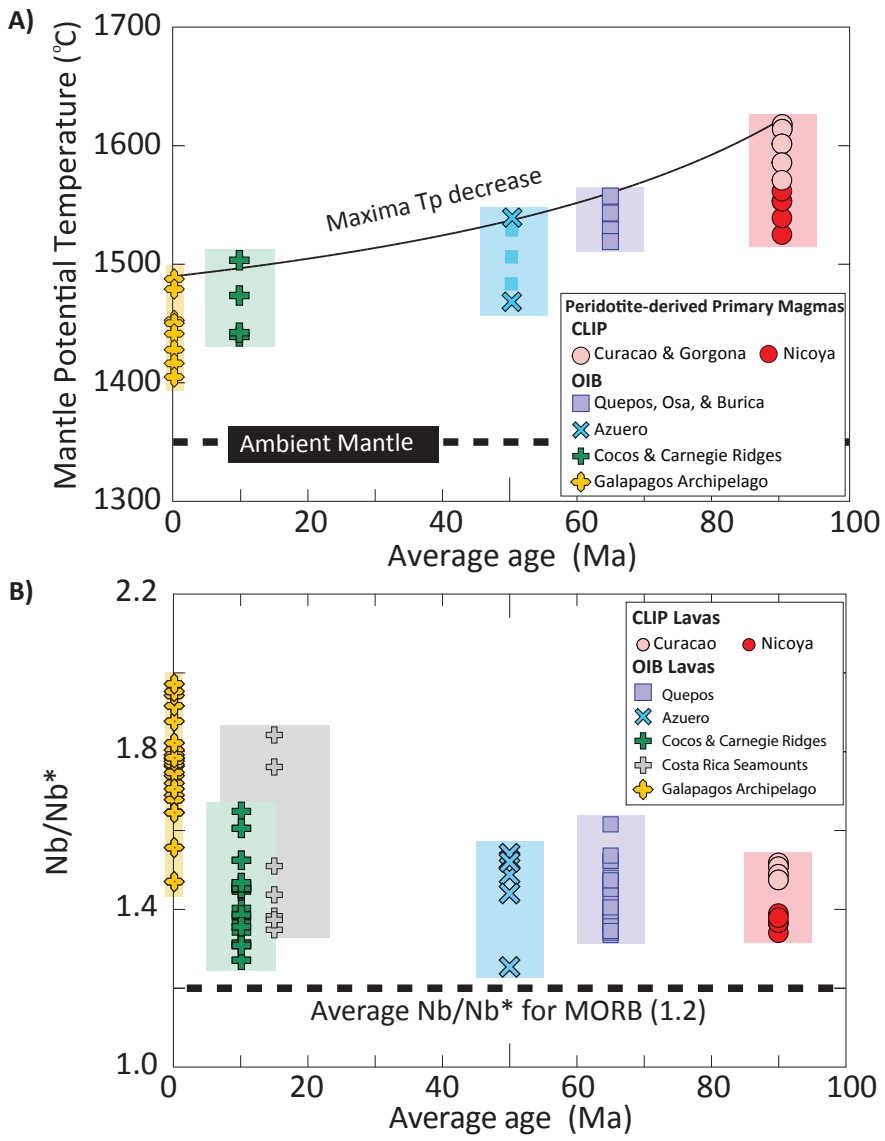

Fig. 7. A) Galápagos plume secular cooling curve modified from Herzberg and Gazel, (2009) using a least squares approximation. Note the drastic decrease in T_p from the time of LIP emplacement to approximately 70-60 Ma. The actual T_p range exhibited for each occurrence like the CLIP at a specific time is typically seen in almost all OIB and LIP occurrences, as reported in Herzberg & Asimow (2008) and Herzberg & Gazel (2009); these authors have attributed the T_p range as a record of plume thermal heterogeneity, higher T_p in the core and lower T_p at the periphery. B) Evolution of the Nb/Nb* vs. time

(Ma) from Galápagos related basalts. Nb/Nb* is defined as $Nb_N/\sqrt{(Th_N \times La_N)}$ where N means normalized to a primitive mantle composition from McDonough and Sun, 1995. Average Nb/Nb* for MORB is calculated from the average MORB composition from Gale et al., 2013. Color bars behind symbols represent the age range of Galápagos units. Notice as the plume cools down the Nb/Nb* ratio increased to a max at 0 Ma (Data from White et al., 1993; Hauff et al., 1997; Allan and Simkin, 2000; Hauff et al., 2000; Hoernle et al., 2000; Blichert-Toft and White, 2001; Geist et al., 2002; Naumann et al., 2002; Werner et al., 2003; O'Connor et al., 2007; Wegner et al., 2010).

Chapter 2: The Hottest Lavas of the Phanerozoic and the Survival of Deep Archean Reservoirs

Abstract

The mantle plume (Wilson, 1963) hypothesis is widely accepted for the formation of large igneous provinces (LIP) and many ocean island basalts (OIB). Petrologic models used to support the mantle plume model suggest that plume-derived melts originated at high mantle temperatures (>1500 °C) relative to those generated at ambient mid ocean ridge conditions (~1350 °C) (Herzberg and Gazel, 2009a). Earth's mantle has also appreciably cooled during its history and the temperatures of modern day basalts are substantially lower than those produced during the Archean (>2.5 Ga), as recorded by komatiites (>1700 °C, e.g. (Herzberg et al., 2010)). Nevertheless, here we show that 89 Ma lavas from the Galapagos Plume-related(Alvarado et al., 1997) Tortugal Suite record mantle temperatures as high as Archean komatiites and ~400°C hotter than the modern ambient mantle (Herzberg et al., 2010). These results are also supported by highly magnesian olivine phenocrysts (Mg# = 94.2) and Al-in-olivine (Coogan et al., 2014) crystallization temperatures of 1570 ± 20 °C. Since mantle plumes are chemically and thermally heterogeneous, we interpret these rocks as the result of melting the hot core of the plume head that produced the Caribbean Large Igneous Province. The Tortugal Suite represents the hottest Phanerozoic lavas of the secularly cooling Galapagos Plume (Herzberg and Gazel, 2009a). We suggest that a reservoir as hot as the one that produced Archean komatiites survived Eons of convection in the deep Earth is still tapped by mantle plumes.

Introduction

Geochemical evidence from hotspot-related lavas offer crucial information about deep planetary recycling processes (Hofmann and White, 1982) and petrological studies indicate that these melts are hotter than ambient mid-ocean ridge basalts (Herzberg and Gazel, 2009a), supporting a hot mantle plume origin. Recent tomographic (French and Romanowicz, 2015) studies advocate that mantle plumes that melt to form large igneous provinces (LIPs) and some ocean island basalts (OIBs) are closely associated with large low shear velocity provinces (LLSVPs), linking hotspots with the deep mantle and providing evidence to the geochemical and lithological heterogeneity of the lower mantle. Mantle plumes originating from the core-mantle boundary can preserve primitive geochemical compositions related to the early stages of planetary accretion that survived eons of crustal recycling, mantle degassing, and mixing of heterogeneous reservoirs (Rizo et al., 2016), thus providing the only "windows" into the deep Earth's composition and evolution.

Primary melts from plume-related lavas provide key information about melting conditions of their mantle sources. Particularly useful are the MgO and FeO contents of a peridotite-derived primary melt (a melt that has not crystallized any mineral phases), which can be used to estimate the thermobarometric conditions during melting (Herzberg and Asimow, 2015; Putirka, 2016). The MgO content of a primary peridotite-derived melt positively correlates to initial melting temperature (Herzberg and Asimow, 2015). For example, primary mid-ocean ridge basalts contain ~10-13.5 wt% MgO (Putirka, 2016; Putirka et al., 2007) while LIPs are derived from primary melts with higher MgO (~12-20 wt%) contents (Herzberg and Asimow, 2015). Melting at extreme P-T (hot,

deep) conditions is thought to have occurred frequently during the Archean (>2.5 Ga) when most ultramafic peridotite-derived lavas (known as komatiites) were produced. Petrological modeling yields high initial melting temperatures (>1700°C, ~400°C hotter than modern day upper ambient mantle temperatures) for samples from the classic komatiite localities (locations in Fig. 1A). Although komatiites have been studied for decades, the melting processes responsible for their formation remain contested. The most widely accepted petrological model suggests that komatiites form via adiabatic decompression melting of relatively anhydrous, anomalously hot mantle plumes. The Gorgona Island case links komatiites with Large Igneous Provinces(Arndt, 1999; Berry et al., 2008; Herzberg, 1992; Walter, 1998) (LIPs). Alternative hypotheses for the genesis of komatiites include fluxed hydrous melting in Archean subduction zones e.g., (Grove and Parman, 2004; Parman et al., 2004), although these melts do not typically have trace element signatures indicative of a subduction origin. Nevertheless, independent of their origin, they represent remnants of a younger Earth, when the temperatures of the ambient mantle and deep Earth reservoirs were substantially hotter (Herzberg et al., 2010).

The 90 Ma lava flows on Gorgona Island remain the only true example of Phanerozoic (<500 Ma) macroscopically spinifex-textured komatiites. Gorgona komatiites are interpreted to be related to the initial melting stages of the Galapagos mantle plume head at ~90 Ma that formed the Caribbean Large Igneous Province (CLIP) (Arndt et al., 1997; Echeverria, 1982; Kerr et al., 1996). Other occurrences of high MgO (~27 wt.%) microspinifex-textured lavas petrogenetically related to the initial melting of the Galapagos Plume also exist in other locations; e.g., the Curacao Lava Formation on the island of Curacao and the Tortugal Suite in Costa Rica (Alvarado et al., 1997) (Fig.

1A). Tortugal olivines are unique relative to other hotspot related terranes with respect to their high Mg# (molar Mg/(Mg+Fe)*100) that reach values up to 94.2 and systematically overlap those of Archean komatiites (Fig. 1B). These olivines are phenocrysts as evidenced by their high Ca, Cr, Al, and Ti contents (relative to residual/lithospheric olivine), abundance of melt inclusions even in the most forsteritic olivine, and normal magmatic zoning from core to rim. Petrologic modeling indicates that these phenocrysts crystallized from a hot, primary peridotite melt and their Ni contents are consistent with crystallization from a melt with ~27 wt.% MgO (Fig 2A), indicative of high initial melting pressure and temperature (Herzberg and O'Hara, 2002; Matzen et al., 2011).

Estimating temperatures using olivine compositions as a thermometer

Although the Mg# of an olivine crystal is related to the temperature at which it crystallized, diffusion and re-equilibration of Fe and Mg (in slowly cooled rocks) within the crystal lattice will alter the original crystallization temperature and skew results (Coogan et al., 2014). Therefore, a more robust way to estimate crystallization temperatures is via olivine-spinel thermometry and analysis of the Al and Cr contents in each respective mineral phase (Coogan et al., 2014),(Wan et al., 2008). We used this method to estimate minimum crystallization temperatures for Tortugal and Curacao olivines in order to compare our results to other high-MgO terranes and LIPs (Figs. 2A-C). This thermometer is advantageous for two main reasons: 1) the slow diffusion of Al and Cr preserves initial olivine-spinel crystallization temperatures and 2) the independence of this thermometer from source lithology composition. It is important to note that although Tortugal spinels have chromium contents higher than the calibrated range for the Al-in-olivine thermometer, there is a strong correlation (using the available

global data) between K_d ($Al_2O_3^{olivine}/Al_2O_3^{spinel}$) and spinel chromium number (molar proportion of Cr/Cr+Al). Because the partition coefficient (K_d) increases proportionally (and with a statistical significance) with increasing spinel Cr-number, then we can conclude that olivines in equilibrium with the most Cr-rich spinels also provide meaningful temperature results(Heinonen et al., 2015). The application of this thermometer to olivine-spinel pairs of komatiites and low calcium boninites also outside the calibrated range yield temperatures within the errors of calculated olivine-melt temperatures (Sobolev et al., 2016). Finally, a new experimental calibration of the Al-in-olivine-spinel thermometer up to 1550 °C and Cr# of spinel up to 0.95 (Sobolev et al., 2015) yields temperature estimates similar to (Coogan et al., 2014) within a ±20 °C uncertainty for Tortugal olivines. Tortugal high-Mg olivines contain abundant micro-inclusions (from 20 μm down to few microns) of spinel, melt, and combined spinel and crystalized melt inclusions. This suggests that small spinel grains already coexisted with melt during crystallization of high-Mg olivines and further justifies the application of the Al-in-olivine geothermometer.

Tortugal olivine phenocrysts indicate the highest Mg# and highest olivine-spinel equilibration temperatures relative to modern Phanerozoic high-MgO intraplate occurrences (Fig. 2B and C). We estimated minimum crystallization temperatures of 1570 ±20°C for the most primitive Tortugal olivine phenocrysts as an average (± 2σ) for the hottest group of points in the high temperature/low-Ti data group. Although spinel typically crystallizes at lower temperatures than olivine, our petrologic modeling suggests that the spinel liquidus shifts to higher temperatures with increasing pressure. Even though our models suggest cotectic olivine-spinel crystallization at lithospheric pressure

(about 0.6 GPa), this pressure effect is insignificant in modifying the estimated Al-in-olivine temperatures (Wan et al., 2008). The temperature range (up to ~150 °C) for the same olivine Mg# (~93) could be due to partial re-equilibration of olivine-spinel on cooling. For comparison with the new Tortugal data, the most primitive Gorgona and Curacao olivine from the CLIP (Mg# 88-92) record minimum crystallization temperatures between 1200-1450 °C and 1200-1350 °C, respectively. Other mantle plume and hotspot related terranes (e.g., Karoo, Emeishan, and Iceland) also record anomalously high crystallization temperatures relative to MORB olivine, yet no locality records temperatures as high as the Tortugal Suite.

For comparison, the Abitibi komatiites record a maximum Al-in-olivine crystallization temperature of only 1450°C, possibly due to late spinel crystallization (Sobolev et al., 2016) (Fig. 2B). Fractional crystallization of olivine from a melt will result in progressively lower olivine-spinel equilibration temperatures; however, even in a narrow window of olivine Mg# (e.g., 91-93) we observe a large temperature variation ranging from 1100 °C in MORB to 1600 °C in our Tortugal samples. Thus, based on both the high Mg# and high olivine-spinel crystallization temperatures, we suggest that Tortugal melts derived via melting of a hot mantle plume. We suggest that melting of the core of Galapagos Plume during the LIP event as the most viable geodynamic interpretation for the origin of the Tortugal ultramafic melts.

Primary melt compositions

To model the meting conditions that generated Tortugal melts, we computed primary melt compositions by adding or subtracting olivine from whole rock compositions until reaching equilibrium with a mantle with an Mg# equal to 94.2

(maximum Mg# observed in the olivine from Tortugal). We assumed a dry and reduced source (based on volatiles in the melt inclusions and on the stoichiometry of spinel compositions (Danyushevsky and Sobolev, 1996; Maurel and Maurel, 1984), respectively) and estimated the Fe^{2+}/Fe^{total} of the melt in equilibrium with spinel to be ~0.95. Sulfur concentrations measured on melt inclusions are also low (max 995 ppm S at the max measured H_2O content, see below in the volatiles discussion) which suggests a relatively reduced primary melt. The V/Sc ratio of Tortugal picrites (5.42 ± 0.57 1σ) are on the lower range relative to modern mid-ocean ridge basalts (6.74 ±1.11, 1σ) and Archean basalts (6.34 ± 0.62, 1σ) also supporting a reduced mantle source for these melts (Li and Lee, 2004).

Our models yielded primary magma solutions with ~10.5 wt.% FeO and ~27 wt.% MgO (Fig 3A), which suggests that these primary melts originated at depths around >10 GPa and record mantle potential temperatures between 1700 and 1800 °C (Fig 3B). These P-T estimates for Tortugal melts are well within the range for Archean komatiites and indicate melting pressures and temperatures that surpass those for the other ultramafic Galapagos LIP terranes (e.g., Curacao and Gorgona, Fig. 3B). One important influence of P-T melting conditions is the amount of volatiles present at the mantle source. To estimate the pre-eruptive volatile content of melts from Tortugal, we analyzed olivine-hosted melt inclusions (MI) in olivines with Mg#s up to 93. The maximum H_2O content from the suite of MI analyzed is 0.24 wt%. Because olivine-hosted MI have the potential to lose water by diffusion of H^+ through the host crystal, this represents a minimum estimate for the water content of the primary melt. Furthermore, we can also use the H_2O/Ce(Dixon et al., 2002) and CO_2/Nb (Michael and Graham, 2015) ratios of

Pacific intraplate lavas (200 and 1029 ppm, respectively) with the Ce and Nb values from the hottest Tortugal sample (TO-080514-1) as another proxy for volatile concentrations. Using this approach, we find that Tortugal melts could be consistent with a maximum of 0.4 wt.% H_2O and 1.6 wt.% CO_2. Addition of these volatiles would result in a ~50 °C decrease (Herzberg, 2016) in the T_p calculation, lowering the T_p maxima from ~1800 to 1750 °C (within the actual T_p uncertainty of ±50 °C(Herzberg and Asimow, 2015)). Therefore, our mantle potential temperatures, along with the high Al-in-olivine crystallization temperatures, support extremely hot, reduced, and relatively dry conditions for the generation of these lavas.

The preservation of deep primitive mantle reservoirs

When compared globally, there is internal consistency between estimated Al-in-olivine temperatures and petrologically modeled mantle potential temperatures for Phanerozoic primitive melts (Fig. 4A). We suggest that the anomalously hot Tortugal melts most likely originated via melting of the hot Galapagos Plume axis while Curacao, Gorgona and, other CLIP lavas probably originated in the adjacent areas of the plume at lower pressures due to plume capture by a mid-ocean ridge (Madrigal et al., 2016) (Fig 4B). Therefore, it is likely that the source of Tortugal melts was significantly hotter, and due to this, the range of depths at which melting occurred was deeper relative to other high-MgO Phanerozoic localities (Fig. 4A and B).

High-degrees of partial melting are expected at such extreme P-T conditions, producing melts depleted in trace element concentrations and resembling the composition of the mantle source. Interestingly, Tortugal melts display enriched trace element concentrations as well as radiogenic isotopic ratios. These melts also display a negative

correlation between $^{143}Nd/^{144}Nd$ and TiO_2 and a positive correlation between $^{143}Nd/^{144}Nd$ and Gd/Yb that suggest mixing between two compositionally distinct melts. We used the correlations between TiO_2 concentrations and other rare earth elements to model the trace element concentrations of Tortugal primary melts as a function of TiO_2. This modeling essentially provides possible solutions to the trace element concentrations of end member melt compositions that mixed to produce the resultant Tortugal Suite. These relationships, paired with the trace element chemistry of Tortugal olivines, provide crucial information regarding mantle source compositions and the magmatic plumbing system of Tortugal. We propose that Tortugal olivines crystallized from two compositionally distinct parental melts: one low-Ti/high-temperature melt, from which most of the magnesium-rich olivines (Mg#>92) crystallized and a second high-Ti melt enriched in light rare earth elements (LREE) with a moderate temperature. It is possible that the former melt derived from high degrees of melting in the hottest part of the Galapagos plume and the latter by low degrees of melting in the less hot part of the plume. Most of the olivines crystallized from the low-Ti depleted melts (with TiO_2<0.5 wt%) at high temperatures and were subsequently mixed and transported along with the high-Ti/LREE-enriched melt. A fertile recycled oceanic crustal component(Hofmann and White, 1982) could be a plausible explanation for the enriched trace element characteristics of Tortugal melts; however, the minor and trace element signatures in Tortugal olivine phenocrysts, as well as the whole rock major element compositions, indicate crystallization from a dominant peridotite source (Fig. 2A). Melted recycled crust embedded within partially melted peridotite may explain the trace element and radiogenic isotope mixing lines. Thus, we suggest that this enriched component could to

be a separate entity within the peridotite matrix. The exact composition and lithology of the enriched component remains unclear and can be further clarified by future geochemical investigations, e.g., helium and osmium radiogenic isotopes, and stable magnesium isotope systematics. What is evident is that Galapagos-related lavas record heterogeneous melt productivity in a secularly cooling plume (Trela et al., 2015) and may result from deep planetary crustal recycling processes and plume entrainment during ascent.

The Tortugal Suite represents an exceptional ultramafic Phanerozoic location. The extreme P-T melting conditions, high olivine crystallization temperatures, and enriched trace element and radiogenic isotope systematics stand as a tribute to the immense compositional and thermal variability of the deep earth (e.g., the LLSVPs) as sampled by mantle plumes. These regions may represent laterally heterogeneous primordial thermochemical piles mixed with recycled oceanic lithosphere (Garnero et al., 2016; Hirose et al., 1999) that do not actively mix into the overlying lower mantle (Garnero et al., 2016; Hofmann and Hart, 1978). Geochemical investigations of Phanerozoic basalts from Baffin Island and the Ontong Java Plateau also show elevated $^{182}W/^{184}W$ ratios ($\mu^{182}W$ up to 50 ppm), implying that mantle plumes in the recent geologic past tapped ancient primordial reservoirs that escaped eons of convective mantle mixing(Jackson et al., 2017; Rizo et al., 2016). Considering that Tortugal melts preserve an Archean mantle temperature and show strong evidence for a recycled crustal lithology, this suite may offer a unique opportunity to study the reservoirs sampled by mantle plumes to answer key questions regarding the interconnectivity between deep mantle convection, the nature

of LLVPs, hotspot track geochemical zonation, and the thermochemical evolution of the early mantle.

A recent numerical study (Andrault et al., 2016) suggested a 4.3 Ga steady-state thermal scenario for the lowermost mantle. If plumes do in fact sample primordial LLSVP material that has not appreciably cooled over 4.3 Ga, then it stands to reason that even modern plumes can produce basaltic melts at similar P-T conditions as inferred during the Archean if this reservoir can reach the surface without sufficiently interacting with cooler ambient upper mantle. Initially hot Phanerozoic plumes captured in spreading ridges during ascent may also mix with cooler upper ambient MORB mantle that would result in a significant decrease in the plumes temperature (Madrigal et al., 2016). The results from Tortugal (and other anomalously hot Phanerozoic locations) imply that if the mantle is still producing melts as hot as during Archean time, then there must exist isolated reservoirs in the deep Earth that preserve Archean temperatures. These hot, Archean-like temperatures preserved at the base of the lower mantle maybe sustained over time by the steady-state temperature conditions at the core mantle boundary. As the core cools and loses heat to the mantle, the temperature at the core-mantle boundary will be near constant as it is buffered by a near two-phase solid-liquid system.

Methods

At the University of Wisconsin-Madison Rare Gas Geochronology Laboratory, $^{40}Ar/^{39}Ar$ incremental heating experiments were conducted on groundmass and mineral separates following the procedures of (Jicha and Brown, 2014). Isotope data were reduced using ArArCalc software version 2.5 (http://earthref.org/ArArCALC/). We report ages with 2σ uncertainties (includes the J uncertainty) and are calculated relative to

a Fish Canyon standard age of 28.201 ± 0.046 Ma(Kuiper et al., 2008) and a value for $\lambda^{40}K$ of 5.463 ± 0.107 x 10^{-10} yr^{-1} (Min et al., 2000). We do not prefer the values for the 40K decay constants or the standard age calibration proposed in (Renne et al., 2011). In fact, numerous Ar/Ar laboratories also do not recognize the (Renne et al., 2011) values for reasons that are well beyond the scope of this paper. Thus, the ages used in this manuscript do not need to be recalculated (Jicha et al., 2016).

Alteration-free rock chips were selected under stereoscopic microscope and powdered in an alumina mill at the Department of Geosciences at Virginia Tech. From these powders, whole rock major and trace element compositions were collected at Virginia Tech by XRF and ICP-MS (Johnson et al., 1999). Curacao picrite samples were processed and analyzed in the geochemistry laboratory at the Department of Geosciences at Virginia Tech following the procedures reported in (Mazza et al., 2014). X-ray fluorescence (XRF) was used to determine major element concentrations. The Relative Standard Deviation for 10 replicates of BHVO-2g was <2.70% for all major elements and accuracy better than 1.74%, with the exception of P_2O_5. Trace elements as well as P_2O_5 were collected from the same fluxed glasses with an Agilent 7500ce ICPMS coupled with a Geolas laser ablation system, following the protocols reported in (Mazza et al., 2014). The data were calibrated against USGS standards BCR-2, BHVO-2, G-2, and BIR-1a, using Ti from XRF as an internal standard and the standard element values reported in (Kelley et al., 2003). The accuracy for 4 replicates of BHVO-2g was better than 5 % for all elements except for Ba, Hf, and Ge (7-9 %). The accuracy for 4 replicates of BIR-1a was better than 5 % for most elements except for Ga, Ge, Ce, Pr, Eu, Tb, Dy, Ho, Tm, Er, Yb, and Lu (5-9 %).

Isotope analyses were performed at the Center for Elemental Mass Spectrometry, University of South Carolina. Sample powders from the same aliquots used for major and trace elements were digested in sub-boiling Teflon-distilled 3:1 HF:HNO_3 (v/v) mixture, and the isotopes were analyzed on aliquots of a single digestion. Pb was separated on an anion resin in HBr, HNO_3 acids. Sr and REE were separated from the bulk rock washes of the Pb chemistry on a cation resin in HCl. Sr was further purified on a Sr-spec resin and Nd on an Ln-resin (both from EICHROM, USA). The radiogenic isotope ratios were determined on a Thermo Neptune multi collector ICPMS with the PLUS upgrade. Sample introduction was with an APEX enhanced sensitivity spray chamber and high sensitivity cones (JET and X-skimmer configuration) resulting in Nd sensitivities in the order of 1400-1500 V / ppm. The NIST SRM-987 Sr standard was determined at $^{87}Sr/^{86}Sr$ = 0.710320 ± 0.000012 (n=12) using $^{86}Sr/^{87}Sr$ = 0.1194 for instrumental fractionation correction. All Sr-isotope ratios are reported relative to the $^{87}Sr/^{86}Sr$ = 0.710250 for the NIST standard to correct for instrument bias. The LaJolla Nd standard was determined at $^{143}Nd/^{144}Nd$ of 0.511858 ± 0.000007 (n = 10) using $^{144}Nd/^{146}Nd$ = 0.7219 for fractionation correction. Pb isotope ratios were determined by the Tl-addition technique(White et al., 2000) using $^{203}Tl/^{205}Tl$ = 0.418922 and assuming identical fractionation factors between Tl and Pb. The Pb/Tl ratio ($^{208}Pb/^{205}Tl \sim 7$) of the samples was kept near identical to the NBS 981 standard by first performing dip checks in the samples and spiking Tl to the appropriate level. The standard NBS-981 was determined at $^{206}Pb/^{204}Pb$ = 16.936 ± 0.001, $^{207}Pb/^{204}Pb$ = 15.940 ±00.1, $^{208}Pb/^{204}Pb$ = 36.694 ±0.003 (n=13).

Measured radiogenic isotope ratios of new Tortugal and Curacao samples were age corrected to initial eruptive values at 90 Ma. We included initial Nd-Pb (age corrected to 90 Ma) ratios of previously studied Quepos samples(Trela et al., 2015) and CLIP basalts and glasses for comparison.

Melt inclusions in olivine from all Tortugal lava samples were completely recrystallized, so it was necessary to experimentally reheat them. Separated olivine grains were heated to 1300^{o}C in vertical heating stage at oxygen fugacity corresponding to QFM buffer at Vernadsky Institute of Geochemistry, Russian Academy of Science, Moscow. Olivine grains were quenched after exposure of 5 minutes at top temperature. The total exposure time of inclusions at temperatures over 800 °C was less than 10 minutes, which precludes any significant loss of H^{+} from the melt inclusions. Grains were grinded and polished to expose inclusions on the surface. Exposed inclusions were then measured by EPMA, SIMS, and Raman spectroscopy.

We used the high precision method of (Batanova et al., 2015) to analyze olivine phenocrysts from Tortugal samples using only the most primitive, unfractionated (samples in olivine control) basalts. Data was collected at the University of Joseph Fourier, Grenoble France on a JEOL JXA-8230 Superprobe using a focused beam (~1 μm in diameter) of 25 kV and 900 nA. We analyzed the San Carlos olivine standard at regular intervals during each analysis to correct for instrumental drift. The average relative 2σ error for major and trace elements on the San Carlos olivine standard (n=45) were: Si ~0.14, Mg ~0.14, Fe ~0.036 and Ni ~0.002, Mn ~0.001, Ca 0.001, Na ~0.002, Al ~0.002, Co ~0.002, P ~0.002, and Ti ~0.0005. An internal house standard (xen-7) was measured at regular intervals to correct for instrumental drift in Zn. The 2σ error for Zn

on xen-7 was ~0.002. The relative accuracy was better than 2% for all oxides except Co (2.8%), P (4.6%), and Zn (17%). Major elements of olivine hosted melt inclusions and clinopyroxene crystals were analyzed at Virginia Tech with a Cameca SX 50 electron microprobe using a focused beam (~1 μm in diameter) of 15 kV and 25 nA.

Olivine hosted melt inclusions and clinopyroxenes were analyzed at Woods Hole Oceanographic Institution. We determined H_2O, CO_2, F, S, and Cl concentrations from ratios of $^{16}O^1H$, (other isotopes of C, F, S, and Cl) to ^{30}Si using a Cs beam and a 1 μm spot size within 50 μm x 50 μm rastered pits in each phase.

We performed petrologic modeling on Tortugal samples following the approach reported in (Herzberg and Asimow, 2015) to constrain melt generation P-T conditions. We incorporated data from other komatiite and high-MgO terranes (i.e., Barberton, Kambalda, Munro, Emeishan, Baffin Island, and Gorgona) using precompiled datasets found on the GEOROC Database. PRIMELT3 MEGA.xlsm software is a user-friendly program in which the operator needs only to import whole rock data composition and specify desired source oxidation state. Melting is assumed to be due to accumulated fractional melting. The software first identifies a range of primary magma composition through olivine addition or subtraction. Olivine is added or subtracted until the software identifies a common melt fraction in multicomponent (CMAS) and FeO-MgO space. In the case of high-MgO basalts, we add/subtract olivine until a primary magma solution in equilibrium with the highest olivine Mg# is reached (Mg#=94 for Tortugal melts). We then apply the experimentally determined equations to estimate T_p, $T^{ol/l}$, and initial melting pressure (P_i). These melting equations are not calibrated for sources that have undergone such extensive melting and therefore restrain us from calculating final melting

pressures (P_f), because komatiites most likely left behind residues of olivine+clinopyroxene+garnet. We, therefore, used the approach of Herzberg and Asimow (2015) to qualitatively estimate P_f. We assume that the final melting temperatures and pressures coincide with the intersection of the adiabat with the maximum pyroxene stability curve (Herzberg et al., 2010)(Fig 3B). Melt productivity essentially stops once opx is melted out of the source and leaves behind a refractory dunite residue.

References:

Alvarado, G.E., Denyer, P., Sinton, C.W., 1997. The 89 Ma Tortugal komatiitic suite, Costa Rica: Implications for a common geological origin of the Caribbean and Eastern Pacific region from a mantle plume. Geology 25, 439-442.

Andrault, D., Monteux, J., Le Bars, M., Samuel, H., 2016. The deep Earth may not be cooling down. Earth and Planetary Science Letters 443, 195-203.

Arndt, N., 1999. Why was flood volcanism on submerged continental platforms so common in the precambrian? Precambrian Research 97, 155-164.

Arndt, N., Kerr, A.C., Tarney, J., 1997. Dynamic melting in plume heads: the formation of Gorgona komatiites and basalts. Earth and Planetary Science Letters 146, 289-301.

Batanova, V.G., Sobolev, A.V., Kuzmin, D.V., 2015. Trace element analysis of olivine: High precision analytical method for JEOL JXA-8230 electron probe microanalyser. Chemical Geology 419, 149-157.

Berry, A.J., Danyushevsky, L.V., O'Neil, H.S.C., Newville, M., Sutton, S.R., 2008. Oxidation state of iron in komatiitic melt inclusions indicates hot Archaean mantle. Nature 455, 960-964.

Coogan, L.A., Saunders, A.D., Wilson, R.N., 2014. Aluminum-in-olivine thermometry of primitive basalts: Evidence of an anomalously hot mantle source for large igneous provinces. Chemical Geology 368, 1-10.

Danyushevsky, L.V., Sobolev, A.V., 1996. Ferric-ferrous ratio and oxygen fugacity calculations for primitive mantle-derived melts: calibration of an empirical technique. Mineralogy and Petrology 57, 229-241.

Dixon, J.E., Leist, L., Langmuir, C.H., Schilling, J.-G., 2002. Recycled dehydrated lithosphere observed in plume-influenced mid-ocean-ridge basalt. Nature 420, 385-389.

Echeverria, L.M., 1982. Komatiites from Gorgona Island, Colombia. George Allen and Unwin, London.

French, S.W., Romanowicz, B., 2015. Broad plumes rooted at the base of the Earth's mantle beneath major hotspots. Nature 525, 95-99.

Garnero, E.J., McNamara, A.K., Shim, S.-H., 2016. Continent-sized anomalous zones with low seismic velocity at the base of Earth's mantle. Nature Geoscience 9, 481-489.

Grove, T.L., Parman, S., 2004. Thermal evolution of the Earth as recorded by komatiites. Earth and Planetary Science Letters 219, 173-187.

Heinonen, J.S., Jennings, E.S., Riley, T.R., 2015. Crystallisation temperatures of the most Mg-rich magmas of the Karoo LIP on the basis of Al-in-olivine thermometry. Chemical Geology 411, 26-35.

Herzberg, C., 1992. Depth and degree of melting of Komatiites. Journal of Geophysical Research 97, 4521-4540.

Herzberg, C., 2016. Petrological Evidence from Komatiites for an Early Earth Carbon and Water Cycle. Journal of Petrology 57, 2271-2288.

Herzberg, C., Asimow, P.D., 2015. PRIMELT3 MEGA.XLSM software for primary magma calculation: Peridotite primary magma MgO contents from the liquidus to the solidus. Geochemistry Geophysics Geosystems 16.

Herzberg, C., Condie, K., Korenaga, J., 2010. Thermal history of the Earth and its petrological expression. Earth and Planetary Science Letters 292, 79-88.

Herzberg, C., Gazel, E., 2009a. Petrological evidence for secular cooling in mantle plumes. Nature 458, 619-623.

Herzberg, C., Gazel, E., 2009b. Petrological evidence for secular cooling in mantle plumes. Nature 458, 619-622.

Herzberg, C., O'Hara, M.J., 2002. Plume-Associated Ultramafic Magmas of Phanerozoic Age. Journal of Petrology 43, 1857-1883.

Hirose, K., Fei, Y.W., Ma, Y.Z., Mao, H.K., 1999. The fate of subducted basaltic crust in the Earth's lower mantle. Nature 397, 53-56.

Hofmann, A.W., Hart, S.R., 1978. Assessment of local and rgional isotopic equilibrium in the mantle. Earth and Planetary Science Letters 38, 44-62.

Hofmann, A.W., White, W.M., 1982. Mantle plumes from ancient oceanic crust. Earth and Planetary Science Letters 57, 421-436.

Jackson, M.G., Konter, J.G., Becker, T.W., 2017. Primordial helium entrained by the hottest mantle plumes. Nature 542, 340-343.

Jicha, B., Singer, B.S., Sobol, P., 2016. Re-evaluation of the ages of 40Ar/39Ar sanidine standards and supereruptions in the western US using a Noblesse multicollector mass spectrometer. Chemical Geology 431, 54-66.

Jicha, B.R., Brown, F.H., 2014. An age on the Korath Range and the viability of 40 Ar/39 Ar dating of kaersutite in Late Pleistocene volcanics, Ethiopia. Quaternary Geochronology 21, 53-57.

Johnson, D.M., Hooper, P.R., Conrey, R.M., 1999. XRF Analysis of rocks and minerals for major and trace elements on a single low dilution Li-tetraborate fused bead. Advances in X-ray Analysis 41, 843-867.

Kelley, K.A., Plank, T., Ludden, J., Staudigel, H., 2003. Composition of altered oceanic crust at ODP Sites 801 and 1149. Geochemistry, Geophysics, Geosystems 4, n/a-n/a.

Kerr, A.C., Marriner, G.F., Arndt, N., Tarney, J., Nivia, A., Saunders, A.D., Duncan, R.A., 1996. The petrogenesis of Gorgona komatiites, picrites and basalts: new field, petrographic and geochemical constraints. Lithos 37, 245-260.

Kuiper, K.F., Deino, A., Hilgen, F.J., Krijgsman, W., Renne, P.R., Wijbrans, J.R., 2008. Synchronizing rock clocks of Earth history. Science 320, 500-504.

Li, Z.-X.A., Lee, C.-T.A., 2004. The constancy of upper mantle fO2 through time inferred from V/Sc ratios in basalts. Earth and Planetary Science Letters 228, 483-493.

Madrigal, P., Gazel, E., Flores, K.E., Bizimis, M., Jicha, B., 2016. Record of massive upwellings from the Pacific large low shear velocity province. Nature Communications 7, 13309.

Matzen, A.K., Baker, M.B., Beckett, J.R., Stolper, E.M., 2011. Fe-Mg Partitioning between Olivine and High-magnesian Melts and the Nature of Hawaiian Parental Liquids. Journal of Petrology 52, 1243-1263.

Maurel, C., Maurel, P., 1984. Etude experimentale de la distribution du ferrique entre spinelle chromifere et bain silicate basique. Bull. Mineral. 107, 25-33.

Mazza, S.E., Gazel, E., Johnson, E.A., Kunk, M.J., McAleer, R., Spotila, J.A., Bizimis, M., Coleman, D.S., 2014. Volcanoes of the passive margin: The youngest magmatic event in eastern North America. Geology 42, 483-486.

Michael, P.J., Graham, D.W., 2015. The behavior and concentration of CO2 in the suboceanic mantle: Inferences from undegassed ocean ridge and ocean island basalts. Lithos 236-237, 338-351.

Min, K., Mundil, R., Renne, P.R., Ludwig, K.R., 2000. A test for systematic errors in 40Ar/39Ar geochronology through comparison with U/Pb analysis of a 1.1-Ga rhyolite. Geochimica et Cosmochimica Acta 64, 73-98.

Parman, S.W., Grove, T.L., Dann, J.C., de Wit, M.J., 2004. A subduction origin for komatiites and cratonic lithospheric mantle. South African Journal of Geology 107, 107-118.

Putirka, K., 2016. Rates and styles of planetary cooling on Earth, Moon, Mars, and Vesta, using new models for oxygen fugacity, ferric-ferrous ratios, olivine-liquid Fe-Mg exchange, and mantle potential temperature. American Mineralogist 101, 819-840.

Putirka, K.D., Perfit, M., Ryerson, F.J., Jackson, M.G., 2007. Ambient and excess mantle temperatures, olivine thermometry, and active vs. passive upwelling. Chemical Geology 241, 177-206.

Renne, P.R., Balco, G., Ludwig, K.R., Mundil, R., Min, K., 2011. Response to the comment by W.H. Schwarz et al. on "Joint determination of 40K decay constants and 40Ar*/40K for the Fish Canyon sanidine standard, and improved accuracy for 40Ar/39Ar geochronology" by P.R. Renne et al. (2010). Geochimica et Cosmochimica Acta 75, 5097-5100.

Rizo, H., Walker, R.J., Carlson, R.W., Horan, M., Mukhopadhyay, S., Manthos, V., Francis, D., Jackson, M., 2016. Preservation of Earth-forming events in the tungsten isotopic composition of modern flood basalts. Science 352, 809-811.

Sobolev, A., Batanova, V., Asafov, E., Gurenko, A.A., Arndt, N., Krasheninnikov, S., Portnyagin, M., Garbe-Schönberg, D., 2015. How Hot and Wet are Mantle Derived Magmas and Their Sources? AGU Fall Meeting.

Sobolev, A.V., Asafov, E.V., Gurenko, A.A., Arndt, N.T., Batanova, V.G., Portnyagin, M.V., Garbe-Schonberg, D., Krasheninnikov, S.P., 2016. Komatiites reveal a hydrous Archaean deep-mantle reservoir. Nature 531, 628-632.

Sobolev, A.V., Hofmann, A.W., Kuzmin, D.V., Yaxley, G.M., Arndt, N.T., Chung, S.L., Danyushevsky, L.V., Elliott, T., Frey, F.A., Garcia, M.O., Gurenko, A.A.,

Kamenetsky, V.S., Kerr, A.C., Krivolutskaya, N.A., Matvienkov, V.V., Nikogosian, I.K., Rocholl, A., Sigurdsson, I.A., Sushchevskaya, N.M., Teklay, M., 2007. The amount of recycled crust in sources of mantle-derived melts. Science 316, 412-417.

Spice, H.E., Fitton, G., Kirstein, L., 2016. Temperature fluctuation of the Iceland mantle plume through time. Geochem. Geophys. Geosyst., 1-12.

Trela, J., Vidito, C., Gazel, E., Herzberg, C., Class, C., Whalen, W., Jicha, B., Bizimis, M., Alvarado, G.E., 2015. Recycled crust in the Galápagos Plume source at 70 Ma: Implications for plume evolution. Earth and Planetary Science Letters 425, 268-277.

Walter, M.J., 1998. Melting of Garnet Peridotite and the Origin of Komatiite and Depleted Lithosphere. Journal of Petrology 39, 29–60.

Wan, Z., Coogan, L.A., Canil, D., 2008. Experimental calibration of aluminum partitioning between olivine and spinel as a geothermometer. American Mineralogist 93, 1142-1147.

White, W.M., Albarede, F., Telouk, P., 2000. High-precision analysis of Pb isotope ratios by multi-collector ICP-MS. Chemical Geology 167, 257-270.

Wilson, J.T., 1963. A possible origin of the Hawaiian Islands. Can. J. Phys. 41, 863-868.

Xu, R., Liu, Y., 2016. Al-in-olivine thermometry evidence for the mantle plume origin of the Emeishan Large Igneous Province. Lithos 266-267, 362-366.

Figures

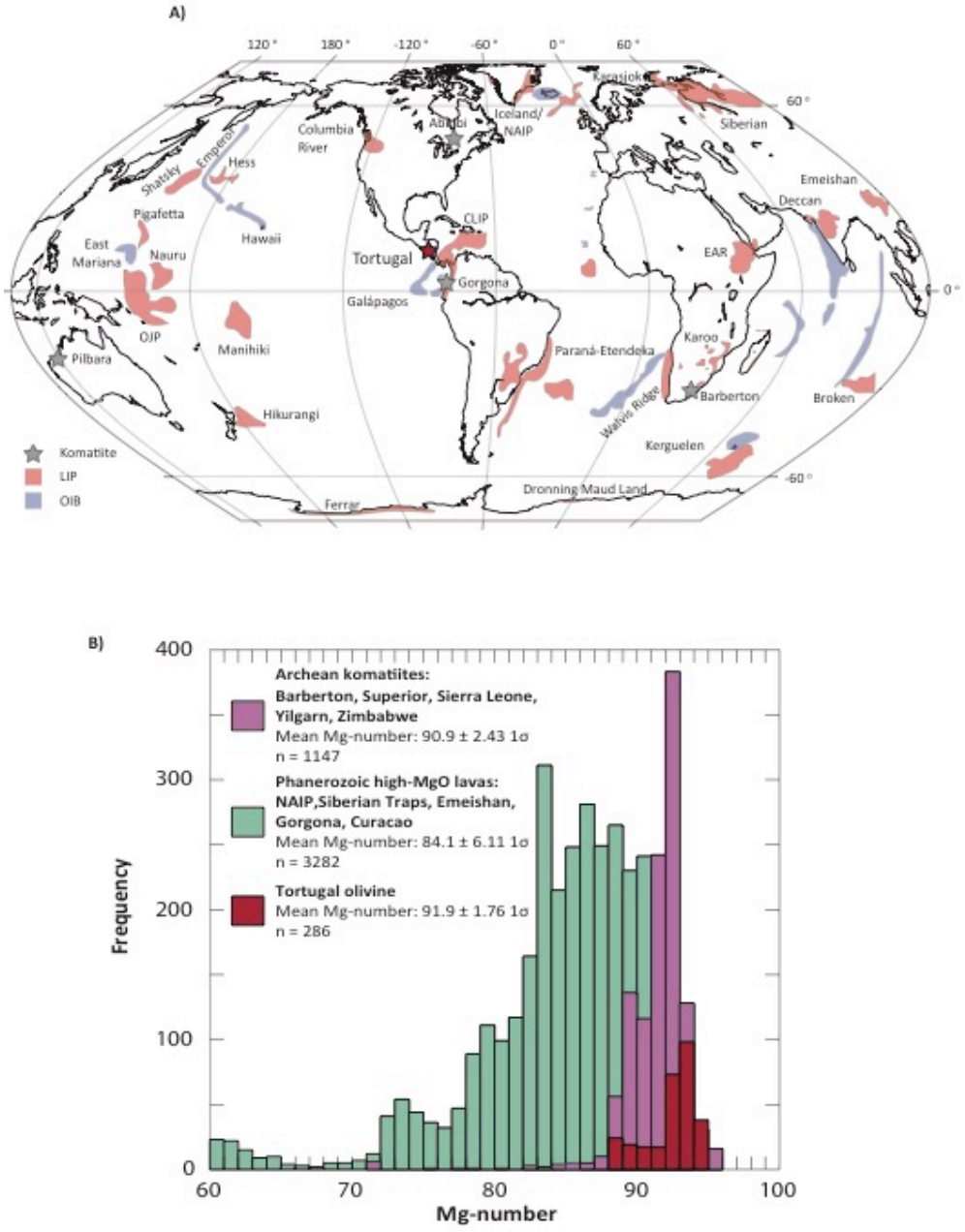

Figure 1: Locations of famous komatiites, hotspot lavas, and the frequency distribution of their olivine Mg-numbers. A) Map highlighting famous komatiite localities including Barberton, Abitibi, Pilbara, and Gorgona (grey stars). Other high-MgO lavas discussed in this study include the Siberian Traps, Emeishan LIP, North Atlantic Igneous Province (NAIP), Baffin Island, and the Karoo LIP. Large igneous

provinces (LIPs) are in red and ocean island basalts (OIBs) are in blue. A red star denotes the Tortugal Suite. OIB locations are shown blue. B) Histogram comparing olivine Mg# for Archean komatiites (purple), high-MgO Phanerozoic lavas (green), and the Tortugal terrane (red). Note that Tortugal olivines have high Mg# and their population overlaps that of Archean komatiites suggesting crystallization from an exceptionally hot melt. Olivine data from (Coogan et al., 2014; Heinonen et al., 2015; Sobolev et al., 2016; Sobolev et al., 2007; Spice et al., 2016; Wan et al., 2008; Xu and Liu, 2016) and the Georoc database (http://georoc.mpch-mainz.gwdg.de/georoc).

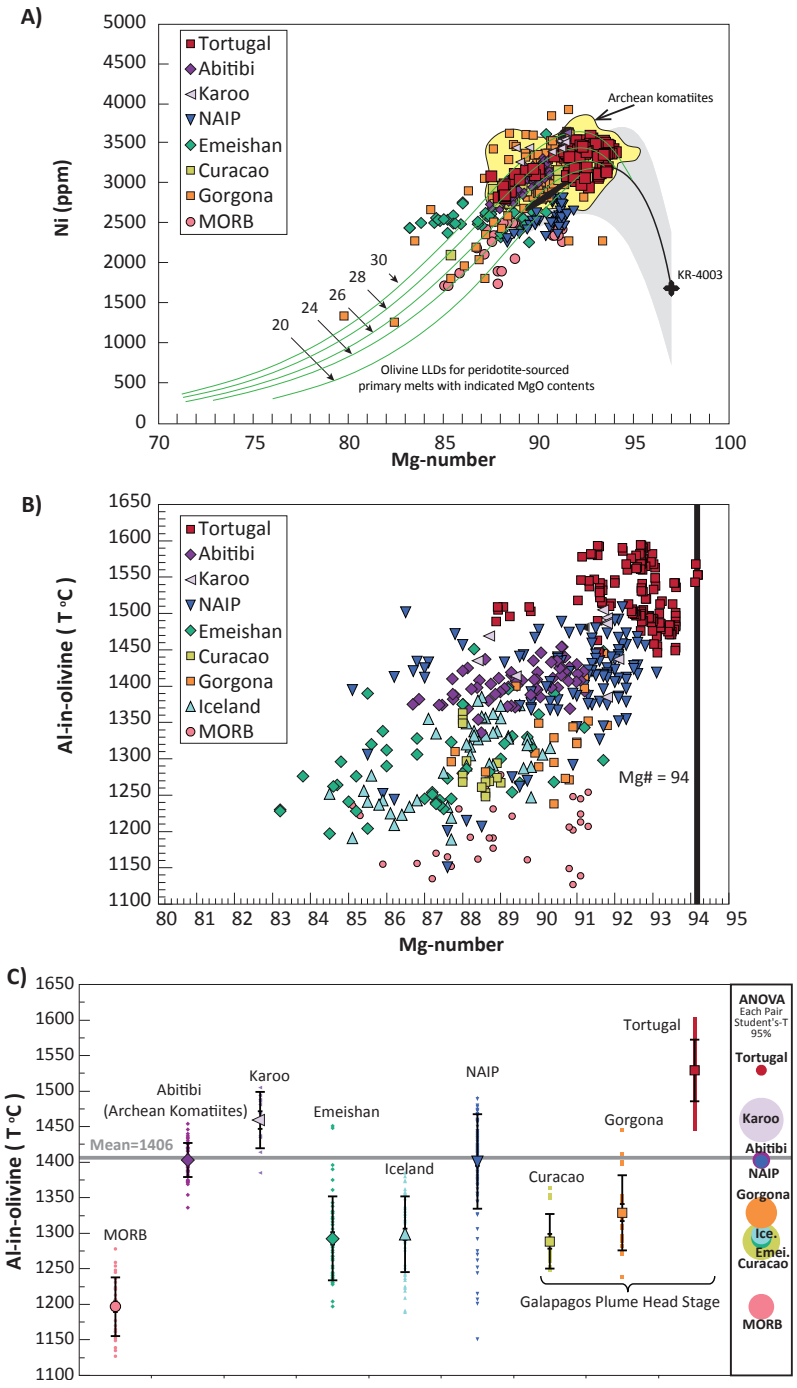

Figure 2: **Global olivine systematics and Al-in-olivine thermometry for komatiites and the hottest Phanerozoic olivines.** A) Graph showing the relationship between Ni (ppm) and Mg-number. The green curves are olivine liquid lines of descent from primary magmas having initial MgO contents between 20 and 30%. Tortugal olivine plot within

the Barberton komatiite olivine field and are consistent with derivation from a primary liquid with 26-30 wt% MgO. Mid-ocean ridge basalt (MORB) olivines are from the East Pacific Rise(Sobolev et al., 2007). B) Results from aluminum-in-olivine thermometry plotted against host olivine Mg#. Tortugal data filtered for low-Ti, high-temperature group of olivines. C) One-way comparison of the results from aluminum-in-olivine thermometer(Coogan et al., 2014). Olivines from the Tortugal terrane record the highest Al-in-olivine crystallization temperatures to date. Circles on the right side of the graph denote the result of analysis of variance (ANOVA) using a Student's-T at the 95% confidence interval for each terrane/location. The radii of the circles are proportional to the standard error of the mean. Olivine trace element data is from (Coogan et al., 2014; Heinonen et al., 2015; Sobolev et al., 2016; Sobolev et al., 2007; Spice et al., 2016; Wan et al., 2008).

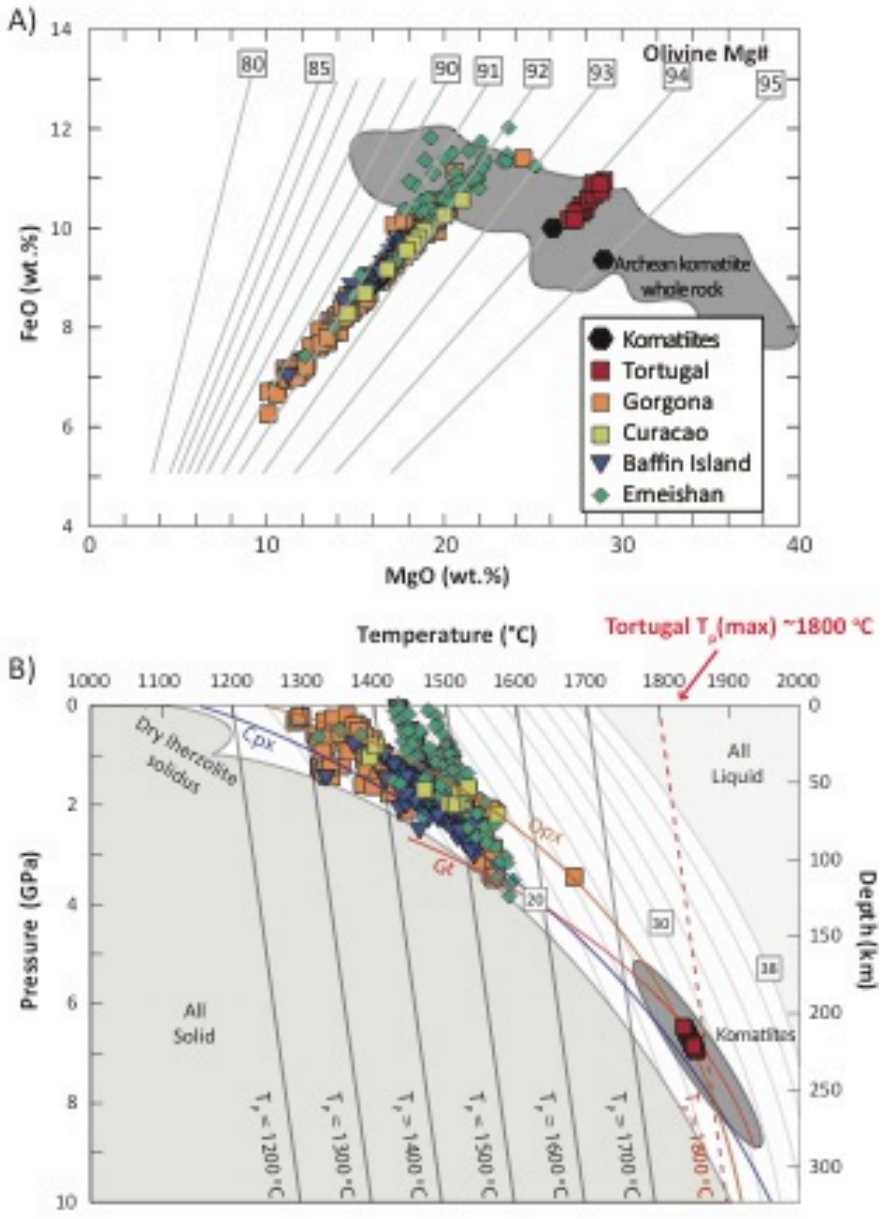

Figure 3: **Primary melt petrologic modeling of hot Phanerozoic lavas.** A) FeO-MgO projection showing primary melt compositions for high-MgO Phanerozoic melts and Archean komatiites formed by accumulated fractional melting[18]. Gray diagonal lines represent equilibrium olivine compositions and the range of Archean komatiite whole rock data is shown for comparison. B) Estimated temperatures and pressures of final melting. The P-T conditions (all locations except Tortugal and Archean komatiites) for P_f

are estimated using the equation T_{OL} (°C) = 935 + 33MgO − 0.37MgO^2 + 54P_F − 2$P_F{}^2$. T^{OL} (°C) is the olivine-liquidus temperature at P_f (Herzberg and Gazel, 2009b). The colored curves (labeled Opx, Cpx, and Gt) represent the maximum temperatures at which these minerals are stable during equilibrium melting of a fertile peridotite (Herzberg and O'Hara, 2002). Tortugal primary melts fall within the estimated range P-T range of Archean komatiites (Herzberg et al., 2010). We assume that melting ceased for Tortugal when all cpx and opx were exhausted.

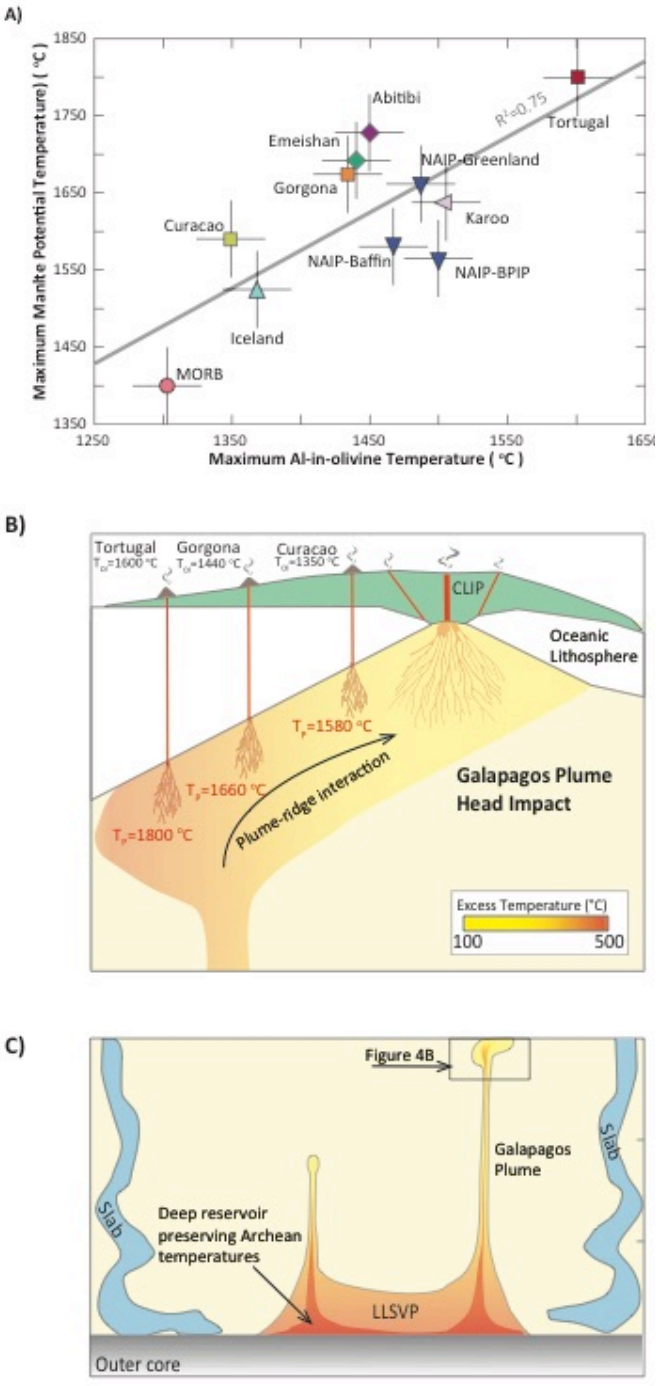

Figure 4: The correlation between two independent thermometers suggests the preservation of deep, hot Archean mantle reservoirs. A) Graph showing our estimated maximum mantle potential temperatures plotted against maximum Al-in-olivine crystallization temperatures. Error bars represent the uncertainty of both

thermometers(Coogan et al., 2014; Herzberg and Asimow, 2015). The Tortugal terrane records the highest T_p and Al-in-olivine crystallization temperatures to date. Al-in-olivine temperature estimates include data from this study and refs. ((Coogan et al., 2014; Heinonen et al., 2015; Sobolev et al., 2016; Spice et al., 2016; Wan et al., 2008) B) Schematic representation for the genesis of Tortugal melts. Tortugal liquids originated via melting the hot, axial core of the plume under high-pressure conditions. Gorgona and Curacao likely melted at lower pressures due to plume capture by a mid-ocean ridge. C) Schematic representation showing the excess temperature of the mantle during the Archean and Phanerozoic relative to modern ambient MORB mantle (1350 °C). Inspired by (Garnero et al., 2016). The North Atlantic Igneous Province (NAIP) has been separated into three locations in this figure including Greenland, Baffin Island, and the British Paleogene Igneous Province (BPIP).

Chapter 3: Long-lived chemical and spatial heterogeneities in the Galapagos mantle plume

Abstract

Mantle plume derived melts provide a unique glimpse into the chemical heterogeneity of the deep mantle that resulted from eons of complex planetary differentiation, recycling, and mixing processes. The Galapagos plume is exceptional in that its lavas sample four distinct isotopic mantle components defined by variations Sr-Nd-Pb radiogenic isotopes space. However, the origin and petrogenetic history of each of these end members still remains debated. In this study, we investigate the spatial and temporal evolution of the four isotopic end members of the Galapagos mantle plume using Sr-Nd-Pb isotopic modeling. We find that the spatial relationship between each of the classically defined Galapagos Domains has remained relatively constant over the last 90 Ma as evidenced by the isotopic compositions of accreted terranes in Costa Rica and Panama. Our new results extend the time scale of distinct isotopic heterogeneity in the source of the plume to at least 70 Ma for the Southern Domain and 90 Ma for the Central, and Northern Domains, suggesting that geochemically zoned plumes rising through the mantle preserve distinct isotopic heterogeneity on the time scale of tens to hundreds of millions of years. Additionally, trace element systematics of olivine crystals from the Galapagos related Azuero and Quepos terranes (Central and Southern Domain respectively) suggest derivation from sources that included recycled components, though with a different isotopic composition.

Introduction

Mantle plumes offer a window into geochemical and geodynamic processes occurring within the deep Earth. These anomalously hot mantle domains sample the lithological and isotopic heterogeneities of the lower mantle (Hofmann and White, 1982; White, 1985) and thus their partial melts, as observed at hotspots (the surface manifestations mantle plumes) can offer a long-lived geochemical record of mantle evolution (Wilson, 1963). Recycling of crustal materials back into that mantle is an important planetary process (Chauvel et al., 2008; Hofmann, 1997; Hofmann and White, 1982; Zindler and Hart, 1986) as it has introduced lithological and isotopic heterogeneities back into the convecting mantle over the course of Earth's evolution. These heterogeneities are samples by plumes rising through the mantle and are manifested in the geochemistry of surficial basaltic lava flows (e.g(Hofmann, 1997). Typical OIB primitive mantle normalized spider diagrams display positive high field strength element (e.g., Nb, Ta, and Ti) enrichments, indicating that a reservoir of refractory subducted oceanic lithosphere has been accumulating in the deep mantle (Jackson et al., 2008; Kamber and Collerson, 2000; McDonough, 1991; Rudnick et al., 2000) and possibly represent the component common to all plume origins (Hart et al., 1992; Stracke, 2005; Zindler and Hart, 1986).

The Galapagos mantle plume it is characterized by spatial (Hofmann and White; White et al.) and temporal lithologic and isotopic variability across different time scales, e.g., millions to tens of millions of years (Blichert-Toft and White., 2001; Hauff et al., 2000a; Hoernle et al., 2004; Vidito et al., 2013; White et al., 1993). Additionally, this plume provides an unparalleled record of plume evolution as both large igneous province

(LIP) and ocean island basalt (OIB) terranes are accreted in the Caribbean and in Central America (Denyer et al., 2006; Denyer and Gazel, 2009; Hoernle et al., 2004; Sinton et al., 1998). Recent studies showed that the Galapagos plume also experienced systematic, secular cooling throughout its 90 Ma history. Herzberg and Gazel (2009) showed that the plume was hottest during the "head" early melting stage that formed the Caribbean Large Igneous Province (CLIP) and subsequent cooled during melting of the plume conduit responsible for generating paleo-ocean island basalt terranes, the linear Cocos and Carnegie, and the present day archipelago produced progressively cooler lavas (Herzberg and Gazel, 2009; Trela et al., 2015). A previous study from our group (Trela et al., 2015) suggested that the appearance of an entrained a dense, recycled oceanic crust (pyroxenite) component in the hotspot source at 70 Ma is contemporaneous with a sharp decrease in mantle potential temperature between 90 and 70 Ma.

Here, we add to this study of the evolution of the Galapagos Plume new whole-rock major and trace element, and isotopic data, and high-precision olivine trace element systematics of picrites and basalts from the 60 to 70 Ma accreted and Azuero terranes (Panama) in order to better understand the significance of recycled component and the implications of planetary-scale crustal recycling processes to constrain the origin of the distinct isotopic components sampled by the present-day Galapagos archipelago. Our goal is to to constrain the timing, origin, and evolution of the four isotopic Galapagos Domains and to determine when this complex spatial zonation (Geist et al.; White and Hofmann) first appeared during the history of the plume and for how long each has been extant by tracing the isotopic composition of these older Galapagos-related terranes through time.

Tectonic History and Isotopic Domains of the Galapagos plume

The early stage of the Galapagos plume-head melting began at ~90 Ma (at near the same location as the current archipelago) and resulted in the formation of the Caribbean LIP (CLIP) (Duncan and Hargraves, 1984; Hauff et al., 1997; Kerr et al., 1996; Pindell and Barrett, 1990; Richards et al., 1989; Sinton et al., 1998); Madrigal et al., 2016]. The over-thickened section of the Farrallon plate (~20 km) migrated northeast and collided with the Greater Antilles Arc (Duncan and Hargraves, 1984; Gazel et al., 2011; Geldmacher, 2003; Hauff et al., 2000b) initiating subduction along the western margin of the CLIP (Duncan and Hargraves, 1984; Geldmacher, 2003)Madrigal et al. 2016] A record of progressive Galapagos plume tail melting (70 Ma to the present) is preserved as accreted OIB terranes along the Pacific coast of Costa Rica and Peninsula, Panama (Hoernle et al., 2002) and along the Cocos and Carnegie ridges, and associated seamounts. The Farrallon slab rifted at ~23 Ma (Lonsdale, 2005) (in close proximity to the hotspot) to form the present day Cocos and Nazca plates. This event resulted in a series of complex plume-ridge interactions and jumps that are preserved in the Cocos, Carnegie, Coiba, and Malpelo hotspot tracks (Hoernle et al., 2002; Werner et al., 2003).

Perhaps the most enigmatic aspect of the Galapagos hotspot is the origin of the unique radiogenic isotope domains manifested in the Sr-Nd-Pb-Hf-He signatures of the modern-day Archipelago. The modern Galápagos platform is divided into four distinct isotopic domains based on their distinctive and consistent isotopic variations in radiogenic Nd-Sr-Pb-Hf and $^{3}He/^{4}He$ ratios (Harpp and White, 2001; Hoernle et al., 2000). The Eastern Domain is the most depleted isotopic end-member (Harpp and White, 2001; Hauff et al., 2000a) with isotopic ratios comparable to mid ocean ridge basalt

(MORB). The Southern or Floreana Domain is the most isotopically enriched with high radiogenic $^{87}Sr/^{86}Sr$ and $^{206}Pb/^{204}Pb$ ratios (Harpp and White, 2001). The Northern Domain includes the Wolf-Darwin Lineament and typically displays minor ^{207}Pb and ^{208}Pb enrichments and low $^{3}He/^{4}He$ ratios (~8.8-6.9 R/R_A) (Harpp and White, 2001; Vidito et al., 2013) and unradiogenic $^{87}Sr/^{86}Sr$ and $^{206}Pb/^{204}Pb$ ratios relative to the Southern Domain (Harpp and White, 2001). Lavas from the Central Domain (e.g., Fernandina) are thought to reflect the primitive composition of the plume. These melts have relatively high $^{87}Sr/^{86}Sr$ and $^{206}Pb/^{204}Pb$ ratios (though not as high as the Southern Domain) (Harpp and White, 2001) and record the highest $^{3}He/^{4}He$ signature (up to 30.3 R/R_A; (Kurz et al., 2014).

A Galapagos origin for the Caribbean Large Igneous Province (CLIP) is largely based on geochrnonolgical and geochemical evidence (Duncan and Hargraves; Kerr et al., 2003; Loewen et al., 2013). The CLIP is thought to represent the early melting stages of the Galapagos mantle plume between 90-95 Ma, that resulted in widespread lava flows in the vicinity of present day Galapagos Archipelago. The CLIP migrated northeast along with Farrallon plate where it collided with the Greater Antilles Arc (Duncan and Hargraves; Kerr et al., 2003; Madrigal et al., 2016). The CLIP related Nicoya Complex (Costa Rica) and Curacao Lava Formation exhibit both geochemical and radiogenic isotope systematic that are consistent with derivation from a Galapagos source (Geldmacher, 2003; Hauff et al., 2000a). Major and trace element systematics (Kerr et al.; Klaver) and radiogenic isotope ratios (Kerr et al., 1996; Hauff et al., 2000) suggest Curacao lavas formed from a common parental melt, consistent with large degrees of partial melting from a plume mantle source (Herzberg and Gazel, 2009). Both the

Nicoya Complex and the Curacao Lava Formation have radiogenic $^{143/144}$Nd and ^{206,207,206}Pb/^{204}Pb ratios consistent with being derived from the Galapagos Central Domain (Hauff et al., 2000a; Trela et al., 2015).

The Quepos terrane (Fig. 1) is an accreted oceanic igneous terrane located along the Pacific side of Costa Rica and is related to melting of the Galapagos mantle plume between 60 and 70 Ma (Frisch et al., 1992; Hauff et al., 1997; Trela et al., 2015). Quepos lavas span the basaltic spectrum from transitional tholeiities to alkaline in nature and display trace element patterns indicating an OIB source with a clear Galápagos radiogenic isotope signature (Geldmacher, 2003; Hauff et al., 2000a; Hauff et al., 2000c). Source age-projection suggests that these melts dominantly plot within the present day Central Domain in terms of their Pb and Nd isotopes systematics (Trela et al., 2015).

Earlier geologic investigations suggested that the Panamanian Pacific coast is underlain by 90 Ma Caribbean basement (Hauff et al., 2000a; Hoernle et al., 2002; Sinton et al., 1998). These studies identified 21-66 Ma OIB terranes in southern Panama and interpreted them as accreted Galapagos OIBs and seamounts and explain the connection between the CLIP and the aseismic Cocos, Carnegie, Coiba, and Malpelo ridges (Hoernle et al., 2002). The Azuero Peninsula, located in the southeastern region of Panama juts into the Pacific Ocean (Fig. 1). The Azuero-Sona fault zone strikes approximately N 50° W and crosscuts the southwestern portion of the peninsula. This feature separates Cretaceous island arc volcanics and minor CLIP related terranes located northeast of the fault from accreted Galapagos OIB terranes to the southwest (Gazel et al., , Lissina, 2005). The terranes in the Azuero Peninsula range in age from 21-66 Ma (Hoernle et al., 2002) and represent accreted seamounts and islands that were formed by decompression

melting of the Galapagos mantle plume. These rocks include well-preserved olivine rich cumulates and basalts that range in composition from thoeliitic to alakalic basalts. Previously studied Azuero picrites and basalts display radiogenic isotope ratios similar to the classically defined Central and Southern domains (Hauff et al., 2000a).

Materials and Methods

We collected picrite and basalt samples along the Pacific coast of the Azuero Peninsula, from in-situ outcrops and the fresh interiors of nearby coastal boulders.

$^{40}Ar/^{39}Ar$ incremental heating experiments were conducted for six sample matrices at the University of Wisconsin-Madison Rare Gas Geochronology Laboratory, on using a 25 Watt CO_2 laser and analyzed using a MAP 215–50 following protocols found in Jicha and Brown (2014). These samples were selected for age determinations complement previously published data on Galapagos accreted terranes in western Costa Rica and Panama (Hauff et al., 2000a). We reduced the data using ArArCalc software version 2.5 (http://earthref.org/ArArCALC/) and report ages with 2σ uncertainties (including the J uncertainty) relative to a Fish Canyon standard age of 28.201 ± 0.046 Ma (Kuiper et al., 2008). We used a value of 5.463 ± 0.107 x 10^{-10} yr^{-1} for $\lambda^{40}K$ (Min et al., 2000).

Alteration-free rock chips were selected under stereoscopic microscope and powdered them in an alumina mill at the Department of Geosciences at Virginia Tech. Fluxed glasses were prepared using those powders and Spex certified ultrapure lithium flux (34.83% $Li_2B_4O_7$ – 64.67% $LiBO_2$ – 0.5% LiBr). Whole rock major and trace element compositions were collected at Virginia Tech by XRF and ICPMS (detailed protocols in (Johnson et al., 1999; Mazza et al., 2014). The Relative Standard Deviation

(RSD) for 10 replicates of BHVO-2g collected as an unknown was <0.24% for all major elements and accuracy better than 1.74%, with the exception of P_2O_5. We obtained trace element concentrations from the same fluxed glasses with an Agilent 7500ce ICPMS coupled with a Geolas laser ablation system. The data were calibrated using USGS standards BCR-2, BHVO-2, G-2, and BIR-1a, using TiO_2 wt% from XRF analyses as an internal standard. We used the standard trace element values reported in (Kelley et al., 2003). The accuracy for four replicates of BHVO-2g was better than 5 % for most elements with exceptions for Ba, Hf, and Ge (7-9 %). The accuracy for four replicates of BIR-1a was better than 5 % for most elements except for Ga, Ge, Ce, Pr, Eu, Tb, Dy, Ho, Tm, Er, Yb, and Lu, which had accuracies ranging from 5-9 %.

Acid-digested aliquots were made from powdered basaltic and picritic material to collect Pb, Nd, and Sr radiogenic isotopes ratios. Column chemistry was done following the protocols reported in (Bizimis et al., 2013; Khanna et al., 2014). Radiogenic isotope ratios were collected using a Neptune multi collector ICPMS at the Center for Elemental Mass Spectrometry, University of South Carolina (USC). We determined Pb isotope ratios by the Tl-addition technique (White et al., 2000) using $^{203}Tl/^{205}Tl = 0.418922$ and assuming equal fractionation factors between Tl and Pb. The Pb/Tl ratio ($^{208}Pb/^{205}Tl \sim 7$) of the samples was kept near identical to the NBS 981 standard by first performing dip checks in the samples and spiking Tl to the appropriate level. The NBS-981 standard was determined at $^{206}Pb/^{204}Pb = 16.935 \pm 0.001$, $^{207}Pb/^{204}Pb = 15.489 \pm 0.001$, $^{208}Pb/^{204}Pb = 36.692 \pm 0.003$ (2 standard deviations, = 8). Isotopic ratios for Nd were normalized to $^{146}Nd/^{144}Nd = 0.7219$ and the Nd standard JNd_i was measured at $^{143}Nd/^{144}Nd = 0.5121$ and 0.512097 ± 0.00002 (n=6) at USC. Isotopic ratios for Sr were normalized to $^{86}Sr/^{88}Sr$

= 0.1194 and replicate analyses of $^{87}Sr/^{86}Sr$ at 0.710311 ± 0.0000045. All Sr measurements are reported relative to NBS-987 where $^{87}Sr/^{86}Sr = 0.710250$.

We used a high precision electron-micro probe method (Batanova et al., 2015) to analyze olivine phenocrysts from Azuero samples using only the most primitive, unfractionated samples in olivine control. Data was collected at the University of Joseph Fourier, Grenoble France on a JEOL JXA-8200 Superprobe using a focused beam (~1 μm in diameter) of 25 kV and 900 nA. We analyzed the San Carlos olivine standard was analyzed at regular intervals during each analysis to correct for instrumental drift. The average relative 2σ error for major and trace elements on the San Carlos olivine standard (n=45) were: Si ~0.14, Mg ~0.14, Fe ~0.036 and Ni ~0.002, Mn ~0.0001, Ca 0.001, Na ~0.002, Al ~0.002, Co ~0.002, P ~0.002, and Ti ~0.0005. An internal house standard (xen-7) was measured at regular intervals to correct for instrumental drift in Zn. The 2σ error for Zn on xen-7 was ~0.002. The relative accuracy was better than 2% for all oxides except Co (2.8%), P (4.6%), and Zn (17%).

Results

The matrix of six Azuero samples (three basalts and three picrites) dated by $^{40}Ar/^{39}Ar$ yielded weighted mean plateau ages of 61.6 ± 0.7, 62.6 ± 0.4, 63.1 ± 0.7, 63.6 ±0.8, 64.4 ± 0.3, and 72.2 ± 3.3 Ma. $^{40}Ar/^{39}Ar$ age dating results from the Quepos terrane yield similar ages between 60 and 70 Ma (Trela et al., 2015). Previously studies of Azuero lavas showed that the $^{40}Ar/^{39}Ar$ ages ranged between 20.8 ± 1.8 and 66.0 ± 0.7 (Hoernle et al., 2002; Sinton et al., 1998). We did not find younger lavas, however, our data agree with previous results and suggest a magmatic pulse between 60 and 70 Ma produced both the Azuero and Quepos terranes during a 10 Ma period.

The majority of lavas from the Azuero Peninsula plot within the picrite and basaltic fields on a total alkali vs. silica classification diagram (Fig. 2A), in a similar space to the lavas Quepos Terrane (Trela et al., 2015). Some basaltic samples are more rich in $Na_2O + K_2O$ (up to 6 wt.%) and show major element chemical similarity to tephrites and trachy-basalts. All of the samples studied here are tholeiites and do not show any affinity to calc-alkaline melts on the classic AFM diagram (Fig. 2A). Samples for the Azuero Peninsula consistently display enrichments in incompatible elements on a primitive mantle normalized spider diagram (Fig. 5). Similar to most intraplate OIBs, these samples display positive high-field strength element enrichments (e.g., Ti, Ta, Nb) as well as depletions in fluid mobile elements (K, Rb, Th, U). The trace element patterns of the Azuero samples from this study closely resemble primitive mantle normalized patterns of current the Galápagos hotspot tracks (the Cocos, Coiba, and Carnegie ridges) as well as the patterns from Quepos terrane (Fig. 5). One subtle, yet important difference in the trace element patterns is that a subset of the Azuero samples are relatively more enriched than Quepos lavas.

Fourteen samples from the Azuero Peninsula were selected for new whole-rock Sr-Nd-Pb isotope ratios. These ratios were first age corrected using an average age of 65 Ma and then used to project the radiogenic ingrowth of the source. We age-corrected radiogenic isotope ratios samples to initial eruptive values using an average age of 65 Ma. Then we calculated the radiogenic composition sources projected from 65 Ma and the CLIP source projected from 90 Ma by inverting primary magma compositions (using IGPET software, (Carr and Gazel, 2016)) from Quepos sample AQ16 (Hauff et al., 2000a), sample AN3 (Hoernle et al., 2004), and AZ-090613-9 (this study) and using the

modal composition of a refertilized peridotite and a melt fraction of F=10%. By projecting the sources of CLIP and Quepos lavas to t = 0 Ma, we account for the radiogenic ingrowth of their respective sources. This allows for proper comparison to the modern Galapagos isotopic domains. We tested the sensitivity of radiogenic source composition to the degree of partial melting and found negligible changes in the source projected Nd and Pb isotope ratios at melt fractions F=10, 20, and 30%. Age corrected Azuero lavas in this study have $^{206}Pb/^{204}Pb$ ratios that range from 19.02 to 19.28. The $^{208}Pb/^{204}Pb$ ratios range from 38.68 to 38.84 while $^{207}Pb/^{204}Pb$ ratios range from 15.58 to 15.64. Age corrected $^{143}Nd/^{144}Nd$ ratios range from 0.512888 to 0.512948. Source projected values (accounting for radiogenic ingrowth in the mantle source of these melts) are plotted in Figure 6 along with modern Galápagos Plume isotopic domains (Harpp and White, 2001; Hauff et al., 2000a) and previously published CLIP, Quepos, and Nicoya data also projected to present day compositions (Hauff et al., 2000a; Hoernle et al., 2004).

We used our high precision olivine data to infer source lithology of both the Quepos and Azuero Terranes and to determine the longevity of the pyroxenite component in the source of the Galapagos plume. A description of our adopted petrologic modeling method was provided previously (Herzberg, 2011; Herzberg et al., 2013; Herzberg et al., 2014). The model has the following components: 1) identification of a primary magma composition, 2) calculation of olivine and clinopyroxene liquid lines of descent (LLDs) 3) estimating olivine compositions that would theoretically crystallize along the LLD, and 4) comparing the theoretical models to the empirically measured olivine compositions. For the olivine/melt distribution coefficients $D^{ol/melt}$ we used the model of

Beattie (1993) for Ni, the model of Herzberg (2004) for Ca and Mn, and we used the model of Toplis (2005) for the Fe-Mg exchange coefficient.

Olivine phenocrysts from the Quepos and Azuero terranes are magnesium rich with Mg# (molar (MgO)/(MgO+FeO)) ranging from 80 to 90.4% (Fig. 3). The olivines contain high Ni contents (2000-4000 ppm) that decrease as a function of Mg#. The Fe/Mn ratios in these phenocrysts has an average value of ~70. Calcium contents range from 1500 ppm to 2700 ppm and increase with decreasing Mg#. Overall, both datasets strongly overlap one another and follow similar LLDs, however, olivines from Azuero tend to contain slightly higher Fe concentrations relative to Quepos phenocrysts (Fig. 4). The implications of this observation are discussed in detail below.

Discussion

Our new $^{40}Ar/^{39}Ar$ strongly suggest the formation of the Azuero and Quepos terranes between 60 and 70 Ma. These two terranes show strong overlap in terms of their major and trace element compositions as well as their olivine trace element characteristics. Both terranes include tholeiitic picrites (phenocrystic charged basalts) that experiences a significant amount of olivine. These rocks are ideal for exploring the internal consistency between different petrological and geochemical indicators for source composition discussed below.

Major element and olivine chemistry record for source composition

The whole rock CaO-MgO contents of these terranes suggest an olivine controlled LLD until ~8 wt.% MgO, where cotectic olivine + clinopyroxene fractionation commenced. The high-MgO nature of these samples and their derivative olivines are therefore ideal for source lithology discrimination studies. As noted by Trela et al.

(2015), samples from the Quepos terrane plot below the peridotite-pyroxenite discrimination line of (Herzberg and Asimow, 2008). It is important to note that no experimentally derived melts from peridotites have ever been reported to plot in the pyroxenite field of Figure 2B (Herzberg and Asimow, 2008). Samples from the Azuero terrane plot on both sides of the discrimination line. This first order approximation suggests that Quepos melts derived from a dominant pyroxenite component while Azuero melts derived from a mixture of both peridotite and pyroxenite components (Fig. 2B). CLIP lavas plot above the discrimination line in the peridotite partial melt field and lavas from the modern day Galapagos Archipelago plot on both sides of the divide indicating a mixed source lithology.

Source lithology can be further constrained using trace element systematics in olivine phenocrysts (Herzberg, 2011; Sobolev et al., 2005). Olivines that crystallize from pyroxenite-derived melts record high Ni, low Ca, and high Fe/Mn and the partitioning of these elements is largely controlled by clinopyroxene and garnet in the source (Sobolev et al., 2005; 2007). Peridotite derived olivines (such as those found in mid-ocean ridge basalts (MORB)), record systematically lower Ni and Fe/Mn and higher Ca relative to olivines that crystallize from pyroxenite derived melts. The observed systematics are largely controlled by the residual mineralogy of the mantle source. For example, nickel is less compatible in clinopyroxene (relative to olivine), and thus, olivines crystallizing from olivine-free pyroxenite sourced melts will contain higher Ni-contents. Similarly, clinopyroxene and garnet sequester Mn and Ca during pyroxenite melting and crystallizing olivine will retain high Fe/Mn ratios and low Ca contents. Oxidized melts could also crystallize olivine with lower Fe/Mn ratios betcause Fe^{3+} is less compatible in

olivine than Fe^{2+} (Krivolutskaya et al., 2012). Previous studies have shown that the partition coefficient of Ni ($D_{Ni}^{ol/melt}$) in olivine depends also on the temperature difference between melt segregation and olivine crystallization. This means that olivines that crystallize from deep peridotite sourced melts will record relatively higher-Ni content than those that crystallize from shallower sourced peridotite melts (Matzen et al., 2013; Putirka et al., 2011). A recent contribution from Matzen et al., (Matzen et al.) shows that variations in NiO of phenocrystic olivine correlates positively with lithospheric thickness and the variation is a natural consequence of the temperature dependence of $D^{ol/l}_{Ni}$. Although the variations in olivine trace element systematics in this study can be explained by $D^{ol/l}_{Ni}$ as a function of lithospheric pressure, we favor the interpretation that source lithology is the dominant control on olivine chemistry in this study for several reasons. A number of studies (Herzberg et al., 2016; Straub et al., 2008; Trela et al., 2015) show that high Ni, low Ca olivines can crystallize from relatively low temperature melts. This is observed in the NiO differences in olivines from the Quepos terrane and Curacao Lava Formation. Petrologic modeling shows that younger 70 Ma Quepos terrane records lower mantle potential temperatures than the 90 Ma Curacao Lava Formation, despite the fact that theses terranes are interpreted to both derive from the Galapagos mantle plume and there is not evidence suggesting significant lithospheric thickening between 90 and 70 Ma. Contrastingly, the cooler Quepos melts crystallized olivine with higher NiO than the Curaco melts. We acknowledge that the ΔT model is a viable explanation for high Ni olivine, although olivines crystallizing from melts produced in such a manner will not record as high of Ni contents as though produced form an olivine-free pyroxenite source. Additionally, the pressure dependence model does not account for

other olivine trace element systematics such as Fe/Mn ratios and Ca contents. Future efforts should focus on holistic approaches to understand olivine trace element systematics and resolve discrepancies between source lithology and pressure-dependence models.

The observed trends in Ca and Ni of our Azuero and Quepos olivines cannot be explained solely by olivine crystallization alone (Fig. 3). High pressure cotectic crystallization of olivine and clinopyroxene in deep magma chambers could explain the observed trends, however, these samples tend lack any observable clinopyroxene.. Thus, our preferred model is that these melt derived from a source that included recycled components (pyroxenite) followed by magma chamber recharge and mixing of melts with variable MgO contents (more details in (Trela et al., 2015)). Interestingly, both the Azuero and Quepos olivine trends can be explained by crystallization of a pyroxenite source primary magma. Azuero olivines have slightly elevated Ca concentrations and lower Fe/Mn ratios (for a give olivine Mg#) relative to Quepos olivines. This is consistent with the CaO-MgO whole rock systematics of the Azuero samples that plot along both sides of the pyroxenite-peridotite discrimination line in Figure 2B.

We compared the Azuero and Quepos olivine systematics with a global data set using the source lithology sensitive ratios 100Mn/Fe vs. Ni/(Mg/Fe)/1000 (Fig. 4A). This diagram is particularly useful as these ratios eliminate the effects of olivine crystallization. Quepos and Azuero olivines have an average Ni/(Mg/Fe)/1000 value of 0.9 and average 100(Mn/Fe) value of 1.45 and plot close to Mauna Kea olivine which have been interpreted to crystallize from an olivine-free pyroxenite source (Sobolev et al., 2007). Olivines derived from peridotite sourced MORB have an average

Ni/(Mg/Fe)/1000 value of ~0.6 and average 100(Mn/Fe) value of 1.6. Quepos and Azuero olivines have an average 100(Ca/Fe) value of 2.3, trending in the direction of Mauna Kea olivines (Fig. 4B). In both Figures 4A and 4B, our analyzed olivines plot closer to a pyroxenite end member as do globally compared olivines from other LIP and OIB localities, e.g., the Canaries, Iceland, and the North Atlantic Igneous Province. Although, both the Quepos and Azuero olivine data strongly overlap each other and have nearly identical and constant 100(Ca/Fe) ratios, the Azuero data has systematically lower 100(Mn/Fe) values and plots closer to the pyroxenitic end member than do Quepos olivines. This observation is in contrast to the major element data (MgO-CaO) that suggests that at least some Azuero melts derived from a peridotite source. We suggest that the most likely explanation for these observed differences lies in the source lithology. Both of these sets of olivine most likely crystallized form a pyroxenite derived melt, however, small variations in the redox state of the mantle source yielded olivines different Fe contents. Fe^{3+} is less compatible in olivine than Fe^{2+} (Krivolutskaya et al., 2012) and more oxidized melts will result in olivines with lower Fe contents. In fact, Azuero olivines show systematically higher Fe contents than Quepos olivines at a given Mn content (not shown). Based on these observations, we suggest that the pyroxenite source of Quepos olivines was more oxidized than the Azuero source. Future melt inclusion studies using vanadium partitioning between olivine and melt could potentially shed light on whether or not there was a different redox state in the mantle source for each respective terrane. Furthermore, the radiogenic isotope compositions described below also suggest unique sources for both the Azuero and Quepos terranes.

Olivine trace element systematics from the modern day Galapagos Archipelago suggest a predominantly peridotite component in the source of the plume with variable involvement of pyroxenite components between the various volcanoes (Vidito et al., 2013). Olivines from the enriched Central and depleted Eastern Domains show the strongest pyroxenite signature in these two parts of the Archipelago. Olivines from Floreana (Southern Domain) indicate crystallization from a melt that is up to 60% pyroxenite. These results suggest that recycled crustal lithologies are not the sole explanation for the isotopic variability of the Galapagos hotspot. Trace element systematics of Azuero (Southern Domain) and Quepos (Central Domain) olivines are generally consistent with the findings of (Vidito et al., 2013).

Trace elements and radiogenic isotopes evidence for long-lived heterogeneities in the Galapagos Plume

The whole rock trace element systematics of the Azuero terrane samples shows a broad similarity to lavas from the modern day Galapagos lavas (Fig. 5). Interestingly, there appear to be two groups that can be distinguished in a primitive mantle normalized spider diagrams. The relative depletions in fluid-mobile elements (e.g., K, Pb, and Sr) and strong relative enrichments in high field strength elements (e.g., Nb, Ti, and Ta) are typical of OIB-intraplate lavas and have been interpreted to result from the entrainment and melting of recycled oceanic crust (Jackson et al., 2008). Both terranes show strongly fractionated heavy rare earth element (HREE) patterns indicative of melting in the presence of garnet that sequesters the HREE. Azuero picrites show strong similarities with, respect to trace element patterns, to the Cocos, Coiba, and Carnegie Ridges, but have stronger depletions in Ba, K, and Sr and more negative HREE slope (Fig. 5).

Source projected radiogenic isotopes for Quepos and Azuero have broadly similar $^{143}Nd/^{144}Nd$ isotopes, yet distinct $^{206}Pb/^{204}Pb$ and $^{208}Pb/^{204}Pb$ ratios (Fig. 6). Azuero lavas most likely were derived from a mantle source with a higher $^{238}U/^{204}Pb$ ratio than Quepos lavas. For comparison, we plotted source projected isotope ratios from other accreted Galapagos-related terranes such as the Tortugal Suite (Costa Rica), the Curacao Lava Formation, and basalts from the Nicoya Peninsula. Quepos samples plot well within the field of the classically defined Central Domain, while Azuero radiogenic isotopes show similarity to the Southern Domain (e.g., the island of Floreana). The Tortugal Suite shows vast isotopic similarity to the classically defined Northern Domain (e.g., the Wolf-Darwin lineament). Although olivines from the two terranes examined in this study suggest crystallization a source that reflect a pyroxenitic component, the radiogenic ratios clearly show a unique source component for each terrane. By doing a source projection of the radiogenic we can adequately compare the source compositions of ancient Galapagos-related islands with the mantle source beneath the current archipelago and determine how it has evolved over time. Our study shows that spatial isotopic (and perhaps lithological) zonation has existed in the Galapagos mantle plume for tens of millions of years. The enigmatic Northern Domain end member has been a distinct Galapagos component since the incipient melting stages of the plume circa 90 Ma evident in the Tortugal suite acceted in Costa Rica (Trela et al., in review) and is still present in the mantle source today as observed in the radiogenic isotope signature of lavas from Wolf, Darwin, and Pinta Islands. Likewise, the Central Domain component has been present in the plume source since 90 ~Ma as shown by lavas from the Nicoya Peninsula and the Curacao Lava

Formation. Azuero lavas are the oldest record of the Southern Domain that extends to at least 70 Ma before present time.

Interestingly, besides evidence of the long-lived heterogeneities sampled by the Galapagos Plume, the spatial relationship between each of the classically defined Galapagos Domains appeared to remain relatively constant over the last 90 Ma. This is evidenced by the isotopic compositions of accreted terranes along the western coasts of Costa Rica and Panama (Fig. 7). Previous studies have suggested that the Central, Southern, and depleted Eastern Domains have existed for at least 20 Ma whereas the Northern Domain has been present for at least 15 Ma (e.g. Hoernle et al., 2000). Our new results extend the time scale of distinct isotopic heterogeneity in the source of the plume to at least 70 Ma for the Southern Domain and 90 Ma for the Central, Northern, and Eastern Domains, suggesting that geochemically zoned plumes rising through the mantle preserve distinct isotopic heterogeneity on the time scale of tens to hundreds of Ma. This relatively stationary heterogeneity if further supported by accreted tracks along the western margin of the Central American coast. Accreted terranes in northern Costa Rica preserve evidence of the Northern Domain end member while further south the Quepos terrane preserves a memory of the Central Domain end member (Fig. 7). Lastly, accreted terranes in the Azuero Peninsula, Panama largely record evidence the Southern Domain sourced the ancient lavas collected in this terrane.

Numerical geodynamic studies proposed that the entrainment of dense recycled oceanic crust within a mantle plume may result in overall lower plume temperatures due to longer transit ascent times that provides the opportunity for greater conductive heat loss to the surrounding mantle, relative to a purely peridotite plume (Farnetani, 2005;

Kumagai et al., 2008; Nolet et al., 2006). Conversely, here is also evidence that mantle plumes are able to entrain greater amounts of dense recycled oceanic crust due to their greater buoyancy (Kumagai et al., 2008). In the case of the Galapagos plume it is possible that entrained recycled oceanic crust was present in the source since its incipient melting stage at 90 Ma, but the high degree of peridotite partial melting during the head stage overprinted this signature, and it is until later stages of the plume evolution that these components became more evident. The radiogenic isotope compositions highlight the longevity of these distinct domains sampled by the plume over the course of 90 Ma. We suggest that the Northern and Central Domains have existed since 90 Ma while the first appearance of the Southern Domain occurred at ~70 Ma during the melting event that formed the accreted-terranes in the Azuero Peninsula Panama.

Conclusions

The accreted Galapagos terranes along the western margins of Panama and Costa Rica provide unparalleled opportunities to study the life-death cycles of mantle plumes and the existence of long-term spatial geochemical and lithological zonation within them. Our new results from the Azuero and Quepos terranes, based on olivine trace element systematics isotope modeling, suggest that both of these terranes resulted from melts that derived from sourced that included recycled components but with different initial radiogenic isotopes signatures that have evolved separately through time. Thus, based on our new results, we suggest that the Galapagos plume is sampling recycled, isotopically distinct reservoirs from the deep mantle, similar to the case of the Hawaiian and Tristan hotspots (Hoernle et al., 2015; Hofmann and Farnetani, 2013). These observations support the idea that mantle plumes are long-lived upwellings of geochemically domains

that can be used to understand the geochemical evolution of the deep regions of the mantle and the processes of global recycling in both space and time.

References

Allan, J.F., Simkin, T., 2000. Fernandina Volcano's evolved, well-mixed basalts: Mineralogical and petrological constraints on the nature of the Galapagos plume. Journal of Geophysical Research 105, 6071-6041.

Batanova, V.G., Sobolev, A.V., Kuzmin, D.V., 2015. Trace element analysis of olivine: High precision analytical method for JEOL JXA-8230 electron probe microanalyser. Chemical Geology 419, 149-157.

Beattie, P., 1993. Olivine-melt and orthopyroxene-melt equilibria. Contributions to Mineralogy and Petrology 115, 103-111.

Bizimis, M., Salters, V.J.M., Garcia, M.O., Norman, M.D., 2013. The composition and distribution of the rejuvenated component across the Hawaiian plume: Hf-Nd-Sr-Pb isotope systematics of Kaula lavas and pyroxenite xenoliths. Geochemistry, Geophysics, Geosystems 14, 4458-4478.

Blichert-Toft, J., White., W.M., 2001. Hf isotope geochemistry of the Galapagos Islands,. Geochem. Geophys. Geosyst. 2.

Carr, M., Gazel, E., 2016. Igpet software for modeling igneous processes: examples of application using the open educational version. Mineralogy and Petrology.

Chauvel, C., Lewin, E., Carpentier, M., Arndt, N.T., Marini, J.-C., 2008. Role of recycled oceanic basalt and sediment in generating the Hf–Nd mantle array. Nature Geoscience 1, 64-67.

Coogan, L.A., Saunders, A.D., Wilson, R.N., 2014. Aluminum-in-olivine thermometry of primitive basalts: Evidence of an anomalously hot mantle source for large igneous provinces. Chemical Geology 368, 1-10.

Denyer, P., Baumgartner, P.O., Gazel, E., 2006. Characterization and tectonic implications of Mesozoic-Cenozoic oceanic assemblages of Costa Rica and Western Panama. Geologica Acta 4, 219-235.

Denyer, P., Gazel, E., 2009. The Costa Rican Jurassic to Miocene oceanic complexes: Origin, tectonics and relations. Journal of South American Earth Sciences 28, 429-442.

Duncan, R., Hargraves, R., 1984. Plate tectonic evolution of the Caribbean region in the mantle reference frame. Geological Society of America Memoirs 162, 81-94.

Duran, P., 2013. Estudio vulcano-estructural y sedimentario del mélange en el Promontorio de Quepos. Masters Thesis-University of Costa Rica.

Farnetani, C.G., 2005. Beyond the thermal plume paradigm. Geophysical Research Letters 32.

Frisch, W., Meschede, M., Sick, M., 1992. Origin of the Central American ophiolites: Evidence from paleomagnetic results. Geological Society of America Bulletin 104, 1301-1314.

Gazel, E., Hayes, J.L., Hoernle, K., Kelemen, P., Everson, E., Holbrook, W.S., Hauff, F., van den Bogaard, P., Vance, E.A., Chu, S., Calvert, A.J., Carr, M.J., Yogodzinski, G.M., 2015. Continental crust generated in oceanic arcs. Nature Geoscience 8, 321-327.

Gazel, E., Hoernle, K., Carr, M.J., Herzberg, C., Saginor, I., den Bogaard, P.v., Hauff, F., Feigenson, M., Swisher, C., 2011. Plume–subduction interaction in southern Central America: Mantle upwelling and slab melting. Lithos 121, 117-134.

Geist, D., White, W.M., Albarede, F., Harpp, K., Reynolds, R., Blichert-Toft, J., Kurz, M.D., 2002. Volcanic evolution in the Galápagos: The dissected shield of Volcan Ecuador. Geochemistry, Geophysics, Geosystems 3, 1 of 32-32 of 32.

Geist, D., White, W.M., McBirney, A.R., 1988. Plume-asthenosphere mixing beneath the Galapagos archipelago. Nature 333, 657-660.

Geldmacher, J., 2003. Hafnium isotopic variations in volcanic rocks from the Caribbean Large Igneous Province and Galápagos hot spot tracks. Geochemistry Geophysics Geosystems 4.

Gurenko, A.A., Sobolev, A.V., Hoernle, K.A., Hauff, F., Schmincke, H.-U., 2009. Enriched, HIMU-type peridotite and depleted recycled pyroxenite in the Canary plume: A mixed-up mantle. Earth and Planetary Science Letters 277, 514-524.

Harpp, K.S., White, W.M., 2001. Tracing a mantle plume: Isotopic and trace element variations of Galapagos seamounts. Geochemistry Geophysics Geosystems 2, 1525.

Hart, S., Hauri, E., Oschmann, L., Whitehead, J., 1992. Mantle plumes and entrainment: isotopic evidence. Science 256, 517-520.

Hauff, F., Hoernle, K., Schmincke, H.-U., Werner, R., 1997. A Mid Cretaceous origin for the Galapagos hotspot: volcanological, petrological and geochemical evidence from Costa Rican oceanic crustal segments. Geol. Rundsch. 86, 141-155.

Hauff, F., Hoernle, K., Tilton, G., Graham, D.W., Kerr, A.C., 2000a. Large volume recycling of oceanic lithosphere over short time scales: geochemical constraints from the Caribbean Large Igneous Province. Earth and Planetary Science Letters 174, 247-263.

Hauff, F., Hoernle, K., Tilton, G., Graham, D.W., Kerr, A.C., 2000b. Large volume recycling of oceanic lithosphere over short time scales:geochemical constraints from the Carribean Large Igneous Province. Earth and Planetary Science Letters 174, 247-263.

Hauff, F., Hoernle, K., van den Bogaard, P., Alvarado, G., Garbe-Schönberg, D., 2000c. Age and geochemistry of basaltic complexes in western Costa Rica: Contributions to the geotectonic evolution of Central America. Geochemistry, Geophysics, Geosystems 1, 1009.

Herzberg, C., 2004. Partial Crystallization of Mid-Ocean Ridge Basalts in the Crust and Mantle. Journal of Petrology 45, 2389-2405.

Herzberg, C., 2011. Basalts as temperature probes of Earth's mantle. Geology 39, 1179-1180.

Herzberg, C., Asimow, P.D., 2008. Petrology of some oceanic island basalts: PRIMELT2.XLS software for primary magma calculation. Geochemistry, Geophysics, Geosystems 9, n/a-n/a.

Herzberg, C., Asimow, P.D., Ionov, D.A., Vidito, C., Jackson, M.G., Geist, D., 2013. Nickel and helium evidence for melt above the core-mantle boundary. Nature 493, 393-397.

Herzberg, C., Cabral, R.A., Jackson, M.G., Vidito, C., Day, J.M.D., Hauri, E.H., 2014. Phantom Archean crust in Mangaia hotspot lavas and the meaning of heterogeneous mantle. Earth and Planetary Science Letters 396, 97-106.

Herzberg, C., Gazel, E., 2009. Petrological evidence for secular cooling in mantle plumes. Nature 458, 619-623.

Herzberg, C., Vidito, C., Starkey, N.A., 2016. Nickel–cobalt contents of olivine record origins of mantle peridotite and related rocks. American Mineralogist 101, 1952-1966.

Hoernle, K., Hauff, F., Bogaard, P.v.d., 2004. 70 m.y. history (139–69 Ma) for the Caribbean large igneous province. Geology 32, 697-700.

Hoernle, K., Rohde, J., Hauff, F., Garbe-Schönberg, D., Homrighausen, S., Werner, R., Morgan, J.P., 2015. How and when plume zonation appeared during the 132 Myr evolution of the Tristan Hotspot.

Hoernle, K., van den Bogaard, P., Wener, R., Lissina, B., Hauff, F., Alvarado, G., Garbe-Schönberg, D., 2002. Missing history (16–71 Ma) of the Galapagos hotspot: Implications for the tectonic and biological evolution of the Americas. Geology 30, 795–798.

Hoernle, K., Werner, R., Morgan, J.P., Garbe-Schönberg, D., Bryce, J., Mrazek, J., 2000. Existence of complex spatial zonation in the Galápagos plume for at least 14 m.y. Geology 28, 435-438.

Hofmann, A., Farnetani, C.G., 2013. Two views of the Hawaiian plume structure. Geochemistry Geophysics Geosystems 14, 5308-5322.

Hofmann, A.W., 1997. Mantle geochemistry: the message from oceanic volcanism. Nature 385, 219-229.

Hofmann, A.W., White, W.M., 1982. Mantle plumes from ancient oceanic crust. Earth and Planetary Science Letters 57, 421-436.

Jackson, M.G., Hart, S.R., Saal, A.E., Shimizu, N., Kurz, M.D., Blusztajn, J.S., Skovgaard, A.C., 2008. Globally elevated titanium, tantalum, and niobium (TITAN) in ocean island basalts with high3He/4He. Geochemistry, Geophysics, Geosystems 9, Q04027, doi:04010.01029/02007GC001876.

Jicha, B.R., Brown, F.H., 2014. An age on the Korath Range and the viability of 40 Ar/39 Ar dating of kaersutite in Late Pleistocene volcanics, Ethiopia. Quaternary Geochronology 21, 53-57.

Johnson, D.M., Hooper, P.R., Conrey, R.M., 1999. XRF Analysis of rocks and minerals for major and trace elements on a single low dilution Li-tetraborate fused bead. Advances in X-ray Analysis 41, 843-867.

Kamber, B., Collerson, K., 2000. Zr/Nb systematics of ocean island basalts reassessed—the case for binary mixing. Journal of Petrology 41, 1007-1021.

Kelley, K.A., Plank, T., Ludden, J., Staudigel, H., 2003. Composition of altered oceanic crust at ODP Sites 801 and 1149. Geochemistry, Geophysics, Geosystems 4, n/a-n/a.

Kerr, A.C., Tarney, J., Marriner, G.F., Klaver, G.T., Saunders, A.D., Thriwall, M.F., 1996. The geochemistry and petrogenesis of the late-Cretaceaous picrites and basalts of Curacao, Netherlands Antilles: a remnant of an oceanic plateau. Contrib. Min. Petrol. 124, 29-43.

Kerr, A.C., White, R.V., Thompson, P.M.E., Tarney, J., Saunders, A.D., 2003. No oceanic plateau-no Caribbean Plate? The seminal role of an oceanic plateau in Caribbean Plate evolution. AAPG Memoir 79, 126-168.

Khanna, T.C., Bizimis, M., Yogodzinski, G.M., Mallick, S., 2014. Hafnium–neodymium isotope systematics of the 2.7 Ga Gadwal greenstone terrane, Eastern Dharwar craton, India: Implications for the evolution of the Archean depleted mantle. Geochimica et Cosmochimica Acta 127, 10-24.

Klaver, G.T., 1987. The Curacao lava formation: an ophiolitic analogue of the anomalously thick layer 2B of the mid-Cretaceous oceanic plateausin the western Pacific and CAribbean. PHD Thesis. University of Amsterdam.

Krivolutskaya, N.A., Sobolev, A.V., Mikhailov, V.N., Plechova, A.A., Kostitsyn, Y.A., Roschina, I.A., Fekiacova, Z., 2012. Parental melt of the Nadezhdinsky Formation: Geochemistry, petrology and connection with Cu-Ni deposits (Noril'sk area, Russia). Chemical Geology 302–303, 87-105.

Kuiper, K.F., Deino, A., Hilgen, F.J., Krijgsman, W., Renne, P.R., Wijbrans, J.R., 2008. Synchronizing rock clocks of Earth history. Science 320, 500-504.

Kumagai, I., Davaille, A., Kurita, K., Stutzmann, E., 2008. Mantle plumes: Thin, fat, successful, or failing? Constraints to explain hot spot volcanism through time and space. Geophysical Research Letters 35.

Kurz, M.D., Rowland, S.K., Curtice, J., Saal, A.E., Naumann, T., 2014. Eruption Rates for Fernandina Volcano, The Galápagos. John Wiley & Sons, Inc, pp. 41-54.

Loewen, M.W., Duncan, R.A., Kent, A.J.R., Krawl, K., 2013. Prolonged plume volcanism in the Caribbean Large Igneous Province: New insights from Curaçao and Haiti. Geochemistry, Geophysics, Geosystems 14, 4241-4259.

Lonsdale, P., 2005. Creation of the Cocos and Nazca plates by fission of the Farallon plate. Tectonophysics 404, 237-264.

Madrigal, P., Gazel, E., Flores, K.E., Bizimis, M., Jicha, B., 2016. Record of massive upwellings from the Pacific large low shear velocity province. Nature Communications 7, 13309.

Matzen, A.K., Baker, M.B., Beckett, J.R., Stolper, E.M., 2013. The Temperature and Pressure Dependence of Nickel Partitioning between Olivine and Silicate Melt. Journal of Petrology 54, 2521-2545.

Matzen, A.K., Baker, M.B., Beckett, J.R., Wood, B.J., Stolper, E.M., 2016. The effect of liquid composition on the partitioning of Ni between olivine and silicate melt. Contributions to Mineralogy and Petrology 172, 3.

Mazza, S.E., Gazel, E., Johnson, E.A., Kunk, M.J., McAleer, R., Spotila, J.A., Bizimis, M., Coleman, D.S., 2014. Volcanoes of the passive margin: The youngest magmatic event in eastern North America. Geology 42, 483-486.

McDonough, W., 1991. Partial melting of subducted oceanic crust and isolation of its residual eclogitic lithology. Philosophical Transactions of the Royal Society of London. Series A: Physical and Engineering Sciences 335, 407-418.

McDonough, W.F., Sun, S.-s., 1995. The composition of the Earth. Chemical Geology 120, 223-253.

Meschede, M., Frisch, W., 1998. A plate-tectonic model for the Mesozoic and Early Cenozoic history of the Caribbean plate. Tectonophysics 296, 269-291.

Min, K., Mundil, R., Renne, P.R., Ludwig, K.R., 2000. A test for systematic errors in 40Ar/39Ar geochronology through comparison with U/Pb analysis of a 1.1-Ga rhyolite. Geochimica et Cosmochimica Acta 64, 73-98.

Naumann, T.R., Geist, D.J., 2002. Petrology and Geochemistry of Cerro Azul Volcano and the Origin of the Petrologic Diversity of the Western Galápagos Shield Volcanoes: An inter-volcano comparison of Cerro Azul, Alcedo, and Sierra Negra. Journal of Petrology 43,, 859-883.

Nolet, G., Karato, S., Montelli, R., 2006. Plume fluxes from seismic tomography. Earth and Planetary Science Letters 248, 685-699.

O'Connor, J.M., Jokat, W., le Roex, A.P., Class, C., Wijbrans, J.R., Keßling, S., Kuiper, K.F., Nebel, O., 2012. Hotspot trails in the South Atlantic controlled by plume and plate tectonic processes. Nature Geoscience 5, 735-738.

Pindell, J.L., Barrett, S.F., 1990. Geological evolution of the Caribbean region: a plate tectonic perspective. The Caribbean region: Boulder, Colorado, Geological Society of America, Geology of North America, v. H, 405-432.

Putirka, K., Ryerson, F.J., Perfit, M., Ridley, W.I., 2011. Mineralogy and Composition of the Oceanic Mantle. Journal of Petrology 52, 279-313.

Richards, M.A., Duncan, R.A., Courtillot, V.E., 1989. Flood Basalts and Hot-Spot Tracks: Plume Heads and Tails. Science 246, 103-107.

Rudnick, R.L., Barth, M., Horn, I., McDonough, W.F., 2000. Rutile-bearing refractory eclogites: missing link between continents and depleted mantle. Science 287, 278-281.

Sinton, C.W., Duncan, R.A., Storey, M., Lewis, J., Estrada, J.J., 1998. An oceanic flood basalt province within the Caribbean plate. Earth and Planetary Science Letters 155, 221-235.

Sobolev, A.V., Hofmann, A., Sobolev, S.V., Nikogosian, I.K., 2005. An olivine-free mantle source of Hawaiian shield basalts. Nature 434, 590-597.

Sobolev, A.V., Hofmann, A.W., Kuzmin, D.V., Yaxley, G.M., Arndt, N.T., Chung, S.L., Danyushevsky, L.V., Elliott, T., Frey, F.A., Garcia, M.O., Gurenko, A.A., Kamenetsky, V.S., Kerr, A.C., Krivolutskaya, N.A., Matvienkov, V.V., Nikogosian, I.K., Rocholl, A., Sigurdsson, I.A., Sushchevskaya, N.M., Teklay, M., 2007. The amount of recycled crust in sources of mantle-derived melts. Science 316, 412-417.

Spice, H.E., Fitton, G., Kirstein, L., 2016. Temperature fluctuation of the Iceland mantle plume through time. Geochem. Geophys. Geosyst., 1-12.

Stolper, E., Sherman, S., Michael, G., Baker, M., Seaman, C., 2004. Glass in the submarine section of the HSDP2 drill core, Hilo, Hawaii. Geochemistry Geophysics Geosystems 5.

Stracke, A., 2005. FOZO, HIMU, and the rest of the mantle zoo. Geochemistry Geophysics Geosystems 6.

Straub, S.M., LaGatta, A.B., Martin-Del Pozzo, A.L., Langmuir, C.H., 2008. Evidence from high-Ni olivines for a hybridized peridotite/pyroxenite source for orogenic

andesites from the central Mexican Volcanic Belt. Geochemistry Geophysics Geosystems 9.

Toplis, M.J., 2005. The thermodynamics of iron and magnesium partitioning between olivine and liquid: criteria for assessing and predicting equilibria in natural and experimental systems. Contributions to Mineralogy and Petrology 149, 22-39.

Tournon, J., Azema, J., 1984. Granophyres and ferrodolerites from the Nicoya Complex (Costa Rica)-possible example of magma immiscibility. Bull. Soc. Géol. Fr. 26, 1336-1347.

Trela, J., Vidito, C., Gazel, E., Herzberg, C., Class, C., Whalen, W., Jicha, B., Bizimis, M., Alvarado, G.E., 2015. Recycled crust in the Galápagos Plume source at 70 Ma: Implications for plume evolution. Earth and Planetary Science Letters 425, 268-277.

Vidito, C., Herzberg, C., Gazel, E., Geist, D., Harpp, K., 2013. Lithological structure of the Galápagos Plume. Geochemistry, Geophysics, Geosystems 14, 4214-4240.

Wegner, W., Worner, G., Harmon, R.S., Jicha, B.R., 2010. Magmatic history and evolution of the Central American Land Bridge in Panama since Cretaceous times. Geological Society of America Bulletin 123, 703-724.

Werner, R., Hoernle, K., Barckhausen, U., Hauff, F., 2003. Geodynamic evolution of the Galápagos hot spot system (Central East Pacific) over the past 20 m.y.: Constraints from morphology, geochemistry, and magnetic anomalies. Geochemistry, Geophysics, Geosystems 4, n/a-n/a.

White, W., Hofmann, A., 1978. Geochemistry of the Galápagos Islands: implications for mantle dynamics and evolution. Year Book Carnegie Inst. Washington 77, 596-606.

White, W.M., 1985. Sources of oceanic basalts: Radiogenic isotopic evidence. Geology 13, 115.

White, W.M., Albarede, F., Telouk, P., 2000. High-precision analysis of Pb isotope ratios by multi-collector ICP-MS. Chemical Geology 167, 257-270.

White, W.M., McBirney, A.R., Duncan, R.A., 1993. Petrology and geochemistry of the Galápagos Islands: Portrait of a pathological mantle plume. Journal of Geophysical Research 98, 19533.

Wilson, J.T., 1963. A possible origin of the Hawaiian Islands. Can. J. Phys. 41, 863-868.

Zindler, A., Hart, S., 1986. Chemical Geodynamics. Annual Review of Earth and Planetary Science 14, 493-571.

Figures

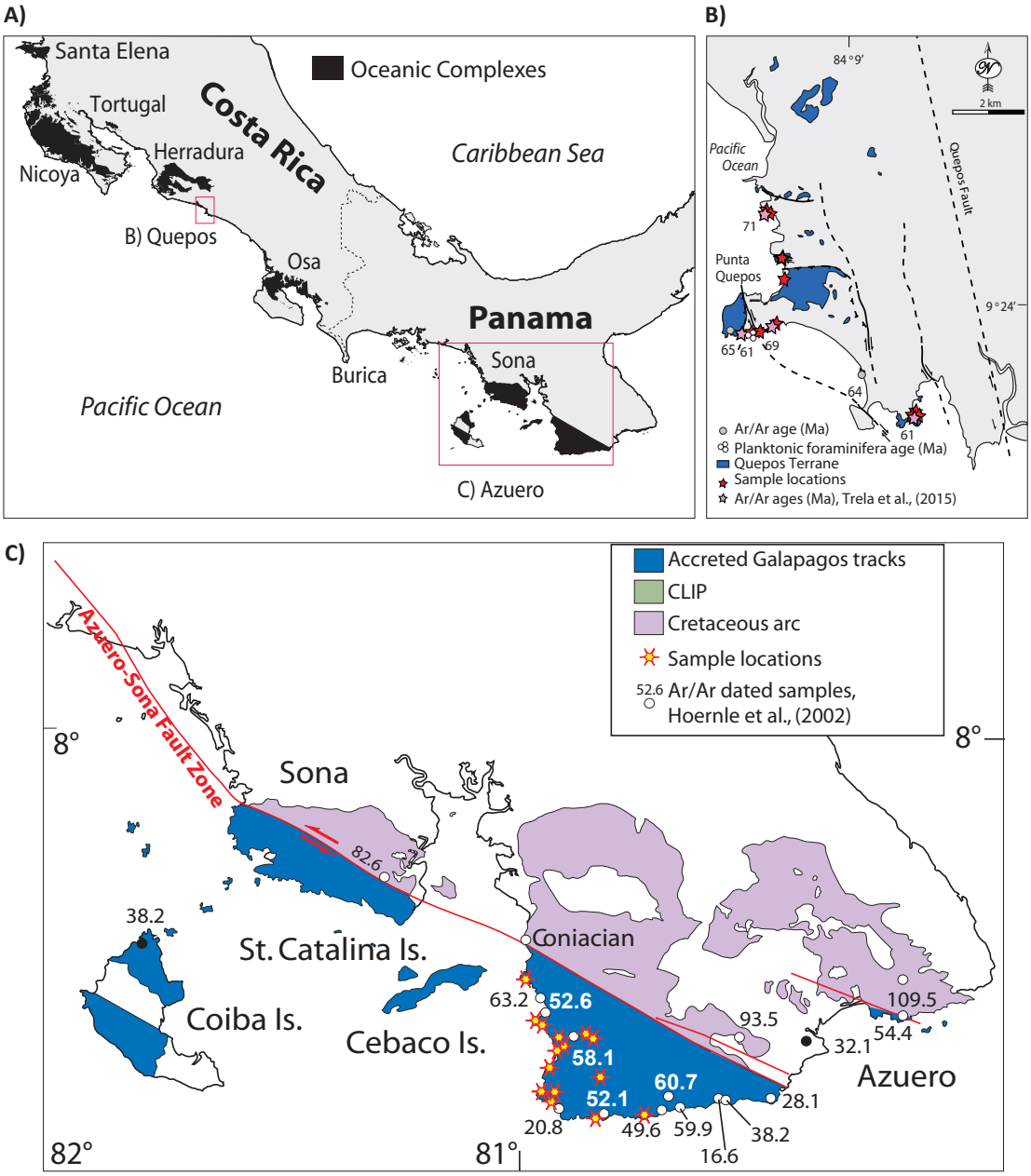

Figure 1. A) Tectonic location of the study area modified from Denyer and Gazel (2009) and Trela et al. (2015). B) Geological map of the Quepos terrane showing sample locations, structures, and areas comprised by basalts and picrites modified from Duran (2013). C) Geological map of the Azuero Peninsula showing sample locations, structures, and areas comprised by basalts and picrites.

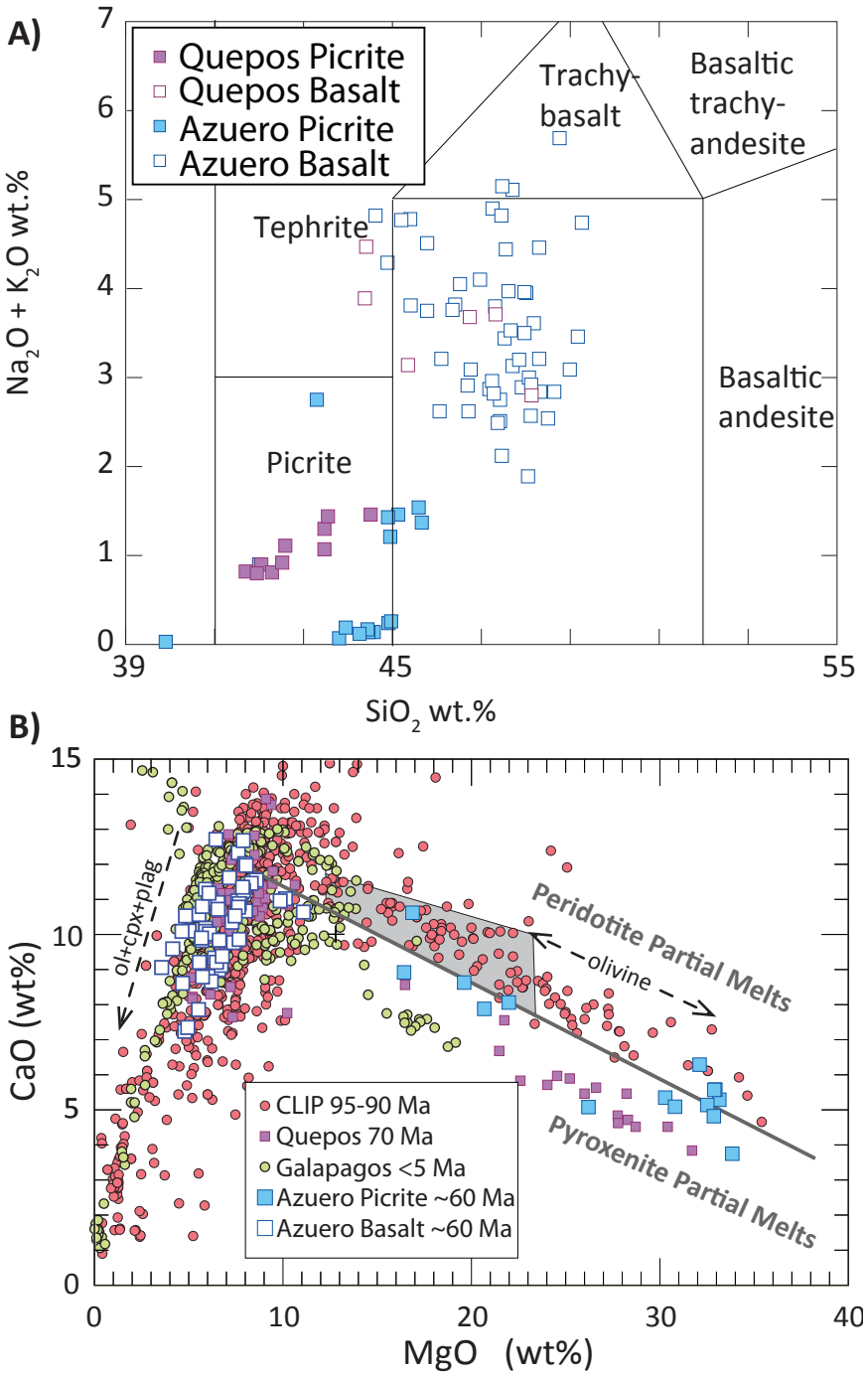

Figure 2. A) Chemical classification of samples using the total alkali versus silica diagram (TAS). Literature data from Hauff et al. (2000c); Meschede and Frisch (1998); Sinton et al. (1998). B) CaO-MgO discrimination diagram between peridotite and

pyroxenite derived magmas from (Herzberg and Asimow, 2008). This model was developed for accumulated fractional melting of peridotite KR4003, and is validated by the fact that no experimental melt compositions from a pure peridotite source plot below the discrimination line. The grey shaded region represents primary magmas of fertile peridotite produced by accumulated fractional melting. Additional data from Stolper et al. (2004) for Mauna Kea and from (Allan and Simkin, 2000; Blichert-Toft and White., 2001; Geist et al., 2002; Hauff et al., 1997; Hauff et al., 2000c; Hoernle et al., 2000; Naumann and Geist, 2002; O'Connor et al., 2012; Wegner et al., 2010; Werner et al., 2003; White et al., 1993) for Galápagos related lavas including accreted terranes in Central America and parts of the CLIP including Nicoya and Curacao.

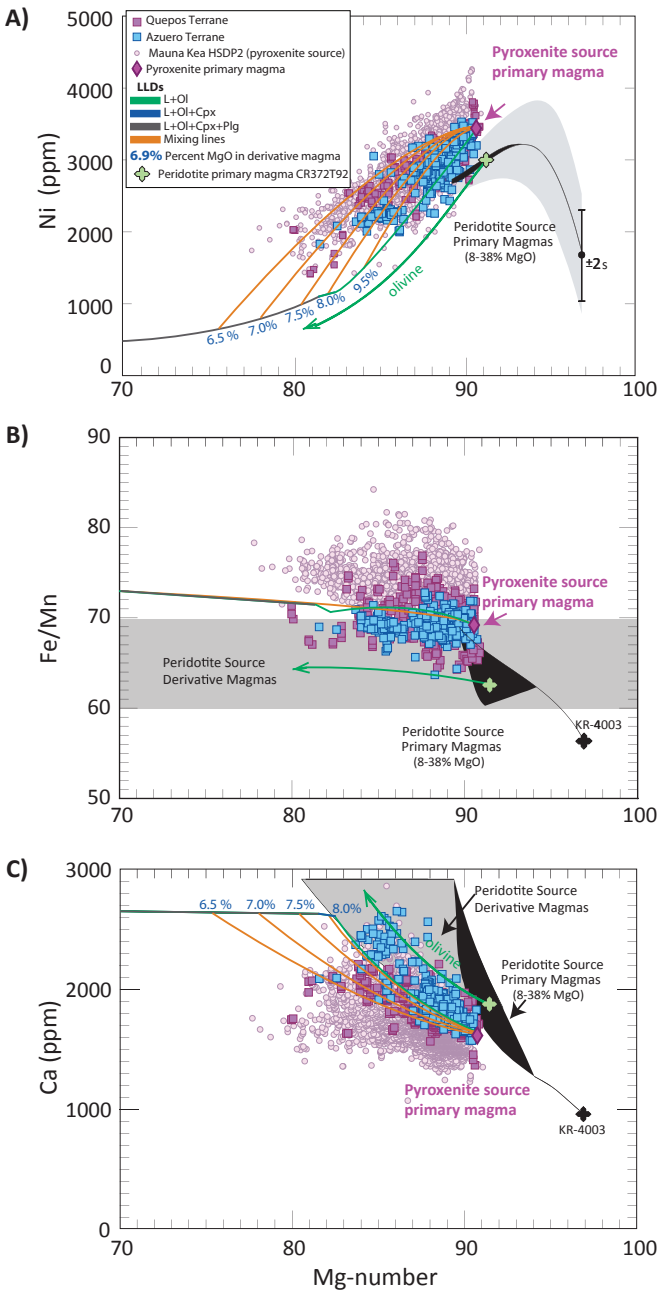

Figure 3. Mg-numbers versus Ni and Ca contents and Fe/Mn for calculated olivines and high-precision olivines from picrites of the ~ 70 Ma Quepos and Azuero terranes. Examples of olivines from a peridotite source primary magma and its derivatives are given by the green cross and arrow, computed from lava sample CR372T92 reported by Tournon and Azema (1984). Quepos olivine compositions are not consistent with

derivation from a normal peridotite source. Notice how the new Quepos data is within range of Mauna Kea data from (Sobolev et al., 2007) interpreted as olivines that crystallized from a pyroxenite-derived primary magma. The trends can be explained by complex olivine+clinopyroxene fractional crystallization or magma recharge. Independent of the explanation, these crystallization trends do not extrapolate to peridotite source primary magmas.

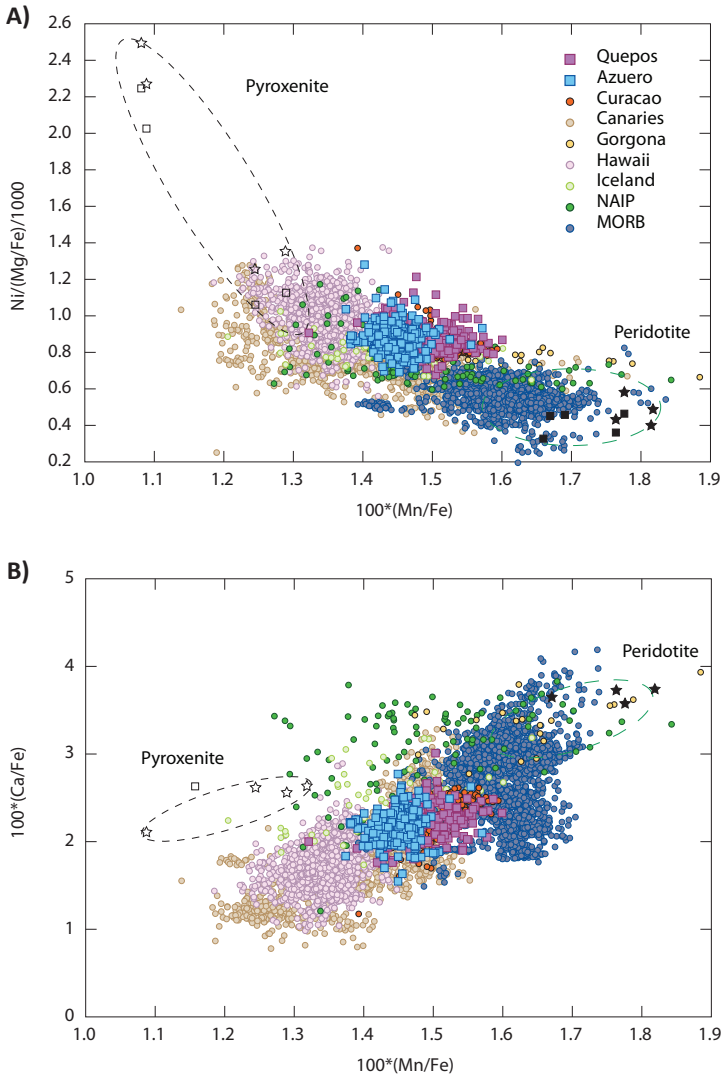

Figure 4. Plot of A) Ni/(Mg/Fe)/1000 and B) 100Mn/Fe vs. 100Ca/Fe used to discriminate between pyroxenite and peridotite source lithology. Azuero and Quepos olivine crystallized principally by a pyroxenite olivine free source through a peridotite source in agreement with the global array of Sobolev et al. (2007). Global olivine data: Ocean Island Basalt (OIB), Hawaii (Sobolev et al., 2007), Quepos (Trela et al., 2015), Canary Islands (Gurenko et al., 2009), Iceland (Spice et al., 2016); Mid Ocean Ridge Basalt (MORB) (Sobolev et al., 2007); Curacao (Trela et al., 2015), Gorgona (Coogan et al., 2014), North Atlantic Igneous Province (NAIP) (Spice et al., 2016).

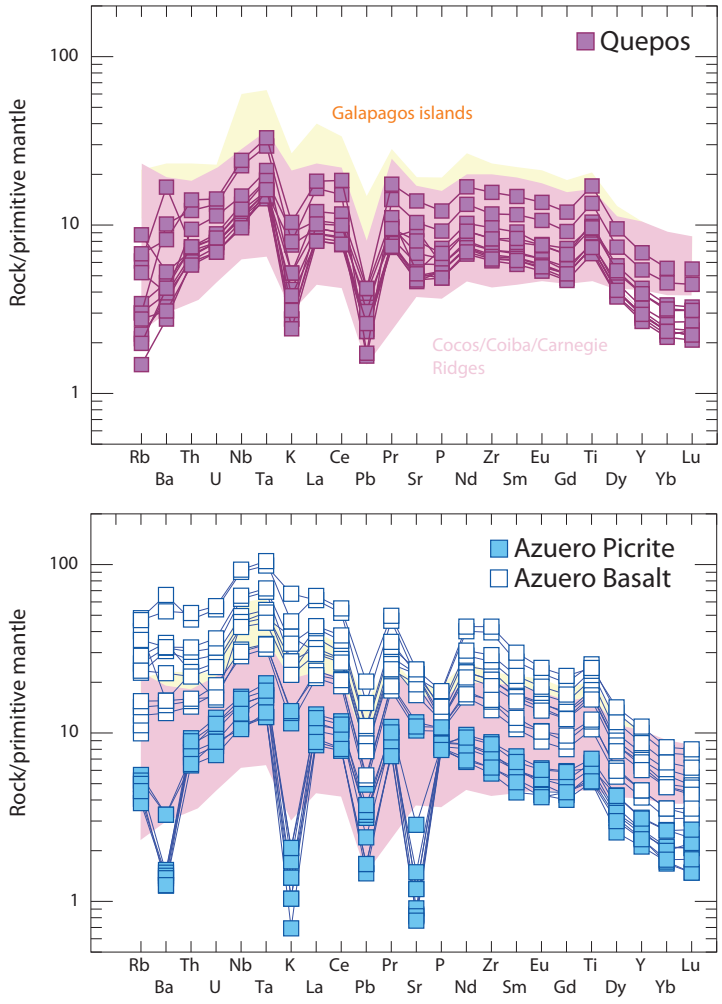

Figure 5. Multi-element spider diagram normalized to primitive mantle (McDonough and Sun, 1995) for A) the Quepos Terrane and B) samples from the Azuero Peninsula.

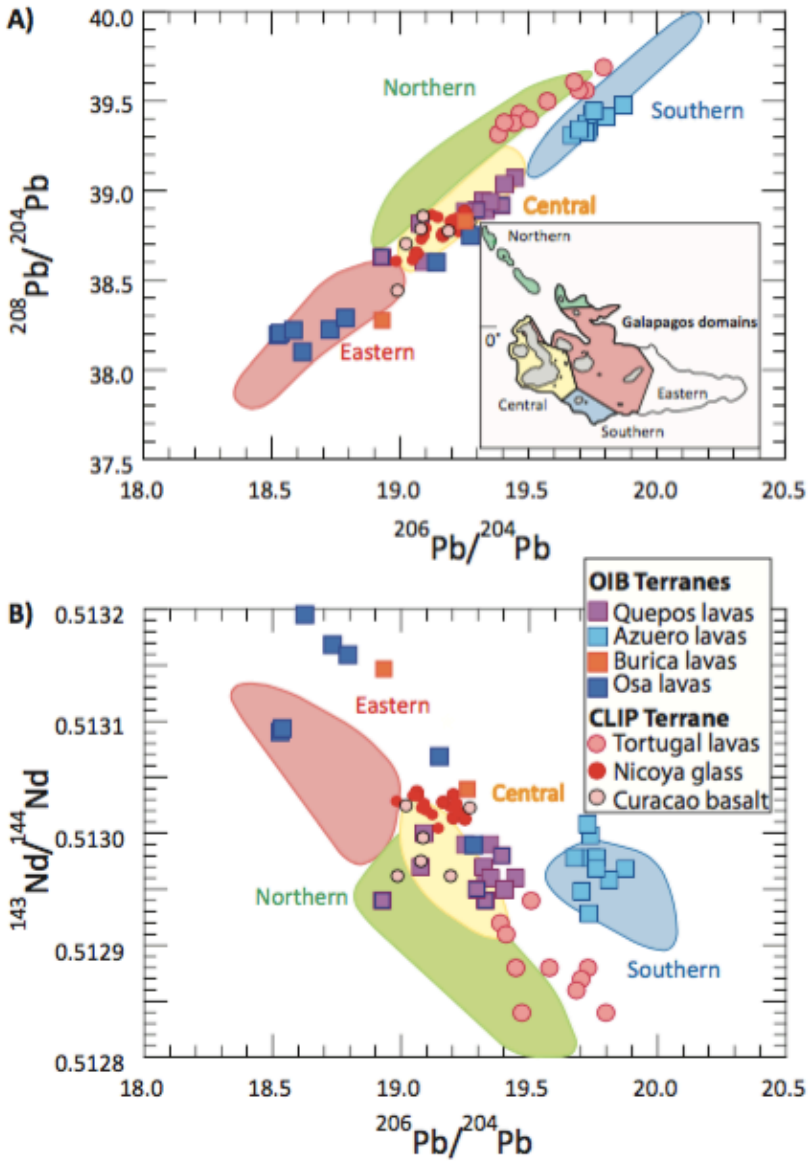

Figure 6. Source projected Pb and Nd isotopes of picrite and basalt samples from the CLIP, Quepos Terrane, Tortugal Suite, and the Azuero Peninsula. Most Quepos samples fall within the Central Galápagos Domain. Tortugal lavas plot within the Northern

Domain and Azuero samples plot within the Southern Domain. Shaded Galápagos Domains for the present day archipelago from Hoernle et al. (2000).

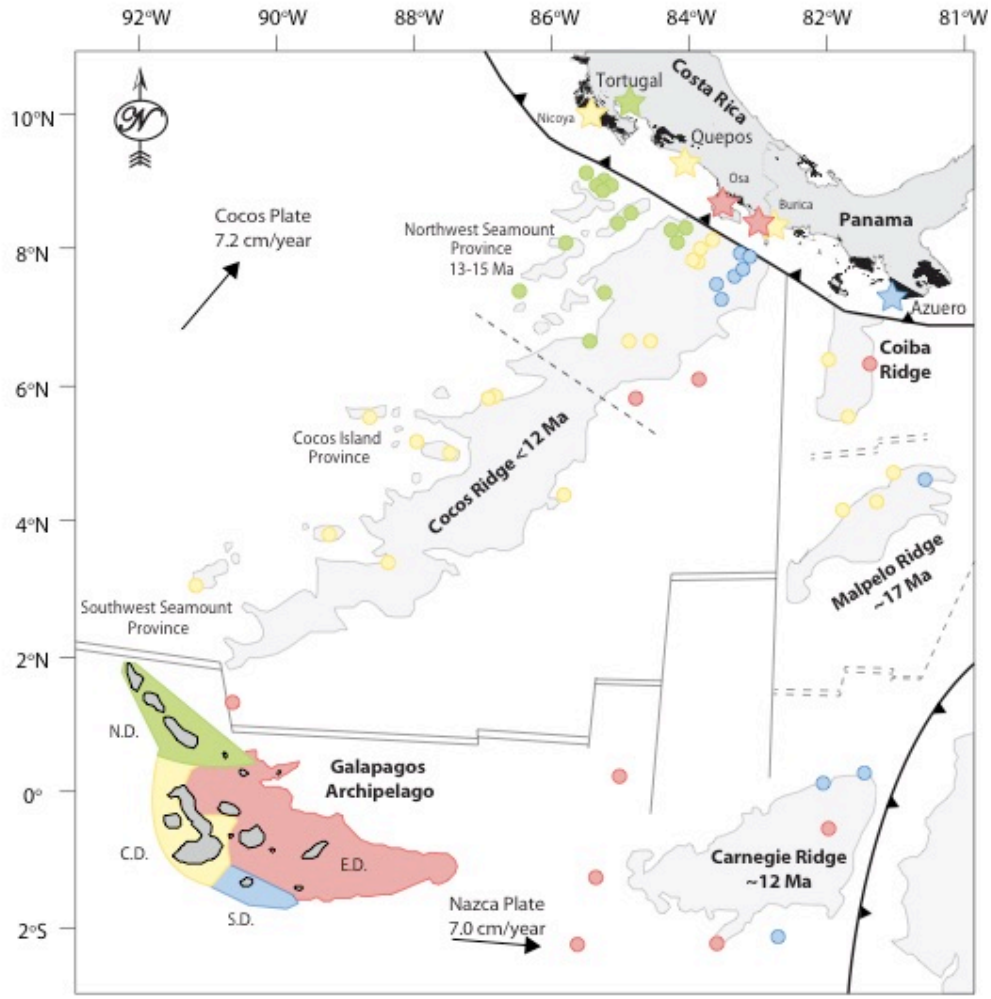

Figure 7. Spatial distribution of Galapagos Domains and their accretion to the western margin of Central America. Modified from (Werner et al., 2003).